

Using multiple signatures to improve accuracy of substorm identification

John D. Haiducek¹, Daniel T. Welling^{2,3}, Steven K. Morley⁴, Natalia Yu. Ganushkina^{3,5}, and Xiangning Chu⁶

¹U.S. Naval Research Laboratory, Washington, DC, USA

²University of Texas at Arlington, Arlington, TX, USA

³Climate and Space Sciences, University of Michigan, Ann Arbor, MI, USA.

⁴Space Science and Applications (ISR-1), Los Alamos National Laboratory, Los Alamos, NM, USA.

⁵Finnish Meteorological Institute, Helsinki, Finland

⁶Laboratory for Atmospheric and Space Physics, University of Colorado Boulder, Boulder, CO

Key Points:

- Combining substorm onsets from multiple types of observations can produce a more accurate list of onset times than any single list
- The resulting onset list exhibits expected behavior for substorms in terms of magnetospheric driving and response
- SWMF has a weak, but consistent and statistically significant skill in predicting substorms

Corresponding author: John Haiducek, jhaiduce@umich.edu

Abstract

We have developed a new procedure for combining lists of substorm onset times from multiple sources. We apply this procedure to observational data and to magnetohydrodynamic (MHD) model output from 1-31 January, 2005. We show that this procedure is capable of rejecting false positive identifications and filling data gaps that appear in individual lists. The resulting combined onset lists produce a waiting time distribution that is comparable to previously published results, and superposed epoch analyses of the solar wind driving conditions and magnetospheric response during the resulting onset times are also comparable to previous results. Comparison of the substorm onset list from the MHD model to that obtained from observational data reveals that the MHD model reproduces many of the characteristic features of the observed substorms, in terms of solar wind driving, magnetospheric response, and waiting time distribution. Heidke skill scores show that the MHD model has statistically significant skill in predicting substorm onset times.

1 Introduction

Geomagnetic substorms consist of an explosive release of stored solar wind energy from the magnetotail, much of which is deposited in the ionosphere. Originally they were observed as an auroral phenomenon [e.g. Akasofu, 1964], consisting of sudden brightening of auroral emissions accompanied by rapid changes in their spatial distribution. It is now recognized that a rapid reconfiguration of the night-side magnetic field, consisting of a plasmoid release and dipolarization, is a fundamental component of the substorm process. The plasmoid release coincides with the formation of field-aligned currents, termed the substorm current wedge, connecting the auroral zone to the magnetotail [e.g. Kepko ., 2015]. When the concept of the current wedge was first introduced, it was imagined as a pair of equal and opposite currents entering and exiting the ionosphere at the same latitude but different longitudes. More recent work has shown evidence that the upward and downward currents may overlap in longitude [Clauer Kamide, 1985], and that the real structure may involve multiple filaments of upward and downward current [Forsyth ., 2014], possibly organized into localized regions of flow-driven current termed “wedgelets” [Liu ., 2013]. However, some doubt has been cast on the wedgelet model [Forsyth ., 2014], and the manner in which wedgelets might contribute to filamentation remains an open question [Kepko ., 2015]. Similarly, the behavior of the earthward flow

49 upon arrival at the inner magnetosphere has not been clearly determined from observa-
50 tions [Sergeev ., 2012].

51 Other open questions remain regarding the conditions that lead to substorm onset,
52 and the timing of events leading to and following from substorm onset. For instance, the
53 question of how substorm onset is influenced by solar wind conditions has not been fully
54 resolved, with some holding that some or all substorms are “triggered” by changes in solar
55 wind conditions [e.g. Caan ., 1977; Lyons ., 1997; Russell, 2000; Hsu McPherron, 2003,
56 2004], and others claiming that the observed characteristics of substorms can be explained
57 without invoking solar wind triggering [e.g. SK. Morley Freeman, 2007; Wild ., 2009;
58 Freeman Morley, 2009; Newell Liou, 2011; Johnson Wing, 2014]. Similarly, the ques-
59 tion of where a substorm originates in geospace (magnetotail, ionosphere, or somewhere
60 else) has remained open for a number of years [e.g. Korth ., 1991; Angelopoulos ., 2008;
61 Rae ., 2009; Henderson, 2009].

62 A major factor limiting progress on these questions is a lack of sufficient observa-
63 tional data, due to the need for simultaneous observations in particular locations, or simply
64 the need for more complete spatial coverage of the magnetosphere. However, addressing
65 this problem directly requires launching additional satellites with the required instrumen-
66 tation, and this is a long and costly process. Global magnetohydrodynamic (MHD) mod-
67 els have the potential to address the problem of limited observational coverage by provid-
68 ing predictions of currents, velocities, and magnetic fields throughout the magnetosphere.
69 These predictions can provide insights into magnetospheric dynamics that would require
70 an impractically large number of spacecraft to obtain using observations alone. The ability
71 of MHD simulations to shed light on substorm dynamics has been demonstrated already
72 by a number of studies [e.g. Si. Ohtani Raeder, 2004; Birn Hesse, 2013; El-Alaoui .,
73 2009]. The capability of MHD models to provide a global, spatially resolved picture of
74 the magnetosphere has been used in previous studies to shed light on cause and effect
75 relationships relating to the evolution of a substorm [e.g. Zhu ., 2004; Raeder ., 2010].
76 However, such results have been limited to single event studies or idealized test cases,
77 which leaves open questions about the degree to which MHD models can reproduce sub-
78 storm dynamics consistently and reliably. Despite years of application of MHD models
79 to substorms, no MHD model has been rigorously validated with regard to its ability to
80 predict substorm onsets.

81 Validating any model (MHD or otherwise) for substorm prediction is complicated
82 by the fact that substantial disagreement remains within the community about what consti-
83 tutes a substorm. While a general consensus exists around several of the main features of
84 substorms, the community has not developed a set of criteria for identifying substorm on-
85 sets that is unambiguous, comprehensive, and widely agreed upon. This remains the case
86 despite decades of attempts to clarify the salient characteristics of substorms [e.g. Aka-
87 sofu, 1964, 1968; Akasofu Meng, 1969; RL. McPherron, 1970; RL. McPherron ., 1973;
88 Pytte, Mcpherron Kokubun, 1976; Pytte, McPherron ., 1976; Caan ., 1978; Rostoker .,
89 1980; Hones, 1984; Lui, 1991; Baker ., 1996; Rostoker, 2002; Sergeev ., 2012; Kepko .,
90 2015]. As a result, different researchers studying the same time period often come to sub-
91 stantially different conclusions about what events should be considered substorms.

92 A major factor contributing to the sometimes discordant results obtained is the fact
93 that substorms produce numerous observational signatures, most of which have substan-
94 tial limitations. Although a substorm is generally regarded as a global phenomenon, many
95 of its effects are localized in a particular region. As a result, gaps in observational data
96 can easily prevent detection of a substorm. For instance, the sparse distribution of ground-
97 based magnetometers can result in negative bay onsets not being detected [Newell Gjer-
98 loev, 2011]. In situ observations are subject to similar limitations: Dipolarizations and
99 plasmoids can only be detected when a satellite is on the night side of the Earth and in
100 the right range of distance, MLT sector, and latitude. Moreover, a plasmoid that propa-
101 gates too slowly relative to the observing spacecraft might go unnoticed [Nishida ., 1986].
102 At the same time, many observational features used to identify substorms can be created
103 by other processes, resulting in false positives. For instance, single-satellite observations
104 may not be able to distinguish a plasmoid from other transient features in the current sheet
105 (such as thickening, thinning, or bending) [Eastwood ., 2005]. A storm sudden commence-
106 ment can result in a negative bay at auroral magnetometers [Heppner, 1955; Sugiura .,
107 1968], as can a pseudobreakup [Koskinen ., 1993; S. Ohtani ., 1993; Aikio ., 1999; Kullen
108 ., 2009]. A discussion of the challenges faced by researchers in distinguishing different
109 magnetospheric phenomena from each other can be found in RL. McPherron [2015].

110 Differences in results obtained when different observational datasets are used can be
111 substantial. An illustrative example is Boakes . [2009], which compared substorm onsets
112 previously published by Frey . [2004] based on analysis of auroral images with energetic
113 particle observations at geosynchronous orbit. Boakes . [2009] found that 26% of the au-

114 roral expansion onsets had no corresponding energetic particle injection even though a
115 satellite was in position to detect such an injection, and suggested that such events might
116 not be substorms.

117 The difficulty in positively identifying substorm onsets presents a problem for val-
118 idation of substorm models. In the absence of a definitive substorm onset list against
119 which to validate a model, those seeking to validate a substorm prediction model are left
120 to choose among the published lists, or create a new one. Given the substantial differences
121 between the existing onset lists, validation against any single onset list leaves open the
122 question of whether the validation procedure is testing the model's ability to predict sub-
123 storms, or merely the model's ability to reproduce a particular onset list, whose contents
124 may or may not really be substorms.

125 One potential way to address the problems of onset list accuracy is to use multi-
126 ple substorm signatures in combination, checking them against each other to remove false
127 positives and avoid missed identifications. The resulting consensus list may prove more
128 reliable than any of its constituent lists, providing a more comprehensive and trustwor-
129 thy set of onsets. Comparing two or three substorm signatures by hand for individual
130 events has been commonplace since the beginning of substorm research [e.g. Akasofu,
131 1960; Cummings Coleman, 1968; Lezniak ., 1968], and a number of researchers have
132 produced statistics comparing onset lists for two or more substorm signatures [e.g. Mold-
133 win Hughes, 1993; Boakes ., 2009; Liou, 2010; Chu ., 2015; Forsyth ., 2015; Kauristie .,
134 2017]. RL. McPherron Chu [2017] demonstrated that a better onset list could be obtained
135 using the midlatitude positive bay (MPB) index and the SML index together than by using
136 either dataset alone.

137 Despite an awareness within the community that multiple observational signatures
138 are required to positively identify a substorm, RL. McPherron Chu [2017] has been the
139 only work to date that uses multiple signatures to create a combined onset list, and no at-
140 tempt to create an onset list using more than two different signatures has been published.
141 This may in part be due to the complexities involved in doing so. As was discussed ear-
142 lier, the absence of a particular signature does not always indicate the absence of a sub-
143 storm, while at the same time some identified signatures may not in fact be substorms.
144 Ideally a combined list should somehow allow for these possibilities and correct for them.

Further complicating matters is the fact that different signatures may be identified at different times for the same substorm [e.g. Rae ., 2009; Liou ., 1999, 2000; Kepko, 2004].

In the present work we present a new procedure which uses multiple substorm signatures to identify substorm onsets. By using multiple datasets consisting of different classes of observations, we reduce the risk of missing substorms due to gaps in individual datasets. At the same time, the new procedure aims to reduce false identifications by only accepting substorm onsets that can be identified by multiple methods. Our procedure is generalizable to any combination of substorm onset signatures, and allows for the possibility that the signatures may not be precisely simultaneous. We demonstrate the technique on observational data from January, 2005. We present evidence that the procedure is successful at reducing false identifications while avoiding missed identifications due to observational data gaps, and that the resulting onset list is consistent with the known characteristics of substorms. Finally, we demonstrate the technique on output from an MHD simulation of the same January, 2005 time period, and show preliminary evidence of predictive skill on the part of the MHD model.

2 Methodology

2.1 Identification of substorm events from combined signatures

Our procedure for combining multiple substorm onset lists consists of first convolving each onset list with a Gaussian kernel. The result of this convolution is re-scaled using an error function (erf) in order to keep the values bounded by 1. The re-scaled convolutions of the onset lists are then summed together to produce a nominal “substorm score.” For a series of onset times τ_{ij} from a set of onset lists i , this score is given by

$$f(t) = \sum_{i=1}^{n_{sig}} \operatorname{erf} \left(\sum_{j=1}^{n_{onset}} \exp \left(-\frac{(t - \tau_{ij})^2}{2\sigma^2} \right) \right), \quad (1)$$

where σ is a tunable kernel width. The i 's each represent a particular substorm onset list. The onset lists each represent a distinct substorm signature and are described in detail in Sections 2.4 and 2.5. The j 's represent the onset times in each onset list. To obtain a list of onset times, we search for local maxima in the score $f(t)$, and keep any maxima that rise above a specified threshold T . If we choose a threshold greater than one, we effectively require that substorm signatures from different lists occur within σ of each

189 **Figure 1.** An illustration of the procedure used to combine multiple substorm onset lists into a single one.
 190 Panels (a-e) show scores obtained by convolving individual onset lists with a Gaussian kernel (using $\sigma = 13.8$
 191 minutes), while (d) shows the combined score obtained by adding together the scores in panels (a-e). The
 192 threshold $T = 1.6$ is marked with a red horizontal line, and vertical dashed lines are drawn through local
 193 maxima of the combined score that exceed this threshold.

173 other in order to identify a substorm. The implications of the choice of threshold T and
 174 kernel width σ will be discussed in more detail later in the paper. We apply this proce-
 175 dure to the onset lists produced from the simulation, and separately apply the procedure to
 176 the observational data.

177 The process is illustrated in Figure 1 for the 24-hour time period of 31 January,
 178 2005. Figure 1 was created using a kernel width $\sigma = 13.8$ minutes and a threshold $T =$
 179 1.6. These values were selected using an optimization process that will be described later.
 180 The specifics of how the signatures were identified will be discussed in Section 2.4, but to
 181 illustrate the convolution procedures it suffices to say that a list of candidate onset times
 182 was identified separately for each signature. Figures 1a-1e show the scores obtained from
 183 the onset list obtained from each signature. Figure 1f shows the sum of the scores in Fig-
 184 ures 1a-1e. The threshold value T is drawn in red, and vertical dashed lines mark the on-
 185 set times identified from local maxima of the combined score that exceed the threshold.
 186 In order to exceed the threshold, signatures from two different lists must occur within a
 187 few minutes of each other, and this occurred seven times during the time period shown in
 188 Figure 1.

194 It is worth noting that the individual onset lists in Figure 1 are substantially differ-
 195 ent from each other, each identifying substorms at different times from the others, and
 196 two including candidate onset times that are not near those in any other list. Our proce-
 197 dure rejects those onsets, such as the dipolarization around 1300 UT and the AL onset
 198 around 1400 UT, which appear only in one list. Near-simultaneous onsets are counted if
 199 two or more occur within approximately σ of each other so that the score rises above the
 200 threshold T . Reducing the threshold would increase the total number of substorm identifi-
 201 cations, while increasing it would lower the number of substorm identifications. The im-
 202 plications of changing the threshold will be explored further in Section 3.2. Note also that
 203 if the score remains above the threshold for a period of time and multiple local maxima

204 are found within that period, all of them are counted as substorm onsets. For example, the
 205 local maxima around 1130 UT and a second one just before 1200 UT are both counted as
 206 substorm onsets.

207 The convolution process effectively acts as a low-pass filter, with the choice of σ
 208 determining the minimum time between successive onsets. As discussed in the introduc-
 209 tion, different substorm signatures may not be detected simultaneously even if they are
 210 related to the same substorm. For instance, Liou . [1999] and Liou . [2000] found geosyn-
 211 chronous energetic particle injections tended to lag the onset of auroral breakup by 1-3
 212 minutes, while the high-latitude magnetic bay can be delayed up to tens of minutes rel-
 213 ative to the onset of auroral breakup. Some of the findings of Liou . [2000] were chal-
 214 lenged by Kepko McPherron [2001] and Kepko [2004], but even Kepko [2004] found that
 215 Earthward plasma flows could precede auroral onset by 1-3 minutes. These results and
 216 others suggest that a kernel width of $\sigma \approx 3$ minutes represents a lower bound for appro-
 217 priate values of σ , unless the analysis is restricted to a set of observational signatures that
 218 have been shown to occur nearly simultaneously. An upper end of the appropriate range
 219 for σ can be identified by noting that previous research has shown that successive sub-
 220 storms rarely occur within 30 minutes of each other [e.g. Borovsky ., 1993; Frey, 2010].
 221 This suggests that σ should be chosen to be under 30 minutes, but leaves substantial room
 222 for tuning. The effects that the choice of σ has on the statistics of the identified substorms
 223 will be explored in a later section of the paper.

224 **2.2 Event description**

225 To test our technique we selected the month of January, 2005. SK. Morley [2007]
 226 and S. Morley . [2009] had previously identified substorms from this time period, and
 227 from the data analyzed in those papers this time period was determined to have a suffi-
 228 cient number of substorms to enable statistical analysis. The substorm database provided
 229 by the SuperMag collaboration (<http://supermag.jhuapl.edu/substorms/>) [Gjerloev, 2012],
 230 which contains onsets identified from the SML index [Newell Gjerloev, 20112] using
 231 the Newell Gjerloev [20111] algorithm, lists 322 substorms during this period, placing
 232 it in the top 3% of 31-day periods included in that dataset. The substorm onset lists from
 233 Borovsky Yakymenko [2017] include 124 AL onsets and 109 energetic particle injections
 234 during January, 2005, placing that month in the top 3% in terms of AL onsets and in the
 235 top 7% in terms of energetic particle injections, compared with other 31-day periods from

236 the same onset lists. Frey . [2004] (whose list has subsequently been updated to include
237 2003-2005 and published online at <http://sprg.ssl.berkeley.edu/image/>) lists 97 substorms
238 in January 2005, placing the month in the top 13% of 31-day periods in that dataset. Chu
239 . [2015] found 167 onsets during this month, placing it in the top 9% of 31-day intervals
240 analyzed in that paper. In addition, two of the “supersubstorms” ($AL < -2500$ nT) identi-
241 fied by Hajra . [2016] occurred during this time period.

242 Three geomagnetic storms occurred during this month: One on January 7 with a
243 minimum Sym-H of -112 nT, one on January 16 with a minimum Sym-H of -107 nT, and
244 one on January 21 with a minimum Sym-H of -101 nT. A table of the minima, maxima,
245 and quartiles of various observed quantities over the course of the month can be found in
246 Haiducek . [2017]. Of particular note is the consistently high solar wind speed (median
247 solar wind speed was 570 km/s), which may have contributed to the relatively high fre-
248 quency of substorms during this period.

249 **2.3 Model description**

250 The simulations presented in this work were performed using the Block-Adaptive
251 Tree Solar-Wind, Roe-Type Upwind Scheme (BATS-R-US) MHD solver [Powell ., 1999;
252 De Zeeuw ., 2000]. This was coupled to the Ridley Ionosphere Model [RIM, Ridley .,
253 2003; Ridley ., 2004] and the Rice Convection Model [RCM, Wolf ., 1982; Sazykin,
254 2000; Toffoletto ., 2003]. The Space Weather Modeling Framework [SWMF, Tóth .,
255 2005, 2012] provided the interface between the different models. The inputs to the model
256 are solar wind parameters (velocity, magnetic field, temperature, and pressure) and F10.7
257 radio flux. The model settings and grid configuration for the simulation are described in
258 detail in Haiducek . [2017], which includes results from the same simulation. (In Haiducek
259 . [2017] the simulation was referred to as “Hi-res w/ RCM” to distinguish it from the
260 other two simulations included in that paper.) The results of Haiducek . [2017] showed
261 that the simulation produced good predictions of the Sym-H, AL, and Kp indices on aver-
262 age. On the other hand, the model was found to under-predict the frequency of occurrence
263 for strongly negative AL values, suggesting a tendency to under-predict the strength or oc-
264 currence rate of substorms.

2.4 Identification of model signatures

The substorm process results in numerous observational signatures that can be leveraged for identification. These include plasmoid releases, magnetic perturbations observable in the auroral zone and at mid latitudes, dipolarization of night-side magnetic fields observable from geosynchronous orbit, Earthward injection of energetic particles, and auroral brightenings. Several of these can be synthesized using MHD as well. Unfortunately, as was discussed in the introduction, all of these signatures can be produced by other processes besides substorms, and this is true for both the observations and the model output. For instance, magnetospheric convection, pseudobreakups and poleward boundary intensifications can cause a negative bay response in the northward magnetic field component at auroral-zone magnetometers, which could be interpreted as substorm onsets [Pytte ., 1978; Koskinen ., 1993; S. Ohtani ., 1993; Aikio ., 1999; Kim ., 2005]. On the other hand, substorms could occur but not be identified because of the limited spatial coverage of observational data, as was shown by Newell Gjerloev [2011] for auroral-zone magnetic field. Substorms could also be missed simply because they produce a response below the threshold selected for analysis [e.g. Forsyth ., 2015]. Even for analysis of model output, many of these factors remain relevant, and we aim to mitigate this by using multiple signatures to identify our substorms. Specifically, we identify dipolarization signatures at 6-7 R_E distances [Nagai, 1987; Korth ., 1991], negative bays in the AL index [Kamide ., 1974; Newell Gjerloev, 2011; Borovsky Yakymenko, 2017], positive bays in the midlatitude positive bay (MPB) index [Chu ., 2015], and plasmoid releases [Hones ., 1984; Ieda ., 2001].

Figure 2 shows examples of substorm signatures from a substorm event on January 2, 2005. This substorm was selected for illustrative purposes because it can be identified by all four of the signatures used in the model output. A handful of previous researchers have identified substorm onsets during the time period shown in the plot (2000-2200 UT). Borovsky Yakymenko [2017] found an AL onset at 2026 UT on this day, and a geosynchronous particle injection at 2130 UT. Chu . [2015] identified an MPB onset at 2112 UT. The SuperMag substorm database (populated using the Newell Gjerloev [2011] algorithm) contains onsets at 2016, 2038, and 2059 UT. Figures 2a-2c show time-series plots of B_z at $x = -7 R_E$ (GSM), the AL index, and the MPB index. Apparent onset times identified from each curve are marked by triangles. Figures 2d-2f show the MHD solution within the x - z (GSM) plane at 5-minute intervals during a plasmoid release. The back-

298 grounds of Figures 2d-2f are colored according to the plasma pressure. Closed magnetic
 299 field lines are plotted in white, and open field lines in black. The Earth is shown as a pair
 300 of black and white semicircles, and surrounded by a grey circle denoting the inner bound-
 301 ary of the MHD domain. The approximate location of the reconnection region is denoted
 302 by a red triangle, and a blue dot marks where $x = -7 R_E$ along the noon-midnight line (this
 303 is the location from which the data in Figure 2a was obtained).

304 **Figure 2.** Model signatures for an example substorm. (a) B_z variations at $x = -7 R_E$ along the GSM x
 305 axis. (b) AL index. (c) MPB index. Apparent substorm onset times are marked with triangles in (a-c). (d-f)
 306 $x - z$ (GSM) cut planes, at 5-minute intervals, colored by pressure. Closed magnetic field lines are drawn in
 307 white, and open field lines in black. Earth is drawn as a pair of black and white semicircles, surrounded by a
 308 grey circle denoting the inner boundary of the MHD domain. The location $x = -7 R_E$, from which the data in
 309 (a) was obtained, is marked a blue circle. The apparent X-line location is marked with a red triangle.

310 **2.4.1 Plasmoid release**

311 A fundamental characteristic of a substorm is the tailward release of a plasmoid[e.g.
 312 Hones ., 1984], and this is the first substorm signature we will describe. In observations,
 313 plasmoids are identified by a bipolar variation of B_z as observed by a spacecraft near the
 314 central plasma sheet [e.g. Slavin ., 1989, 1992; Ieda ., 2001; Eastwood ., 2005]. MHD
 315 models provide data throughout the magnetosphere rather than being limited to a few
 316 point observations, and this enables several additional techniques for identifying plas-
 317 moids. One approach is to plot variables such as temperature, velocity, and magnetic
 318 field over time for different x coordinates along a line through the central plasma sheet
 319 at midnight. This produces a 2-D map showing the time evolution of the MHD solution
 320 in the plasma sheet, in much the same way that keograms are used to visualize the time
 321 evolution of auroral emissions [Raeder ., 2010]. Plasmoids appear in such maps as tail-
 322 ward propagating magnetic field perturbations, with corresponding tailward flow velocity.
 323 Another approach for identifying plasmoids was proposed by Honkonen . [2011], who
 324 used the magnetic field topology derived from an MHD simulation to identify a plasmoid,
 325 which they define as a set of closed field lines that enclose a region of reconnecting open
 326 field lines. Probably the most common method is to plot magnetic field lines in the $x-z$

327 plane, looking for evidence of a flux rope in the form of wrapped up or self-closed field
 328 lines, as in e.g. Slinker . [1995].

329 The method of visually identifying plasmoids by searching for regions of wrapped-
 330 up field lines is the one used in the present work. We require that such features be located
 331 in or near the central plasma sheet, and that they exhibit tailward motion. For each such
 332 plasmoid, we record the time of the first indication of tailward motion, and the x and z
 333 coordinates of the apparent X-line at that time. Plasmoids for which the X-line is beyond
 334 $35 R_E$ down-tail are ignored. Figures 2d-2f show examples of the images that are used for
 335 this analysis. For the event in Figure 2, the first apparent tailward motion occurred at 2059
 336 UT, and this time is shown in Figure 2d. The X-line occurs at around $x=-32 R_E$, and the
 337 plasmoid extends from there to $-60 R_E$. Figures 2e and 2f show the same plasmoid 5 and
 338 10 minutes after release. Tailward motion is clearly apparent, with the center of the plas-
 339 moid moving from $x \approx -55$ to $x \approx -80 R_E$ in 10 minutes.

340 **2.4.2 Dipolarization**

341 While the plasmoid propagates tailward, the magnetic fields Earthward of the X-line
 342 undergo a dipolarization. Previous studies have identified dipolarizations by searching for
 343 sharp increases in B_z [e.g. Lee Lyons, 2004; Runov ., 2009; Birn ., 2011; Runov ., 2012;
 344 Liu ., 2013; Frühauff Glassmeier, 2017] or elevation angle

$$\theta = \tan^{-1} \left(\frac{B_z}{\sqrt{B_x^2 + B_y^2}} \right) \quad (2)$$

345 [e.g. RL. McPherron, 1970; Coroniti Kennel, 1972; Noah Burke, 2013] within the night-
 346 side magnetotail. A number of studies have also used a decrease in

$$|B_r| = \left| \frac{x B_x + y B_y}{\sqrt{x^2 + y^2}} \right|, \quad (3)$$

347 coincident with the increase in B_z or θ , as criteria for identifying a dipolarization onset
 348 [e.g. Nagai, 1987; Korth ., 1991; Schmid ., 2011; Liou ., 2002]. Automated procedures
 349 for identifying dipolarizations have been developed by Fu . [2012] and Liu . [2013]. We
 350 found the Fu . [2012] algorithm unsuitable for our purposes because it uses flow veloc-
 351 ity as part of its criteria, for which we had no observational data from the GOES satel-

352 lites used in the analysis. The Liu . [2013] algorithm was designed for THEMIS and uses
 353 B_z alone for event selection. Since our data was from 6-7 R_E from the Earth (where the
 354 fields differ substantially from those seen by THEMIS), we developed a new algorithm
 355 which uses variations in B_z , $|B_r|$, and θ to identify dipolarizations from the model output.
 356 The new procedure is described in detail in Appendix A: . The algorithm was used to
 357 identify dipolarization signatures along the orbits of GOES 10 and 12, and at a fixed point
 358 located at $x = -7 R_E$ in GSM coordinates on the sun-Earth line; this point is identified by
 359 a blue circle in Figures 2d-2f. A plot of B_z at $x = -7 R_E$ is shown in Figure 2a, and two
 360 dipolarization onsets identified using our procedure are marked on the plot with triangles.
 361 The first of these is closely aligned with the plasmoid release time.

362 **2.4.3 Auroral-zone negative bay**

363 The dipolarization process can be interpreted as a partial redirection of cross-tail
 364 current into the ionosphere [e.g. Bonnevier ., 1970; RL. McPherron ., 1973; Kamide .,
 365 1974; Lui, 1978; Kaufmann, 1987]. The ionospheric closure of this current results in a
 366 negative bay in the northward component of the magnetic field on the ground in the au-
 367 roral zone [Davis Sugiura, 1966]. As a result, substorm onsets can be identified by sharp
 368 negative diversions of the AL index. A number of algorithms have previously been devel-
 369 oped for identifying substorm onsets from the AL index, including the Newell Gjerloev
 370 [2011] (SuperMag) algorithm and the Substorm Onsets and Phases from Indices of the
 371 Electrojet (SOPHIE) algorithm [Forsyth ., 2015].

372 In the present paper we identify AL onsets using the algorithm presented in Borovsky
 373 Yakymenko [2017]. This algorithm was chosen for its simplicity and because it produces
 374 a distribution of inter-substorm timings that is consistent with that obtained from other
 375 signatures, as Borovsky Yakymenko [2017] demonstrated through comparison with tim-
 376 ings of energetic particle injections. We apply the Borovsky Yakymenko [2017] algorithm
 377 to a synthetic AL index computed from the model output using virtual magnetometers as
 378 described in Haiducek . [2017]. An example AL onset is shown in Figure 2b. A nega-
 379 tive bay onset, marked by a triangle, occurs just before 2100 UT, just after the plasmoid
 380 release at 2054 UT.

2.4.4 Midlatitude positive bay

The integrated effect of the currents closing between the tail and auroral zone results in a northward diversion of the ground magnetic field in the mid latitudes, called a midlatitude positive bay [MPB, RL. McPherron ., 1973]. Often MPB's are identified manually through examination of individual magnetometers [e.g. R. McPherron, 1972; RL. McPherron ., 1973; Caan ., 1978; Nagai ., 1998; Forsyth ., 2015]. However, the ASYM-H index may also be used [Iyemori Rao, 1996; Nosé ., 2009]. More recently, Chu . [2015] and RL. McPherron Chu [2017] have developed procedures to compute what they call the MPB index, which is specifically designed to respond to a midlatitude positive bay, along with procedures for identifying substorm onsets using the MPB index. In the present paper we use the MPB index implementation described in Chu . [2015] and its accompanying onset identification procedure. To evaluate the MPB index from the model output, we use a ring of 72 virtual magnetometers placed at a constant latitude of 48.86° and evenly spaced in MLT. We compute estimated magnetic fields for the locations of these magnetometers by performing a Biot-Savart integral over the entire MHD domain, and to this add the contributions of the Hall and Pedersen currents computed using RIM; this procedure is described in Yu Ridley [2008]; Yu . [2010]. Using the estimated magnetic fields at these virtual magnetometer locations, we compute the MPB index and associated substorm onsets using the procedures described in Chu . [2015]. An example of the MPB response is shown in Figure 2c. The MPB onset time occurs roughly 10 minutes after the plasmoid release time, but is well aligned with the second of the two dipolarizations in Figure 2a.

2.5 Identification of substorm events from observational data

When possible, we use the same procedures to identify substorm signatures in the observational data as we do with the model output. This includes the dipolarizations, AL index, and MPB index. In some cases modifications are required due to limitations in the availability of observational data; for instance ground-based magnetometers are normally restricted to being placed on land with suitable terrain, and the locations of satellite observations are constrained by orbital mechanics. On the other hand, some observations rely on physical phenomena that cannot be modeled by the MHD code, such as energetic particle injections and auroral brightenings. In an effort to obtain the best possible identifications of observed substorms, we use as many observational datasets as possible, which

413 for this time period included GOES magnetic field observations, the AL and MPB indices,
414 energetic particle injections at geosynchronous orbit, and auroral brightenings.

415 We identify AL onsets by applying the procedure from Borovsky Yakymenko [2017]
416 to the SuperMag SML index [Newell Gjerloev, 2011]. For simplicity, we will use the
417 term AL throughout the paper to refer to both the observed SML index and the synthetic
418 AL computed from the model output. For the observed MPB index and observed MPB
419 onset times we use the values from the analysis previously published in Chu . [2015]. We
420 identify dipolarizations by applying the procedure described in Appendix A: to measure-
421 ments obtained with the magnetometers onboard GOES 10 and 12 [Singer ., 1996].

422 In addition to the dipolarization, another substorm signature that can be observed at
423 geosynchronous orbit is the Earthward injection of energetic electrons and protons [e.g.
424 Lezniak ., 1968; DeForest McIlwain, 1971]. Previous studies have identified a temporal
425 association between such particle injections and auroral zone magnetic signatures [e.g.
426 Lezniak ., 1968; Kamide McIlwain, 1974; Weygand ., 2008], along with a connection be-
427 tween energetic particle injections and dipolarizations [e.g. Sauvaud Winckler, 1980; Birn
428 ., 1998]. In the present work we use energetic particle injections identified by Borovsky
429 Yakymenko [2017] using the Synchronous Orbit Particle Analyzer (SOPA) instrument
430 [Cayton Belian, 2007] on the LANL-1990-095, LANL-1994-085, and LANL-97A satel-
431 lites. The list of particle injections found in the supplemental data of Borovsky Yaky-
432 menko [2017] is used as-is.

Some of the energetic particles produced by the substorm enter the ionosphere and
cause a brightening and reconfiguration of the aurora. These can be observed from the
ground using all-sky imagers, or from cameras onboard spacecraft. For the month of
January, 2005, observations from the Imager for Magnetopause-to-Aurora Global Explo-
ration (IMAGE) spacecraft are available for this purpose. The IMAGE spacecraft was in
a highly elliptical polar orbit with an apogee of 45,600 km and an orbital period of 14
hours, providing 8-10 hours per orbit of good conditions for imaging the northern auro-
ral oval [Frey ., 2004]. Frey . [2004] examined images from the Far Ultraviolet Imager
(FUV) instrument onboard IMAGE, and produced a list of northern hemisphere substorm
onsets for the years 2000-2002, since updated to include 2003-2005 and available online at
http://sprg.ssl.berkeley.edu/sprite/ago96/image/wic_summary/substorms/. We use the January, 2005 portion of this list as part

3 Results

3.1 Substorm waiting times

The distribution of substorm waiting times (the amount of time that passes between successive substorms) gives an indication of the occurrence frequency for substorms. A number of previous papers have examined waiting times, including Borovsky . [1993] which identified substorm onsets from energetic particle injections and found the modal waiting time to be around 2.75 hours. Chu . [2015] and RL. McPherron Chu [2017] analyzed MPB onsets and reported modal waiting times of 80 and 43 minutes, respectively. Kauristie . [2017] reported modal waiting times of 32 minutes for AL onsets identified by Juusola . [2011] and 23 minutes for SML onsets identified by the Newell Gjerloev [2011] procedure. Hsu McPherron [2012] obtained a modal waiting time of about 1.5 hours for AL onsets, about 2 hours for onsets identified from tail lobe fields, and about 2.5 hours for Pi 2 onsets. Freeman Morley [2004] reproduced the waiting time distribution from Borovsky . [1993] using a solar wind driven substorm model.

To visualize the distributions of waiting times, we use kernel density estimates (KDEs) [Parzen, 1962], which approximate the probability density function of a distribution by convolving samples from the distribution with a Gaussian kernel. The resulting curve can be interpreted in the same way as a normalized histogram. Since the waiting times can take only positive values, while the Gaussian kernels used in the KDE give nonzero probabilities for negative values, we perform the KDE in logarithmic space and transform the result to linear space for plotting as described in Appendix C: . For some of our KDE plots we have estimated confidence intervals using a bootstrapping procedure described in Appendix D: . This provides a means to assess whether the waiting time distribution obtained from the model is significantly different from the observed distribution, in a statistical sense.

To test the sensitivity of the waiting time distributions to the choice of kernel width and threshold, we plotted waiting time distributions for a range of each parameter, as shown in Figure 3. Figure 3 shows the distribution of waiting times for the model and for the observations using three different choices of threshold and four different kernel widths, ranging from $\sigma = 5$ minutes to $\sigma = 20$ minutes. The y-axis of each panel shows the probability densities of waiting time, and the x axis shows the waiting times. Figures 3a, 3b, and 3c show waiting time distributions from the observations, while Figures 3d, 3e, and

471 **Figure 3.** Distributions of substorm waiting times for a range of identification thresholds and kernel widths
 472 used in the identification procedure. a), b), and c): Observed waiting time distributions. d), e), and f): MHD
 473 waiting time distributions. a) and d): Threshold=1.0; b) and e): Threshold=1.5; c) and f): Threshold=2.0.

465 3f show waiting time distributions obtained from the MHD simulation. Figures 3a and 3d
 466 show thresholds of 1.0, Figures 3b and 3e show thresholds of 1.5, and Figures 3c and 3f
 467 show thresholds of 2.0. Within each plot, the kernel width σ used in the substorm iden-
 468 tification procedure is varied from $\sigma = 5$ minutes to $\sigma = 20$ minutes. $\sigma = 5$ minutes is
 469 plotted in red with a dash-dot pattern, $\sigma = 10$ minutes in green with dots, $\sigma = 15$ minutes
 470 in orange with dashes, and $\sigma = 20$ minutes in blue as a solid line.

474 From Figure 3, it is apparent that both the threshold and the kernel width affect
 475 waiting time distributions substantially. The modal waiting time varies from approximately
 476 0.25 to 2.5, while the height of the peak varies from greater than 0.3 to less than 0.1.

477 In order to choose appropriate values of σ and T for the remainder of the analysis,
 478 we aimed to reproduce the mean and mode waiting times from the AL onset list published
 479 by Borovsky Yakymenko [2017]. Only the waiting times during January, 2005 were used.
 480 The Borovsky Yakymenko [2017] AL onset list was chosen because it contained 124 sub-
 481 storm onsets (corresponding to a mean waiting time of 6.0 hours), which was the median
 482 among the currently published onset lists that cover the month of January, 2005. This led
 483 to the choice of $T_{obs}=1.60$, $\sigma_{obs} = 13.8$ min, $T_{model} = 1.72$, and $\sigma_{model} = 20$ min.

484 Figure 4 shows the waiting time distribution obtained from the observational data
 485 (thick blue line) and the model (orange line), along with waiting time distributions from
 486 five previously published substorm onset lists that cover January, 2005. The 95% confi-
 487 dence interval of the observed distribution is denoted with light blue shading. The total
 488 number of substorms in each list, which corresponds to the mean waiting time, is listed
 489 in parentheses in the legend. The Supermag list was something of an outlier compared
 490 with the others, and its mode is not visible with the chosen axis limits. Figure B.1 in the
 491 appendix shows the full Supermag waiting time distribution for January, 2005.

496 Figure 4 shows that the waiting time distribution of the Borovsky Yakymenko [2017]
 497 AL list (the green dashed curve) falls near the middle of the published lists in terms of its
 498 waiting time distribution, not only in terms of the mean waiting time but also in terms of

492 **Figure 4.** Distributions of substorm waiting times from the present paper (thick solid lines), compared with
 493 other published lists that cover the same time period (dashed lines). The shaded region denotes the 95% con-
 494 fidence interval for the observed waiting time distribution in the present work. The total number of substorms
 495 in each list (which corresponds to the mean waiting time) is given in parentheses in the legend.

499 the mode and overall shape of the distribution. The observed onset list developed for the
 500 current paper (blue curve) produces a waiting time distribution that is very close to that
 501 of the Borovsky Yakymenko [2017] AL list. The MHD model produces a waiting time
 502 distribution with a higher peak probability, but it falls entirely within the 95% confidence
 503 interval of the observed distribution.

504 Figure 5 compares the waiting time distributions of the combined lists with those
 505 of the individual onset lists used to create the combined lists. The observed onsets are
 506 shown in light blue, with the 95% confidence interval represented as a shaded region of
 507 lighter blue. The MHD results are shown in dark blue. Figure 5a shows the AL onsets,
 508 Figure 5b shows dipolarization onsets, Figure 5c shows MPB onsets, and Figure 5d shows
 509 all signatures in combination.

510 **Figure 5.** Substorm waiting times for MHD and observations. a) AL onsets only b) Dipolarizations only,
 511 and c) MPB onsets only d) All signatures combined.

512 The distributions of waiting time between AL onsets (Figure 5a) show a modal wait-
 513 ing time of around 1 hour for the simulation and 2 hours for the observations. This is
 514 shorter than the 2.75 hours reported by Borovsky . [1993], and longer than the results
 515 of Juusola . [2011] and Newell Gjerloev [2011], but it is comparable to the approxi-
 516 mately 1 hour reported by Hsu McPherron [2012]. The model distribution for AL waiting
 517 time falls within the confidence intervals of the observed distribution for shorter (<1.5
 518 hours) waiting times, though the model underestimates prevalence of 2-6 hour waiting
 519 times somewhat.

520 Dipolarizations produce a much narrower waiting time distribution (Figure 5b), with
 521 the modes of both the modeled and observed distributions occurring at less than one-half
 522 hour of waiting time. This suggests that the dipolarizations are substantially more frequent

523 than AL onsets. The model reproduces the observed waiting time distribution reasonably
 524 well, straying only slightly outside the confidence bounds of the observed distribution.

525 The observed waiting time distribution for MPB onsets (Figure 5c) has a mode
 526 around 1 hour, in between those of the dipolarizations and AL onsets. The model waiting
 527 time distribution has its mode positioned fairly close to that of the observed distribution,
 528 but the height of the peak is noticeably higher, and well outside the confidence bounds of
 529 the observed distribution. This suggests that the model produces MPB onsets with similar
 530 dynamics to reality in terms of recovery time, but that the onsets occur more often. One
 531 possible reason for this is that the model MPB index was computed using virtual magne-
 532 tometers distributed evenly across all longitudes, while the observed MPB index is neces-
 533 sarily computed using real magnetometers, for which substantial gaps in spatial coverage
 534 may have prevented some substorms from producing an MPB signature.

535 3.2 Forecast metrics

536 In order to evaluate the predictive capabilities of the model, we first apply the pro-
 537 cedure described in Section 2.1 to the onset lists from the model and separately to the ob-
 538 served onset lists, in order to produce a combined onset list for each. We next divide the
 539 month into 30-minute bins, and determine whether a substorm onset from each combined
 540 list was present in each bin. We then classify each bin according to whether a substorm
 541 was identified in the model, observations, neither, or both. The four categories are com-
 542 monly displayed in a two-by-two table called a contingency table, as shown generically in
 543 Table 1: In the upper left corner (a) are true positives, the bins in which a substorm was
 544 found in both the model and the observations. Next are false positives (b), in which sub-
 545 storms were found in the model only. In the bottom row of the table are false negatives
 546 (c), in which substorms were found in the observations only, and true negatives (d), in
 547 which no substorm was found.

		Observations	
		Y	N
Predictions	Y	a	b
	N	c	d

548 **Table 1.** A generic contingency table.

549 To produce a contingency table using our data from January, 2005, we first produced
 550 lists of substorm onsets using the procedure described in Section 2.1, and the parameters
 551 T_{model} , T_{obs} , σ_{model} , and σ_{obs} set to the values given in Section 3.1.

552 Table 2 shows the contingency table produced from the onset lists obtained using
 553 our procedure. We obtained 124 positive bins from the model list, 25 of which were true
 554 positives. We obtained 122 positive bins from the observed list. Since the observed list
 555 contains 124 substorms, this indicates that two of the 30-minute bins contained two sub-
 556 storms from the observed list.

		Observations	
		Y	N
SWMF	Y	25	99
	N	97	1267

557 **Table 2.** Contingency table for SWMF vs. observations

558 From the values in the contingency table we compute several metrics summarizing
 559 the predictive abilities of the model. These include Probability of Detection (POD), Prob-
 560 ability of False Detection (POFD), and the Heidke skill score (HSS), all of which are in
 561 common use in space weather applications [e.g. Lopez ., 2007; Welling Ridley, 2010;
 562 Pulkkinen ., 2013; Ganushkina ., 2015; Glocer ., 2016; Jordanova ., 2017; SK. Morley .,
 563 2018]. The POD, given by

$$\text{POD} = \frac{a}{a + c}, \quad (4)$$

564 [Wilks, 2011] indicates the relative number of times a substorm was forecast when one
 565 occurred in observations. A model that predicts all the observed events will have a POD
 566 of 1. POFD, given by

$$\text{POFD} = \frac{b}{b + d} \quad (5)$$

567 indicates the relative number of times that a substorm was forecast when none occurred.
 568 Smaller values of POFD indicate better performance, and a model with no false predic-
 569 tions will have a POFD of 0.

570 Skill scores are a measure of relative predictive accuracy [e.g. Wilks, 2011]. The
 571 Heidke Skill Score (HSS) is based on the proportion correct (PC), defined as

$$\text{PC} = \frac{a + d}{a + b + c + d}, \quad (6)$$

572 which measures the fraction of correct predictions relative to the total number of predic-
 573 tions. A perfect forecast would have a PC of 1. The HSS adjusts PC relative to a refer-
 574 ence value, PC_{ref} , which is the value of PC that would be obtained by a random forecast
 575 that is statistically independent of the observations, and is given by

$$\text{PC}_{ref} = \frac{(a + b)(a + c) + (b + d)(c + d)}{(a + b + c + d)^2}. \quad (7)$$

576 The HSS is obtained from PC_{ref} as

$$\text{HSS} = \frac{\text{PC} - \text{PC}_{ref}}{1 - \text{PC}_{ref}} = \frac{2(ad - bc)}{(a + c)(c + d) + (a + b)(b + d)}. \quad (8)$$

577 The HSS ranges from -1 to 1, where 1 represents a perfect forecast, 0 is equivalent to a
 578 no-skill random forecast, and -1 represents the worst possible forecast.

579 All of the above metrics are subject to sampling uncertainties, meaning that any par-
 580 ticular value could be obtained simply by chance, and might not be representative of the
 581 model's overall abilities. To address this, we estimate 95% confidence intervals for each
 582 metric. The 95% confidence interval is a range in which we estimate that each metric will
 583 fall for 95% of a given number of random samples of the dataset. Since no analytical for-
 584 mulas are known for computing confidence intervals for the HSS [Stephenson, 2000], we
 585 estimate the confidence interval using bootstrapping [e.g. Conover, 1999]. This approach
 586 was used previously by SK. Morley . [2018], and the procedure is described in detail in
 587 Appendix D: .

588 We now apply the above forecast metrics to our substorm onset lists. Figure 6 shows
 589 receiver operating characteristic (ROC) curves for the MHD model. An ROC curve, by

609 **Figure 6.** ROC curves for the MHD simulation. The threshold score for identifying substorms from the
 610 model output is varied to produce each curve, resulting in changes in the probability of detection (POD) and
 611 probability of false detection (POFD). Each curve is computed using a particular threshold score T_{Obs} for
 612 identifying observed substorms; the thresholds and number of observed substorm identifications are listed
 613 in the legend. The case of the observed threshold equal to 1.6 is highlighted with a bold line, and the case of
 614 model threshold and the observed threshold equal to 1.72 along this line is highlighted with a black circle.

590 definition, shows the probability of detection (POD) of a predictive model as a function
 591 of the probability of false detection (POFD), as the threshold for event identification is
 592 varied [e.g. Ekelund, 2012; Carter ., 2016]. Such curves are commonly used in evaluat-
 593 ing predictive models; a notable recent example from the space weather field is Liemohn
 594 . [2018]. For a perfect forecast, the ROC curve would pass through the upper left corner
 595 of the plot (POD=1 and POFD=0), so the closer the ROC curve comes to the upper left
 596 corner of the plot, the greater the overall accuracy of the forecast. To produce the curves
 597 in Figure 6, the threshold T_{model} used to identify a substorm in the model output is var-
 598 ied along the length of each curve, while the threshold T_{obs} for identifying an observed
 599 substorm is held fixed. Each curve is computed using a different threshold value T_{obs} for
 600 identifying an observed substorm. $T_{obs} = 0.5$ is shown in blue, $T_{obs} = 1.60$ is shown in
 601 orange, $T_{obs} = 2.0$ is shown in green, and $T_{obs} = 2.5$ is shown in red. The total number
 602 of observed substorms obtained with each threshold is shown in parentheses in the legend.
 603 The orange curve, corresponding to an observed threshold of 1.6, is drawn in bold since
 604 that is the threshold that was chosen for use throughout the paper, except for tests like this
 605 one in which the thresholds are varied. A black circle denotes the model threshold of 1.72
 606 along this green curve. A diagonal grey line shows where POD equals POFD, indicating
 607 no skill. For a forecast, POD should exceed POFD, and this is the case along the entire
 608 length of each curve (except for the case POD = POFD = 0, where equality is expected).

615 Note that although a typical ROC curve continues to POD = POFD = 1, ours ends
 616 at POFD \approx 0.2. The reason for this is that the practice of using local maxima in the sub-
 617 storm score places a ceiling on the POD and POFD based on the characteristics of the
 618 underlying substorm onset lists. If the substorm score has no local maxima within a given
 619 30-minute window, no substorm will be identified regardless of what threshold is used.
 620 Also note that the curves corresponding to higher values of T_{obs} produce higher values of

621 POD. While higher POD is desirable, in this case it comes at the cost of an unrealistically
 622 low total number of substorms in the observations (and correspondingly, an unrealistically
 623 high average waiting time). Rather than maximizing POD, we chose instead in the present
 624 work to choose thresholds T_{obs} and T_{model} that produce realistic statistics in terms of sub-
 625 storm waiting time.

626 Figure 7 shows the Heidke skill score (HSS) as a function of the frequency bias (the
 627 ratio of the total number of model substorm bins to the total number of observed sub-
 628 storm bins). Figure 7 was produced by varying the modeled and observed thresholds in
 629 the same manner as was done to produce Figure 6. This provides a means to test the sen-
 630 sitivity of HSS to changes in these thresholds. The x -axis value is obtained by dividing
 631 the total number of substorm bins obtained from model output by the total number of bins
 632 obtained from the observational data. Different observed thresholds are identified by color
 633 and shape in the same manner as Figure 6, with error bars denoting the 95% confidence
 634 interval for each skill score. Also like Figure 6, the case of the observed threshold equal
 635 to 1.6 is drawn with bold lines, and the case of the model threshold equal to 1.72 with the
 636 observed threshold equal to 1.6 is marked with a black circle.

637 For a perfect forecast, the model should produce the same number of substorms as
 638 occur in the observations, in which case the frequency bias on the x -axis of Figure 7 will
 639 equal one. Since we chose the thresholds T_{obs} and T_{model} so that they produce the same
 640 mean waiting time, the black circle corresponding to our chosen thresholds corresponds
 641 with a frequency bias very close to one.

642 For a skill score to represent a true predictive skill, it should be significantly greater
 643 than zero, in a statistical sense. This is indicated by the lower end of the 95% confidence
 644 interval being greater than zero. A forecast satisfying this criterion is estimated to pro-
 645 duce an HSS greater than zero 95% of the time. Figure 7 shows that the skill scores ob-
 646 tained from the MHD model are significantly greater than zero in the majority of cases.
 647 The only exception is a single case where $T_{obs} = 2.5$, which as discussed earlier produced
 648 an unrealistically large mean waiting time in the observed onset list.

658 Figure 8 shows the same analysis as Figure 7, but with the kernel width σ_{model} de-
 659 creased from 20 minutes to 10 minutes. This provides a means to test the sensitivity of
 660 HSS to the kernel width σ . The style and axes are the same as Figure 7, and the case of
 661 the modeled threshold set to 1.6 and observed threshold both set to 1.74 is again iden-

649 **Figure 7.** Heidke skill score as a function of the frequency bias (the ratio of the number of model substorm
 650 bins to the number of observed substorm bins). The threshold scores T_{obs} and T_{model} for identifying sub-
 651 storms have been varied to test the sensitivity of skill scores and frequency biases to these thresholds. Each
 652 color and shape corresponds to a particular threshold score T_{obs} for identifying observed substorms; the
 653 thresholds and number of observed substorm bins are listed in the legend. For a given observed threshold,
 654 different skill scores and frequency biases are obtained by varying the threshold for identifying a model sub-
 655 storm. Error bars represent the 95% confidence interval for each skill score. The case of observed threshold
 656 equal to 1.6 is drawn in bold, and the case of the model threshold equal to 1.72 with the observed threshold
 657 equal to 1.6 is marked with a black circle.

666 **Figure 8.** Heidke skill score as a function of frequency bias, using a kernel width $\sigma_{model} = 10$ minutes in-
 667 stead of the $\sigma_{model} = 20$ minutes width used elsewhere. The format is the same as Figure 7.

662 tified with a black circle. Figure 8 shows that the skill scores are sensitive to the choice
 663 of kernel width. Halving the kernel width reduces many of the skill scores by about half.
 664 However, a majority (all but five) remain significantly greater than zero as determined by
 665 their estimated 95% confidence intervals.

668 Table 3 shows the total number of events, POD, POFD, and HSS for each of the
 669 substorm onset lists obtained from the model output. The first row of the table, labeled
 670 “All,” shows the metrics computed from all signatures, combined into a single onset list
 671 using the methodology in Section 2.1, while the remaining rows show results for indi-
 672 vidual signatures. With the exception of the last column of the table, all quantities are
 673 obtained by testing each signature in the model output with observed signatures of the
 674 same category (for instance, model AL is compared with observed AL). These numbers
 675 are absent for the plasmoids since there was no observational plasmoid data with which
 676 to compare. Two columns are shown for HSS. The first (labeled “HSS, same signature”)
 677 is computed using model and observed substorm onset lists obtained using the signature
 678 identified at the beginning of that row (all signatures combined in the case of the first
 679 row). The second uses the same model onset list as the first, but the observed onset list
 680 is the one obtained using all signatures combined together. This gives an indication of
 681 how well the individual model signature predicts the combined (all signatures) observed
 682 substorm onsets. For the POD, POFD, and HSS, a bar over the number identifies the last
 683 significant digit, as determined by the limits of the 95% confidence interval. For the skill

684 scores, the limits of the confidence intervals are shown in brackets. The lower limits of
 685 the confidence intervals are positive for every case except the plasmoids, indicating that
 686 the skill scores are significantly greater than zero.

	SWMF events	Obs. events	POD	POFD	HSS, same signature	HSS, all signatures
All	124	124	$0.\bar{2}0$	$0.0\bar{7}2$	$0.1\bar{3}1$ [0.061, 0.20]	$0.1\bar{3}1$ [0.062, 0.20]
AL	85	130	$0.\bar{1}8$	$0.0\bar{4}5$	$0.1\bar{6}6$ [0.089, 0.24]	$0.1\bar{2}5$ [0.052, 0.20]
MPB	201	167	$0.\bar{2}7$	$0.1\bar{1}1$	$0.1\bar{4}8$ [0.085, 0.21]	$0.1\bar{2}9$ [0.065, 0.19]
dipolarizations	166	96	$0.\bar{2}6$	$0.0\bar{8}9$	$0.1\bar{2}1$ [0.052, 0.19]	$0.0\bar{8}3$ [0.02, 0.1]
plasmoids	447	–	–	–	–	$0.0\bar{4}2$ [-9×10^{-4} , 0.09]

687 **Table 3.** Forecast metrics for each signature

688 Of all the signatures, the plasmoids releases do the least well at predicting the ob-
 689 served substorms. The AL and MPB signatures produce higher skill scores than the dipo-
 690 larizations, but the confidence intervals for all three overlap so the differences between
 691 them may not be statistically significant.

692 Far more plasmoid releases (447 in total) were identified than any other substorm
 693 signature, with the next most common signature being MPB onsets with only 166 occur-
 694 rences. This strongly implies that the plasmoid release list contained a large number of
 695 false positives. While we have confidence that all the plasmoids were real (in the sense
 696 that they occurred within the simulation), the much smaller number of AL and MPB on-
 697 sets (85 and 201, respectively) suggests that only a few of them were substorm related.
 698 The total number of events in the combined substorm list obtained from the simulation is
 699 only 124. This means that more than two thirds of the plasmoid releases were rejected by
 700 our substorm identification procedure, and indicates that the procedure used to combine
 701 signatures is largely successful at eliminating false positive identifications.

702 3.3 Superposed epoch analysis

703 We now present superposed epoch analyses (SEAs) of parameters related to the so-
 704 lar wind driving during substorms and to the geomagnetic signatures of the substorms.

705 SEA consists of shifting a set of time-series data $y(t)$ to a set of epoch times t_k , producing
 706 a group of time-series $y_k = y(t - t_k)$ from which properties common to the epoch times
 707 can be estimated [e.g. Samson Yeung, 1986]. Common properties of the SEA may be
 708 estimated and visualized in a variety of ways. For instance, SK. Morley . [2010] plotted
 709 shaded regions representing the 95% confidence interval for the median and interquartile
 710 range, and Katus Liemohn [2013] plotted 2-D histograms colored according to the num-
 711 ber of SEA members passing through each cell of the histogram, while Hendry . [2013]
 712 created images colored according to the total electron flux observed by the Medium En-
 713 ergy Proton and Electron Detector among all SEA members, binned by epoch time and
 714 L-shell. Probably the most common approach to visualizing an SEA is to use a measure
 715 of central tendency such as the mean or median to obtain a new time-series $\hat{s}(t)$ that es-
 716 timates the typical behavior of $y(t)$ in the vicinity of the epoch times t_k . In the present
 717 work we will use the median of y_k to accomplish this. The epoch times t_k will come from
 718 one of two lists of substorm onset times (one derived from the MHD simulation and the
 719 other from the observations).

720 Computing an SEA using our substorm onset times serves as a diagnostic to deter-
 721 mine whether the onset times identified by our selection procedure are consistent with pre-
 722 viously reported behavior for substorms, in terms of both the solar wind driving and the
 723 geomagnetic response. With the model substorm onsets, the SEAs also provide a means to
 724 test how closely the model's behavior during substorms follows the observed behavior of
 725 the magnetosphere.

726 Figure 9 shows SEAs of the observational data and the model output, with the epoch
 727 times corresponding to substorm onset times obtained using each of the methods described
 728 in Section 2.5. SEAs obtained using the combined onset list (produced as described in
 729 Section 2.1 with the parameters given in Section 3.1) are shown as a thick blue curve,
 730 along with all the individual signatures: MPB onsets (orange), IMAGE/FUV (green), plas-
 731 moids (red), AL (purple), LANL (brown), and dipolarizations (pink). The left column
 732 (Figures 9a-9d) shows observed results, while the right column (Figures 9e-9h) shows the
 733 MHD results. The variables plotted on the y axes are IMF B_z (Figures 9a and 9e), solar
 734 wind ϵ (Figures 9b and 9f), the AL index (Figures 9c and 9g), and the MPB index (Fig-
 735 ures 9d and 9h). IMF B_z is in GSM coordinates. ϵ provides an estimation of the rate at
 736 which solar wind energy is entering the magnetosphere [Perreault Akasofu, 1978], and is
 737 given by

$$\epsilon = |u_x| \frac{|\mathbf{B}|^2}{\mu_0} \sin\left(\frac{\theta_{clock}}{2}\right)^4, \quad (9)$$

where u_x is the sunward component of solar wind velocity, \mathbf{B} is the IMF, and θ_{clock} is the IMF clock angle.

Figure 9. Superposed epoch analyses of IMF B_z , ϵ , AL, and MPB, comparing onsets identified from the model and from the observations. The left column shows SEAs computed using epoch times from the observations, while the right column shows SEAs computed using epoch times from the simulation. The AL and MPB data come from the respective datasets used to create the onsets (observations or model run), and the other values come from the solar wind data input to the model. The lines show the median value for all epoch times as a function of the time offset. The thick blue line (labeled “All” in the legend) shows the SEA computed with epoch times from the combined onset list using all signatures, while thinner colored lines show SEAs obtained using epoch times from the individual signatures.

From the SEA of IMF B_z (Figures 9a and 9e), it is apparent that the observed substorms are typically preceded by a decrease in IMF B_z , with the minimum B_z occurring just before the onset time and a recovery back to near-zero B_z following the onset. Similar behavior is present in both the model and the observations, but the decrease in B_z is somewhat sharper for the model onsets (with the exception of the plasmoids, which have a particularly weak decrease in B_z). The decrease is evident for all of the onset lists. In addition to the plasmoids, the AL onsets stand out significantly. When using AL onsets for the epoch times (both for observations and model) the minimum B_z occurs slightly later, which may be an indication that the AL onsets precede the other signatures on average. The model AL onsets are preceded by a 1-2 nT increase 1-2 hours prior to onset, and a particularly sharp decrease just prior to onset. The tendency of substorms to occur near a local minimum in IMF B_z has been previously reported, and our results for both observations and MHD are qualitatively similar to those obtained by SEA in previous studies [e.g. Caan ., 1975, 1978; Newell ., 2001; Freeman Morley, 2009; Newell Liou, 2011; Walach Milan, 2015].

Figures 9b and 9f show that all onset lists correspond with an increase in ϵ prior to onset, with a maximum occurring prior to onset, or in the case of AL, just after onset. A separate SEA of the solar wind velocity component u_x (not shown) showed no apprecia-

766 ble trend, which indicates that the trend in ϵ is driven almost entirely by variation in IMF
 767 B_z . However, despite a lack of change in u_x before and after onset, we found that some
 768 classes of onsets seem to be associated with higher or lower u_x ; most notably dipolariza-
 769 tions were associated with higher u_x than any other signature type, and this is responsible
 770 for the higher ϵ values associated with dipolarizations. As with B_z , ϵ undergoes a sharp
 771 transition prior to the model AL onsets, and the plasmoid release times are associated
 772 with only a very weak increase and decrease in ϵ .

773 In the SEA of observed AL (Figure 9c), a sharp decrease occurs at onset. This oc-
 774 curs for the combined onset list and for all of the individual signatures except for the dipo-
 775 larizations. Dipolarizations are associated with a downward trend in AL but the decrease
 776 begins earlier and is more gradual. The behavior of the observed AL index is qualitatively
 777 similar to what was obtained by previous authors. The approximately 2 hour recovery time
 778 is similar to the results of e.g. Caan . [1978]; Forsyth . [2015], but the -500 nT minimum
 779 is lower than their results. Both Caan . [1978] and Forsyth . [2015] analyzed multi-year
 780 time periods, and the lower minimum AL obtained here may simply be due to the fact that
 781 the analysis covers a much shorter time period which was chosen for its relatively large
 782 amount of substorm activity. In the model output (Figure 9g), AL onsets are also associ-
 783 ated with a sharp decrease at onset, but the MPB onsets, dipolarizations, and plasmoids
 784 are associated with gradual decreases in AL. When AL onsets alone are used for the on-
 785 set list, an increase occurs in the hour prior to onset, followed by a decrease similar to
 786 that obtained from the SEA of observed AL onsets. When all the model signatures are
 787 combined, the increase 1 hour prior to onset is absent (although a more gradual, possibly
 788 unrelated increase occurs 1-3 hours prior to onset), and the associated decrease in AL is
 789 weaker than occurs in observations.

790 It is notable that while the combined signature list from the observations produces a
 791 robust decrease at onset in the SEA of AL, the same cannot be said of the combined on-
 792 set list obtained from the model. A possible explanation is that combining signatures does
 793 not preferentially eliminate weak substorms, but rather tends to eliminate those that are
 794 too far from the average for a given input dataset. The fact that the average in the model
 795 involves a weaker onset reflects the fact that the model produces weaker variations in AL
 796 in general, as was noted for the same simulation in Haiducek . [2017]. The weak associa-
 797 tion between dipolarizations and AL onsets in the observations may be due in part to the
 798 fact that only two satellites are used to identify dipolarizations (versus three for the LANL

799 energetic particle injections). The model output uses dipolarizations identified from a third
800 location (which is ideally positioned on the sun-Earth line), and in the model output the
801 dipolarizations do not contrast as strongly from the other datasets in terms of their associ-
802 ated AL response.

803 From Figure 9d, it can be seen that all of the observed signatures are associated
804 with an increase in MPB beginning at onset. Dipolarizations are associated with an addi-
805 tional gradual increase prior to onset, with the rate of increase becoming greater at the on-
806 set time. When all signatures are combined, the associated increase in MPB is noticeably
807 stronger than for any single signature alone. For all curves except the one produced using
808 dipolarizations as the signature, the shape is qualitatively similar to the superposed epoch
809 analysis shown in Chu . [2015] for MPB onsets, which similar to our results showed peaks
810 between 50 and 250 nT and recovery times on the order of 1 hour. With the model output
811 (Figure 9h), all of the signatures are also associated with an increase in MPB. However,
812 the magnitude of this increase varies substantially from one signature to another. Plasmoid
813 releases are associated with the weakest increase in MPB, while AL onsets are associated
814 with the strongest increase. Combining all signatures together does not intensify the as-
815 sociated MPB response as it does for the observations: The combined MPB curve falls in
816 between those of the AL, dipolarization, and MPB onsets.

817 It is worth noting that plasmoid releases are only very weakly associated with changes
818 in driving conditions (IMF and ϵ) or in response indicators (AL and MPB). This is re-
819 lated to the fact that many more plasmoid releases were identified than any other signature
820 (see Table 3), which means that many plasmoid releases may have no associated auroral
821 or geosynchronous response, or the response might be below the threshold for selection.
822 Such plasmoids may be too weak or too far down-tail to have a substantial effect close
823 to the Earth. The state of the fields and plasmas in the inner magnetosphere may also in-
824 fluence how much energy from the plasmoid release is transported Earthward. Similarly,
825 dipolarizations are also only weakly associated with changes in driving conditions and
826 magnetospheric response, though they are more strongly associated than plasmoids are.
827 Like the plasmoids, dipolarizations are observed in the magnetosphere and most likely
828 some of them occur without a strong coupling to the ionosphere that would produce a typ-
829 ical substorm response.

4 Discussion

In the present paper we have demonstrated a procedure to combine multiple substorm onset lists into a single list. We applied this procedure to observational data and to MHD output from the same one-month period. By performing superposed epoch analysis we demonstrated that the resulting onset list is consistent with previous results in terms of the solar wind driving and the geomagnetic response as measured by ground-based magnetometers. We showed that the total number of substorms and the waiting time distributions are also consistent with previous results. Finally, we showed preliminary evidence that our MHD model has statistically significant predictive skill and is able to reproduce the observed waiting time distribution, as well as some of the observed features in terms of driving and response.

4.1 Effectiveness of combining signatures

The approach of combining onset lists obtained using different techniques into a single combined list appears to at least partially address the problems of false identifications and data gaps. More than twice as many plasmoid releases were identified from the model output than were obtained by analyzing any single observational signature, yet the total number of substorms identified in the model output is far smaller than the number of plasmoid releases, indicating that the vast majority of plasmoid releases were rejected for lack of an associated AL, MPB, or dipolarization signature. At the same time, data gaps in the observations account for significant under-counting of dipolarization signatures, but the total number of observed substorms in the combined list is significantly higher than the total number of dipolarizations. This suggests that the combined inputs from other observed signatures were able to compensate for the lack of continuous night-side magnetic field observations in geosynchronous orbit.

We chose tuning parameters so that the resulting onset list has a mean and mode waiting time that is on par with previously published results for the same time period. The resulting waiting time distribution is qualitatively similar to previously published results [by e.g. Borovsky *et al.*, 1993; Chu *et al.*, 2015; Kauristie *et al.*, 2017; Borovsky & Yakymenko, 2017]. The modal waiting time of around 1-1.5 hours is consistent with previously published results covering January, 2005, and the distribution shape is very close to that of the Borovsky & Yakymenko [2017] results for that time period, reproducing not only the

861 mean and mode for which we optimized, but also the shape of the distribution. We also
 862 find that SEAs of our combined onset lists reproduce many of the expected behaviors for
 863 substorms, such as a local maximum in IMF B_z [e.g. Caan ., 1975, 1978; Newell ., 2001;
 864 Freeman Morley, 2009; Newell Liou, 2011; Walach Milan, 2015] and a negative bay in
 865 AL [Kamide ., 1974; Caan ., 1978; Forsyth ., 2015, e.g.] that occur around the substorm
 866 onset time. This indicates that, on average, the magnetosphere exhibited dynamics previ-
 867 ously reported for substorms around the times included in the combined onset lists.

868 **4.2 Paths for improving the substorm identifications**

869 We have demonstrated that the mean and mode waiting time of substorms identified
 870 by our method can be controlled by adjusting its tuning parameters: The detection thresh-
 871 old T and the kernel width σ . While we chose to optimize these parameters to reproduce
 872 the waiting time distribution of a previously published substorm onset list, this may not
 873 be the best approach in all situations. In general it is possible to determine a range of val-
 874 ues for each parameter beyond which reasonable results are no longer expected. For in-
 875 stance, setting the kernel width too low can greatly reduce the number of events selected,
 876 and in extreme cases can result in no events being selected at all. An overly large kernel
 877 width would cause unrelated signatures to be counted together, potentially inflating the
 878 total number of events. However, at some point increasing the kernel width may cause a
 879 decrease in the number of events as independent events are merged together. We have se-
 880 lected a kernel widths σ of 14-20 minutes, but kernel widths as small as 5 minutes and as
 881 large as 25 minutes might be considered reasonable. Similarly, the threshold T can have
 882 a substantial effect on the total number of events selected, as was illustrated in Figures 6
 883 and 7 in which the total number of observed events varies from 47 to 250 as the detection
 884 threshold is varied.

885 The relationship between the threshold T , kernel width σ , and what events are se-
 886 lected depends on the number of signatures used as well as the statistical characteristics
 887 of each signature, such as their waiting time distributions. As a result, the threshold needs
 888 to be adjusted whenever signatures are added or removed. In the present work we opti-
 889 mized T and σ to produce a waiting time distribution that is comparable with previously
 890 published results. However, this approach is only possible for time periods that have ex-
 891 isting published lists to which to compare. An alternative approach might be to construct
 892 a heuristic based on the number of onset lists that are combined. A simple way to do this

893 would be to scale the threshold according to the number of onset lists used. The thresh-
894 old might be adjusted down for time periods in which one or more signatures is known to
895 contain a data gap.

896 It is also worth noting that our procedure weights all signatures equally, convolving
897 each with the same kernel function and adding them together. It would certainly be pos-
898 sible to instead apply weight factors during summation, for instance if one signature was
899 considered more reliable than another. Lacking an objective means to determine appropri-
900 ate weight factors, we have decided not to apply variable weights to the individual signa-
901 tures in the present work. However, in the future it might be appropriate to introduce such
902 weight factors. One way to do this is to compute weighting factors based on the average
903 waiting time in each onset list. This would weight signatures such as plasmoids that occur
904 very frequently (and probably are not always associated with substorms) less heavily than
905 those that occur infrequently. Another approach might be to develop a reliability measure
906 of some sort, which could be applied to each signature and used to compute its weight
907 factor. For some signatures, it might be appropriate to weight individual onsets according
908 to a measure of event strength associated with that signature. For instance, the amount of
909 change in AL within a specified time after onset could be used as a measure of AL onset
910 strength, and AL onsets with large changes could be weighted more strongly than those
911 with small changes.

912 The use of a Gaussian kernel imposes a temporal symmetry, where onsets are treated
913 as being related or not according to how close they occur in time relative to each other,
914 without regard to which signature precedes the other. However, in reality a particular class
915 of signature may tend to occur before or after onset, and the amount of time relative to
916 onset may not be uniform. Our own data suggest that changes in AL may tend to precede
917 other signatures, for instance. This could be accounted for by using a non-Gaussian ker-
918 nel shape, which could be selected individually for each signature based on its tendency to
919 lead or follow other signatures.

920 The tunability of our procedure, along with the possible modifications described in
921 this section, give it a significant amount of flexibility. This enables it to be optimized to
922 produce desired characteristics in terms of what events are identified. An obvious ap-
923 proach to optimization is to adjust the tuning parameters to best fit established criteria
924 for identifying substorms. However, the lack of a community consensus on precise pro-

925 cedures, benchmarks, or tests for correct substorm identification precludes this approach.
926 This lack of such a consensus has been an issue in the community for a while, and has
927 been noted by a number of authors [e.g. Rostoker ., 1980; RL. McPherron Chu, 2017,
928 2018]. While we can readily compare our list against existing ones, as has been done by
929 a number of researchers [e.g. Moldwin Hughes, 1993; Boakes ., 2009; Liou, 2010; Chu
930 ., 2015; Forsyth ., 2015; Kauristie ., 2017], fundamentally such comparisons tell us about
931 the similarities and differences between the lists and not which list is most correct. In the
932 meantime, optimizing for known characteristics of substorms, rather than a specific list, is
933 probably the best approach.

934 If our identification procedure is used applied for operational purposes, another im-
935 portant consideration in choosing detection thresholds is the needs of forecast customers.
936 In this case, factors such as the costs and risks associated with false positive and false
937 negative detections should be considered. Is the cost of responding to a false positive
938 prediction greater or less than the cost incurred when a substorm arrives unannounced?
939 Of course, this probably depends on the strength of an event, and ideally the procedure
940 should be tuned in a manner that makes stronger events more likely to be identified.

941 **4.3 Substorm prediction with MHD**

942 One of the possible operational applications for our identification procedure is the
943 development of a substorm forecast product. This could be done using an MHD model
944 as we demonstrated in the present work, although the technique of combining multiple
945 types of signatures can certainly be applied to other types of models. The ability to simu-
946 late a substorm with an MHD model has been demonstrated previously [e.g. Lyon ., 1981;
947 Slinker ., 1995; Raeder ., 2001; Wang ., 2010]. However, previous efforts simulating sub-
948 storms with MHD have covered time periods lasting no more than a few days and at most
949 several substorms, preventing a rigorous analysis of the model's predictive skill. In the
950 present paper we used a one-month simulation including over 100 substorms, which is
951 sufficient to enable computation of forecast accuracy metrics such as POD, POFD, and
952 HSS. To our knowledge, this is the first attempt to rigorously evaluate an MHD model for
953 its ability to predict substorms.

954 In our test, the MHD model demonstrated consistently positive predictive skill, with
955 zero or negative skill scores occurring only in extreme cases of high or low detection

956 thresholds. The skill scores achieved are significantly greater than zero, but they are closer
957 to zero (no skill) than they are to one (perfect skill). This certainly leaves room for im-
958 provement, and also begs the question of whether scores on this level are sufficiently high
959 to be of practical use. Looking to evaluations of existing operational models, one can find
960 some examples of tropospheric models that deliver performance on this level, particularly
961 for long lead time forecasts of difficult to predict phenomena such as precipitation [e.g.
962 Barnston ., 1999]. However, such comparisons are of limited utility not only because of
963 the differences in the system being modeled, but also difference in the lead time and the
964 temporal and spatial granularity of the forecast. Ultimately, an assessment of operational
965 usefulness depends on the manner in which the forecast is used by customers, including
966 the operational impact and mitigation strategies available.

967 **4.4 Paths for improved MHD modeling of substorms**

968 An obvious path forward with the MHD model is to explore whether this initial
969 demonstration of predictive skill can be improved upon. The first step would be to con-
970 duct tests of different configurations of the model to determine the sensitivity of results to
971 parameters such as grid resolution and boundary conditions. Another possible path for im-
972 provement is the incorporation of non-ideal MHD and other physical processes that were
973 not incorporated in the simulation shown here. A likely candidate for this is the inclusion
974 of additional resistive terms. It has long been recognized that resistivity plays an impor-
975 tant role in controlling magnetotail dynamics such those associated with substorms. Birn
976 Hones Jr. [1981], for instance, demonstrated that an X-line formation and plasmoid release
977 could be induced in an MHD simulation by abruptly increasing the amount of resistiv-
978 ity. In the present work, as with many efforts involving MHD simulation, we rely entirely
979 on numerical resistivity to enable reconnection to occur. Our results show that numeri-
980 cal resistivity can produce substorms at a realistic rate, as evidenced by the fact that the
981 total number of substorms is in line with other lists from the same time period, and the
982 waiting time distribution produced by the model is close to that produced by the obser-
983 vations. This means that our numerical resistivity is realistic enough that the model can
984 capture important aspects of the system dynamics. However, improved prediction of sub-
985 storms may require a more realistic resistivity model. One approach is to introduce Hall
986 resistivity, which has been shown by observations to play a role in magnetotail reconnec-
987 tion [Øieroset ., 2001]. Hall MHD has been implemented in SWMF [Tóth ., 2008], but

988 has not been tested in the context of substorm prediction. Another approach that may im-
989 prove substorm-related reconnection physics is the use of a particle-in-cell (PIC) model in
990 place of MHD in and near the reconnection region. This has been demonstrated by Tóth .
991 [2016] and Chen . [2017] for magnetospheric simulations, but again has not been tested
992 for substorm prediction. On the other hand, the PIC approach, while promising for its
993 ability to capture aspects of reconnection physics that are not incorporated in ideal MHD,
994 is likely too computationally expensive for operational use in the near term.

995 Besides night-side reconnection, coupling between the magnetosphere and iono-
996 sphere plays an important role in the substorm process. For instance, ionospheric con-
997 ductivity influences the strength and spatial distribution of field-aligned currents within
998 the magnetosphere [e.g. Ridley ., 2004]. However, there is considerable room for im-
999 provement in the models of this conductance, particularly in the auroral zone. SWMF
1000 currently estimates auroral-zone conductance using an empirical relationship based on
1001 the strength of field-aligned currents, since MHD does not directly estimate the precipi-
1002 tating fluxes that determine the conductivity in reality [Ridley ., 2004]. Welling . [2017]
1003 showed that SWMF is frequently used to simulate conditions that fall outside the range
1004 of validity for the existing conductance model. Efforts are currently ongoing to develop
1005 an improved empirical model for this purpose [Mukhopadhyay ., 2018]. However, this
1006 approach has limitations because the conductance depends on other factors besides the
1007 field-aligned current, including particle precipitation, that are not modeled by MHD. An
1008 alternative might be to estimate the conductivity using the particle distributions in an in-
1009 ner magnetosphere model such as RCM, but this would likely require the development of
1010 new empirical relationships between precipitating fluxes and conductivity. Other improve-
1011 ments to the MHD model that could influence magnetosphere-ionosphere coupling include
1012 the use of anisotropic pressure [Meng ., 2012, 2013], polar outflow [Glocer, Tóth, Gom-
1013 bosí Welling, 2009], and multi-fluid MHD [Glocer, Tóth, Ma ., 2009], all of which have
1014 been implemented in BATS-R-US and demonstrated in magnetospheric simulations, but
1015 none of which have been tested for their effect on substorm prediction. The initial tests of
1016 anisotropic pressure and polar outflow in SWMF (Meng . [2012] and Glocer, Tóth, Gom-
1017 bosí Welling [2009], respectively) both showed that simulations using those models have
1018 increased tail stretching compared with BATS-R-US simulations that do not use them, and
1019 increased tail stretching could have a significant influence on substorm dynamics since the

1020 substorm growth stage is associated with magnetotail stretching [e.g. Kaufmann, 1987;
1021 Sergeev ., 1990].

1022 Of the enhancements mentioned above, ionospheric outflow may be particularly im-
1023 portant because it has been shown to be associated with substorms. For instance Øieroset
1024 . [1999] and Wilson . [2004] both found that ionospheric outflow increases by a factor of
1025 two on average from quiet time to substorm onset, and that stronger substorms are asso-
1026 ciated with higher rates of ionospheric outflow. Modeling results have shown that iono-
1027 spheric outflow can influence magnetospheric dynamics in general [e.g. Winglee ., 2002;
1028 Wiltberger ., 2010] and substorm strength and onset times in particular [e.g. Welling .,
1029 2016]. Such results suggest that exploration of ionospheric outflow may be a fruitful path
1030 toward improved substorm prediction.

1031 **5 Conclusions**

1032 The conclusions of the paper can be summarized as follows:

- 1033 1. We have demonstrated a new technique for substorm identification that combines
1034 multiple substorm signatures to reduce false positive identifications as well as re-
1035 duce missed identifications.
- 1036 2. The technique can be tuned to produce a mean and mode waiting time that are
1037 comparable to previously published results.
- 1038 3. The magnetospheric driving and response at the substorm onset times identified
1039 using our technique is consistent with expected behavior during substorms.
- 1040 4. When our substorm identification technique is applied to output from an MHD sim-
1041 ulation, we obtain a distribution of waiting times that is comparable to the observa-
1042 tional data, driving conditions that are similar to those at the observed epoch times,
1043 and a magnetospheric response that is qualitatively similar to (though quantitatively
1044 different from) the observed response.
- 1045 5. The MHD simulation has weak, but statistically significant, skill in predicting sub-
1046 storms.

1047 **A: Procedure for identifying dipolarizations**

1048 Our procedure aims to find points that satisfy the following criteria:

- 1049 • Local minimum of θ
- 1050 • Onset of a rapid increase in B_z and θ
- 1051 • Near a local maximum of $|B_r|$

1052 The procedure consists of first finding local minima in θ by searching for points that
 1053 are less than both of their immediate neighbors (endpoints in the data are not considered).
 1054 Neighboring points around each of these local minima are checked against a set of thresh-
 1055 olds to determine whether they satisfy the criteria given above. Given a minimum in θ ,
 1056 denoted by the subscript i , we specify a set of ranges $m : n$ relative to i , and a threshold
 1057 B_z or $|B_r|$ must satisfy within that range in order for i to be considered a dipolarization
 1058 candidate. The thresholds are defined as follows:

$$\begin{aligned}
 \max(B_{z_{i:i+10}}) &> B_{z_i} + 2 \\
 \max(B_{z_{i:i+30}}) &> B_{z_i} + 10 \\
 \max(B_{z_{i:i+60}}) &> B_{z_i} + 16 \\
 \min(|B_r|_{i-10:i-2}) &< |B_r|_i - 0.25 \\
 \min(|B_r|_{i+2:i+20}) &< |B_r|_i - 0.5 \\
 \min(|B_r|_{i+10:i+40}) &< |B_r|_i - 2
 \end{aligned} \tag{A.1}$$

1059 The thresholds for B_z require an immediate increase in B_z (2 nT in 10 minutes),
 1060 which proceeds to at least 10 nT within 30 minutes and 16 nT within 60 minutes. This is
 1061 not a particularly fast increase; the thresholds are designed to identify all dipolarizations
 1062 and not only the strong ones.

1063 The thresholds for $|B_r|$ require an increase of at least 0.25 nT within the 10 minutes
 1064 preceding the candidate onset, a decrease of 0.5 nT within the following 20 minutes, and
 1065 a decrease of 2 nT within the following 40 minutes. These are fairly weak criteria, and
 1066 are designed to select candidate onsets occurring near a local maximum, without requiring
 1067 the maximum be particularly strong nor that the onset candidate occur exactly at the local
 1068 maximum in $|B_r|$.

1069 An additional procedure aims to prevent counting multiple onset times for a single
 1070 dipolarization event. If an onset j is followed by an onset k within the preceding 60 min-
 1071 utes, then we require

$$\max(B_{zj:k}) > 0.25\max(B_{zk:k+60}); \quad (\text{A.2})$$

1072 that is, the maximum B_z between j and k must exceed 25% of the maximum B_z
 1073 reached following onset k . If this threshold is not satisfied, the onset having the lowest
 1074 value of θ is kept and the other is discarded. Finally, for a candidate dipolarization to be
 1075 included in the final list, the satellite providing the observations must be located on the
 1076 night side; that is, $\text{MLT} < 6$ or $\text{MLT} > 18$.

1077 The chosen thresholds are not particularly stringent individually, but in combina-
 1078 tion produce a set of dipolarizations that resembles what has been previously reported for
 1079 ensembles of dipolarizations. To demonstrate this, we performed a superposed epoch anal-
 1080 ysis (SEA) of the magnetic fields for the two GOES satellites in the observations. This is
 1081 shown in Figure A.1, which shows superposed epoch analyses of $|B_r|$, B_z , and θ for dipol-
 1082 arization onsets identified from the observational data and each of the three model runs.
 1083 In this figure, and throughout the paper, plots comparing the model runs to each other and
 1084 to observations use a common color scheme: Observations are shown in light blue, the
 1085 Hi-res w/ RCM simulation in medium blue, the Hi-res w/o RCM simulation in orange,
 1086 and the SWPC simulation in green. The lines in Figure A.1 represent the median of the
 1087 SEA. The number of dipolarizations identified for each dataset is shown in parentheses in
 1088 the legend. Although the thresholds specified allow for as little as a 16 nT increase in 60
 1089 minutes, the median increase is much faster, closer to 20 nT in 20 minutes. This is similar
 1090 to what has been reported in previous studies such as Liou . [2002]. The peaks in $|B_r|$ are
 1091 less pronounced than what occurs in Liou . [2002]. This could probably be addressed with
 1092 more stringent criteria for $|B_r|$, at the cost of possibly missing some dipolarizations.

1093 **Figure A.1.** Superposed epoch analysis of B_r , B_z , and inclination angle θ for all dipolarization onset times.

1094 **B: Comparison of inter-substorm intervals obtained using the Borovsky and Newell** 1095 **algorithms**

1096 Figure B.1 shows distributions of waiting times for AL onsets identified using the
 1097 Borovsky Yakymenko [2017] algorithm (blue curve), for AL onsets identified using the
 1098 Supermag algorithm [Newell Gjerloev, 2011] (orange curve) and for energetic particle
 1099 injections identified from LANL satellite data by Borovsky Yakymenko [2017] (green

1100 curve). The Supermag algorithm stands out with a modal 1-hour waiting time, while both
 1101 the AL onsets and the LANL particle injections from Borovsky Yakymenko [2017] pro-
 1102 duce a modal 3-hour waiting time. The fact that the Borovsky Yakymenko [2017] algo-
 1103 rithm produces a waiting time distribution that resembles that obtained using particle in-
 1104 jections contributed to the decision to use the Borovsky Yakymenko [2017] algorithm for
 1105 substorm identification in the present work.

1106 **Figure B.1.** Substorm waiting times for onsets obtained using the Borovsky (blue curve) and Supermag
 1107 (orange curve).

1108 **C: Log-space computation of KDE**

1109 In Section 3.1 we visualize distributions of substorm waiting times using kernel den-
 1110 sity estimation (KDE). A KDE estimates a probability density function (PDF) by convolv-
 1111 ing samples of the PDF with a kernel function. For a set of n samples X_i and a kernel
 1112 function $K(x)$, the KDE is given by

$$\hat{f}(x) = \frac{1}{nh} \sum_{i=1}^n K\left(\frac{x - X_i}{h}\right). \quad (\text{C.1})$$

1113 In this paper we take $K(x)$ to be a Gaussian. However, this introduces a difficulty
 1114 because the waiting times can take only positive values (meaning that the underlying PDF
 1115 is nonzero only for positive x), while $K(x)$ takes nonzero values everywhere (including
 1116 negative x). To correct for this, we compute the KDE of $\log X_i$, and evaluate this KDE for
 1117 $\log x$. Since this log-space transform alters the spacing (and in turn the estimated densi-
 1118 ties), we must correct this by multiplying the resulting KDE by $\frac{1}{x}$ (the derivative of $\log x$):

$$\hat{f}'(x) = \frac{1}{x} \hat{f}(\log x). \quad (\text{C.2})$$

1119 **D: Bootstrapping procedure to estimate confidence intervals for forecast metrics** 1120 **and probability densities**

1121 The sampling distribution for the HSS is not known [Stephenson, 2000], and this
 1122 means that no analytical formula is available to estimate the confidence interval. We in-
 1123 stead employ a bootstrapping procedure [e.g. Conover, 1999], which involves randomly

1124 sampling the binary event sequence in order to obtain an estimated distribution for the
 1125 skill score. This is done as follows: Given a sequence of n observed bins o_i and n pre-
 1126 dicted bins p_i , we take a sequence of n random samples, with the same indices taken from
 1127 both sequences. For instance, if $n = 9$, we might have

$$o = [0, 0, 1, 1, 0, 0, 1, 0, 1] \quad (\text{D.1})$$

1128 and

$$p = [0, 1, 0, 1, 0, 0, 0, 1, 1]. \quad (\text{D.2})$$

1129 We then generate a sequence of n random integers representing indices to be sam-
 1130 pled from o and p , for instance we might randomly obtain the indices $[8, 1, 4, 4, 2, 6, 5, 0, 3]$,
 1131 which would result in

$$o' = [1, 1, 1, 1, 1, 0, 0, 1, 0] \quad (\text{D.3})$$

1132 and

$$p' = [1, 0, 0, 1, 0, 1, 0, 1, 1], \quad (\text{D.4})$$

1133 from which we can compute a new HSS. We repeat this process N times (typically
 1134 we use $N = 4000$). The 95% confidence interval for HSS is the 2.5th and 97.5th per-
 1135 centiles of the N skill scores obtained from the N sampled distributions. The same proce-
 1136 dure is applied to estimate confidence intervals for POD and POFD.

1137 To obtain a confidence interval for a kernel density estimate, a similar procedure
 1138 is applied: Given a sequence of n values x_i for which a KDE is to be computed, n we
 1139 generate a sequence of n random integers to be used as indices for x_i to produce a new
 1140 sequence x'_j . A KDE $f_j(y)$ is computed from each sequence x'_j , and these points are eval-
 1141 uated at a series of points y_k . This process is repeated $N = 2000$ times, producing $n \times N$
 1142 probability density estimates $p_{jk} = f_j(y_k)$. For each y_k , the 95% confidence interval of
 1143 the KDE is estimated as the 2.5th and 97.5th percentile of the p_j values obtained for that
 1144 evaluation point y_k .

1145 **Acknowledgments**

1146 Thanks to Ruth Skoug of Los Alamos National Laboratory for finding solar wind
1147 data from the Advanced Composition Explorer (ACE) satellite to cover gaps in the pub-
1148 licly available Level 2 datasets.

1149 We gratefully acknowledge the SuperMAG collaborators (<http://supermag.jhuapl.edu/info/?page=acknowledgement>)
1150 for providing the SML index data.

1151 GOES magnetometer data were obtained from CDAWeb (<https://cdaweb.sci.gsfc.nasa.gov/>).

1152 The Spacepy python library [SK. Morley ., 2011; S. Morley ., 2014; Burrell ., 2018]
1153 was used for a number of tasks related to reading and analyzing data in this paper. It is
1154 available at github.com/spacepy/spacepy.

1155 Portions of the work of J. Haiducek leading to these results were performed while
1156 he held a National Research Council (NRC) Research Associateship award at the U.S.
1157 Naval Research Laboratory.

1158 Portions of the work of J. Haiducek leading to these results were financially sup-
1159 ported by the U.S. Veterans Administration under the Post/911 GI Bill.

1160 Contributions by S. K. Morley were performed under the auspices of the US De-
1161 partment of Energy and were partially supported by the Laboratory Directed Research and
1162 Development program (award 20170047DR).

1163 **References**

1164 Aikio1999Aikio, AT., Sergeev, VA., Shukhtina, MA., Vagina, LI., Angelopoulos, V.

1165 Reeves, GD. 1999jun. Characteristics of pseudobreakups and substorms observed in
1166 the ionosphere, at the geosynchronous orbit, and in the midtail Characteristics of pseu-
1167 dobreakups and substorms observed in the ionosphere, at the geosynchronous orbit, and
1168 in the midtail. *Journal of Geophysical Research: Space Physics*104A612263–12287.
1169 <http://doi.wiley.com/10.1029/1999JA900118> 10.1029/1999JA900118

1170 Akasofu1960Akasofu, SI. 1960sep. Large-scale auroral motions and polar magnetic distur-
1171 bances—I A polar disturbance at about 1100 hours on 23 september 1957 Large-scale
1172 auroral motions and polar magnetic disturbances—I A polar disturbance at about 1100
1173 hours on 23 september 1957. *Journal of Atmospheric and Terrestrial Physics*19110–25.

- 1174 <http://www.sciencedirect.com/science/article/pii/0021916960901033> 10.1016/0021-
1175 9169(60)90103-3
- 1176 Akasofu1964Akasofu, SI. 1964apr. The development of the auroral substorm
1177 The development of the auroral substorm. *Planetary and Space Science*1014273.
1178 <https://www.sciencedirect.com/science/article/pii/0032063364901515> 10.1016/0032-
1179 0633(64)90151-5
- 1180 Akasofu1968PolarMagnetosphericSubstormsAkasofu, SI. 1968. Polar and Magnetospheric
1181 Substorms Polar and Magnetospheric Substorms. Dordrecht, The NetherlandsSpringer
1182 Netherlands.
- 1183 Akasofu1969Akasofu, SI. Meng, CI. 1969jan. A study of polar magnetic substorms
1184 A study of polar magnetic substorms. *Journal of Geophysical Research*741293–313.
1185 <http://doi.wiley.com/10.1029/JA074i001p00293> 10.1029/JA074i001p00293
- 1186 Angelopoulos2008Angelopoulos, V., McFadden, JP., Larson, D., Carlson, CW., Mende,
1187 SB., Frey, H.Kepko, L. 2008aug. Tail reconnection triggering substorm onset. Tail
1188 reconnection triggering substorm onset. *Science (New York, N.Y.)*3215891931–5.
1189 <http://www.ncbi.nlm.nih.gov/pubmed/18653845> 10.1126/science.1160495
- 1190 Baker1996NeutralLineModelBaker, DN., Pulkkinen, TI., Angelopoulos, V., Baumjohann,
1191 W. McPherron, RL. 199606. Neutral Line Model of Substorms: Past Results and
1192 Present View Neutral line model of substorms: Past results and present view. *Journal of*
1193 *Geophysical Research: Space Physics*101A612975-13010. 10.1029/95JA03753
- 1194 Barnston1999Barnston, AG., Leetmaa, A., Kousky, VE., Livezey, RE., O'Lenic,
1195 E., Van den Dool, H.Unger, DA. 1999sep. NCEP Forecasts of the El Niño
1196 of 1997-98 and Its U.S. Impacts NCEP Forecasts of the El Niño of 1997-98 and
1197 Its U.S. Impacts. *Bulletin of the American Meteorological Society*8091829–
1198 1852. <http://journals.ametsoc.org/doi/abs/10.1175/1520-0477> 10.1175/1520-
1199 0477(1999)080<1829:NFOTEN>2.0.CO;2
- 1200 Birn2013Birn, J. Hesse, M. 2013jun. The substorm current wedge in MHD simu-
1201 lations The substorm current wedge in MHD simulations. *Journal of Geophysical*
1202 *Research: Space Physics*11863364–3376. <http://doi.wiley.com/10.1002/jgra.50187>
1203 10.1002/jgra.50187
- 1204 Birn1981Birn, J. Hones Jr., EW. 1981. Three-Dimensional Computer Modeling of Dy-
1205 namic Reconnection in the Geomagnetic Tail Three-Dimensional Computer Modeling
1206 of Dynamic Reconnection in the Geomagnetic Tail. *J. Geophys. Res.*86A86802–6808.

- 1207 <http://dx.doi.org/10.1029/JA086iA08p06802> 10.1029/JA086iA08p06802
- 1208 Birn2011Birn, J., Nakamura, R., Panov, EV. Hesse, M. 2011jan. Bursty bulk flows and
1209 dipolarization in MHD simulations of magnetotail reconnection Bursty bulk flows and
1210 dipolarization in MHD simulations of magnetotail reconnection. *Journal of Geophysical*
1211 *Research: Space Physics*116A1A01210. <http://doi.wiley.com/10.1029/2010JA016083>
1212 10.1029/2010JA016083
- 1213 Birn1998Birn, J., Thomsen, MF., Borovsky, JE., Reeves, GD., McComas, DJ., Belian, RD.
1214 Hesse, M. 1998may. Substorm electron injections: Geosynchronous observations and
1215 test particle simulations Substorm electron injections: Geosynchronous observations and
1216 test particle simulations. *Journal of Geophysical Research: Space Physics*103A59235–
1217 9248. <http://doi.wiley.com/10.1029/97JA02635> 10.1029/97JA02635
- 1218 Boakes2009Boakes, PD., Milan, SE., Abel, GA., Freeman, MP., Chisham, G. Hubert, B.
1219 2009. A statistical study of the open magnetic flux content of the magnetosphere at
1220 the time of substorm onset A statistical study of the open magnetic flux content of the
1221 magnetosphere at the time of substorm onset. *Geophysical Research Letters*364L04105.
1222 <http://dx.doi.org/10.1029/2008GL037059> L04105 10.1029/2008GL037059
- 1223 Bonnevier1970Bonnevier, B., Boström, R. Rostoker, G. 1970jan. A three-dimensional
1224 model current system for polar magnetic substorms A three-dimensional model current
1225 system for polar magnetic substorms. *Journal of Geophysical Research*751107–122.
1226 <http://doi.wiley.com/10.1029/JA075i001p00107> 10.1029/JA075i001p00107
- 1227 Borovsky1993Borovsky, JE., Nemzek, RJ. Belian, RD. 1993mar. The occur-
1228 rence rate of magnetospheric-substorm onsets: Random and periodic substorms
1229 The occurrence rate of magnetospheric-substorm onsets: Random and periodic
1230 substorms. *Journal of Geophysical Research: Space Physics*98A33807–3813.
1231 <http://doi.wiley.com/10.1029/92JA02556> 10.1029/92JA02556
- 1232 Borovsky2017Borovsky, JE. Yakymenko, K. 2017mar. Substorm occurrence rates,
1233 substorm recurrence times, and solar wind structure Substorm occurrence rates,
1234 substorm recurrence times, and solar wind structure. *Journal of Geophysical Re-*
1235 *search: Space Physics*12232973–2998. <http://doi.wiley.com/10.1002/2016JA023625>
1236 10.1002/2016JA023625
- 1237 Burrell2018SnakesOnASpaceshipBurrell, AG., Halford, AJ., Klenzing, J., Stoneback, RA.,
1238 Morley, SK., Annex, AM.Ma, J. 201811. Snakes on a Spaceship - An Overview
1239 of Python in Heliophysics Snakes on a Spaceship - An Overview of Python in He-

- liophysics. *Journal of Geophysical Research: Space Physics*1231210384-10402.
10.1029/2018JA025877
- Caan1975Caan, MN., McPherron, RL. Russell, CT. 1975jan. Substorm and interplanetary magnetic field effects on the geomagnetic tail lobes Substorm and interplanetary magnetic field effects on the geomagnetic tail lobes. *Journal of Geophysical Research*801191–194. <http://doi.wiley.com/10.1029/JA080i001p00191>
10.1029/JA080i001p00191
- Caan1977Caan, MN., McPherron, RL. Russell, CT. 1977oct. Characteristics of the association between the interplanetary magnetic field and substorms Characteristics of the association between the interplanetary magnetic field and substorms. *Journal of Geophysical Research*82294837–4842. <http://doi.wiley.com/10.1029/JA082i029p04837>
10.1029/JA082i029p04837
- Caan1978Caan, MN., McPherron, RL. Russell, CT. 1978mar. The statistical magnetic signature of magnetospheric substorms The statistical magnetic signature of magnetospheric substorms. *Planetary and Space Science*263269–279. <https://www.sciencedirect.com/science/article/pii/0032063378900922> 10.1016/0032-0633(78)90092-2
- Carter2016ROCingCarter, JV., Pan, J., Rai, SN. Galandiuk, S. 201606. ROC-Ing along: Evaluation and Interpretation of Receiver Operating Characteristic Curves ROC-Ing along: Evaluation and interpretation of receiver operating characteristic curves. *Surgery*15961638-1645. 10.1016/j.surg.2015.12.029
- Cayton2007Cayton, T. Belian, RD. 2007. Numerical modeling of the Synchronous Orbit Particle Analyzer (SOPA, Version 2) that flew on S/C 1990-095 Numerical modeling of the Synchronous Orbit Particle Analyzer (SOPA, Version 2) that flew on S/C 1990-095 . Los Alamos, NMLos Alamos National Laboratory. <http://permalink.lanl.gov/object/tr?what=info:lanl-repo/lareport/LA-14335>
- Chen2017Chen, Y., Tóth, G., Cassak, P., Jia, X., Gombosi, TI., Slavin, JA.Henderson, MG. 2017oct. Global Three-Dimensional Simulation of Earth's Dayside Reconnection Using a Two-Way Coupled Magnetohydrodynamics With Embedded Particle-in-Cell Model: Initial Results Global Three-Dimensional Simulation of Earth's Dayside Reconnection Using a Two-Way Coupled Magnetohydrodynamics With Embedded Particle-in-Cell Model: Initial Results. *Journal of Geophysical Research: Space Physics*1221010,318–10,335. <http://doi.wiley.com/10.1002/2017JA024186>

- 1273 10.1002/2017JA024186
- 1274 Chu2015Chu, X., McPherron, R.L., Hsu, T.S., Angelopoulos, V. 2015apr. So-
1275 lar cycle dependence of substorm occurrence and duration: Implications for on-
1276 set Solar cycle dependence of substorm occurrence and duration: Implications
1277 for onset. *Journal of Geophysical Research A: Space Physics*12042808–2818.
1278 <http://doi.wiley.com/10.1002/2015JA021104> 10.1002/2015JA021104
- 1279 Clauer1985Clauer, C.R., Kamide, Y. 1985. DP 1 and DP 2 current sys-
1280 tems for the March 22, 1979 substorms DP 1 and DP 2 current systems for
1281 the March 22, 1979 substorms. *Journal of Geophysical Research*90A21343.
1282 <http://doi.wiley.com/10.1029/JA090iA02p01343> 10.1029/JA090iA02p01343
- 1283 Conover1999Conover, W.J. 1999. *Practical nonparametric statistics Practical nonparametric*
1284 *statistics (3rd)*. Hoboken, NJWiley.
- 1285 Coroniti1972Coroniti, F.V., Kennel, C.F. 1972jul. Changes in magnetospheric config-
1286 uration during the substorm growth phase Changes in magnetospheric configuration
1287 during the substorm growth phase. *Journal of Geophysical Research*77193361–3370.
1288 <http://doi.wiley.com/10.1029/JA077i019p03361> 10.1029/JA077i019p03361
- 1289 Cummings1968Cummings, W.D., Coleman, P.J. 1968jul. Simultaneous Magnetic Field
1290 Variations at the Earth's Surface and at Synchronous, Equatorial Distance. Part I. Bay-
1291 Associated Events Simultaneous Magnetic Field Variations at the Earth's Surface and at
1292 Synchronous, Equatorial Distance. Part I. Bay-Associated Events. *Radio Science*37758–
1293 761. <http://doi.wiley.com/10.1002/rds196837758> 10.1002/rds196837758
- 1294 Davis1966Davis, T.N., Sugiura, M. 1966feb. Auroral electrojet ac-
1295 tivity index AE and its universal time variations Auroral electrojet activ-
1296 ity index AE and its universal time variations. *Journal of Geophysi-
1297 cal Research*713785–801. <http://dx.doi.org/10.1029/JZ071i003p00785>
1298 <http://doi.wiley.com/10.1029/JZ071i003p00785> 10.1029/JZ071i003p00785
- 1299 DeZeeuw2000De Zeeuw, D., Gombosi, T., Groth, C., Powell, K., Stout, Q. 2000. An
1300 adaptive MHD method for global space weather simulations An adaptive MHD method
1301 for global space weather simulations. *IEEE Transactions on Plasma Science*2861956–
1302 1965. <http://ieeexplore.ieee.org/document/902224/> 10.1109/27.902224
- 1303 DeForest1971DeForest, S.E., McIlwain, C.E. 1971jun. Plasma clouds in the magnetosphere
1304 Plasma clouds in the magnetosphere. *Journal of Geophysical Research*76163587–3611.
1305 <http://doi.wiley.com/10.1029/JA076i016p03587> 10.1029/JA076i016p03587

- 1306 Eastwood2005Eastwood, JP., Sibeck, DG., Slavin, JA., Goldstein, ML., Lavraud, B., Sit-
 1307 nov, M.Dandouras, I. 2005jun. Observations of multiple X-line structure in the
 1308 Earth's magnetotail current sheet: A Cluster case study Observations of multiple X-
 1309 line structure in the Earth's magnetotail current sheet: A Cluster case study. *Geo-*
 1310 *physical Research Letters*3211L11105. <http://doi.wiley.com/10.1029/2005GL022509>
 1311 10.1029/2005GL022509
- 1312 Ekelund2012ROCCurvesEkelund, S. 201203. ROC Curves—What Are They and How
 1313 Are They Used? ROC Curves—What are They and How are They Used? *Point of*
 1314 *Care*11116-21. 10.1097/POC.0b013e318246a642
- 1315 El-Alaoui2009El-Alaoui, M., Ashour-Abdalla, M., Walker, RJ., Peroomian, V., Richard,
 1316 RL., Angelopoulos, V. Runov, A. 2009aug. Substorm evolution as revealed
 1317 by THEMIS satellites and a global MHD simulation Substorm evolution as re-
 1318 vealed by THEMIS satellites and a global MHD simulation. *Journal of Geo-*
 1319 *physical Research*114A8A08221. <http://doi.wiley.com/10.1029/2009JA014133>
 1320 10.1029/2009JA014133
- 1321 Forsyth2014Forsyth, C., Fazakerley, AN., Rae, IJ., J. Watt, CE., Murphy, K., Wild,
 1322 JA.Zhang, Y. 2014feb. In situ spatiotemporal measurements of the detailed azimuthal
 1323 substructure of the substorm current wedge In situ spatiotemporal measurements of the
 1324 detailed azimuthal substructure of the substorm current wedge. *Journal of Geophysical*
 1325 *Research: Space Physics*1192927–946. <http://doi.wiley.com/10.1002/2013JA019302>
 1326 10.1002/2013JA019302
- 1327 Forsyth2015Forsyth, C., Rae, IJ., Coxon, JC., Freeman, MP., Jackman, CM., Gjer-
 1328 loev, J. Fazakerley, AN. 2015dec. A new technique for determining Sub-
 1329 storm Onsets and Phases from Indices of the Electrojet (SOPHIE) A new tech-
 1330 nique for determining Substorm Onsets and Phases from Indices of the Electrojet
 1331 (SOPHIE). *Journal of Geophysical Research: Space Physics*1201210,592–10,606.
 1332 <http://doi.wiley.com/10.1002/2015JA021343> 10.1002/2015JA021343
- 1333 Freeman2004Freeman, MP. Morley, SK. 2004jun. A minimal substorm
 1334 model that explains the observed statistical distribution of times between sub-
 1335 storms A minimal substorm model that explains the observed statistical distribu-
 1336 tion of times between substorms. *Geophysical Research Letters*3112L12807.
 1337 <http://doi.wiley.com/10.1029/2004GL019989> <http://dx.doi.org/10.1029/2004GL019989>
 1338 10.1029/2004GL019989

- 1339 Freeman2009Freeman, MP. Morley, SK. 2009nov. No evidence for externally trig-
 1340 gered substorms based on superposed epoch analysis of IMF B z No evidence for ex-
 1341 ternally triggered substorms based on superposed epoch analysis of IMF B z. Geo-
 1342 physical Research Letters3621L21101. <http://doi.wiley.com/10.1029/2009GL040621>
 1343 10.1029/2009GL040621
- 1344 Frey2010CommentSubstormTriggeringFrey, HU. 2010. Comment on “Substorm Triggering
 1345 by New Plasma Intrusion: THEMIS All-Sky Imager Observations” by Y. Nishimura
 1346 et Al. Comment on “Substorm triggering by new plasma intrusion: THEMIS all-sky
 1347 imager observations” by Y. Nishimura et al. *Journal of Geophysical Research: Space*
 1348 *Physics*115A12A12232. 10.1029/2010JA016113
- 1349 Frey2004Frey, HU., Mende, SB., Angelopoulos, V. Donovan, EF. 2004oct.
 1350 Substorm onset observations by IMAGE-FUV Substorm onset observa-
 1351 tions by IMAGE-FUV. *Journal of Geophysical Research*109A10A10304.
 1352 <http://doi.wiley.com/10.1029/2004JA010607> 10.1029/2004JA010607
- 1353 Fruhauff2017Frühauff, D. Glassmeier, KH. 2017nov. The Plasma Sheet as Natu-
 1354 ral Symmetry Plane for Dipolarization Fronts in the Earth’s Magnetotail The Plasma
 1355 Sheet as Natural Symmetry Plane for Dipolarization Fronts in the Earth’s Mag-
 1356 netotail. *Journal of Geophysical Research: Space Physics*1221111,373–11,388.
 1357 <http://doi.wiley.com/10.1002/2017JA024682> 10.1002/2017JA024682
- 1358 Fu2012Fu, HS., Khotyaintsev, YV., Vaivads, A., André, M. Huang, SY. 2012may.
 1359 Occurrence rate of earthward-propagating dipolarization fronts Occurrence rate of
 1360 earthward-propagating dipolarization fronts. *Geophysical Research Letters*3910L10101.
 1361 <http://doi.wiley.com/10.1029/2012GL051784> 10.1029/2012GL051784
- 1362 Ganushkina2015Ganushkina, NY., Amariutei, OA., Welling, D. Heynderickx, D. 2015jan.
 1363 Nowcast model for low-energy electrons in the inner magnetosphere Nowcast model
 1364 for low-energy electrons in the inner magnetosphere. *Space Weather*13116–34.
 1365 <http://doi.wiley.com/10.1002/2014SW001098> 10.1002/2014SW001098
- 1366 Gjerloev2012SuperMAGDataProcessingGjerloev, JW. 201209. The SuperMAG Data Pro-
 1367 cessing Technique The SuperMAG data processing technique. *Journal of Geophysical*
 1368 *Research: Space Physics*117A9. 10.1029/2012JA017683
- 1369 Glocer2016Glocer, A., Rastätter, L., Kuznetsova, M., Pulkkinen, A., Singer, HJ., Balch,
 1370 C.Wing, S. 2016jul. Community-wide validation of geospace model local K-index
 1371 predictions to support model transition to operations Community-wide validation

- 1372 of geospace model local K-index predictions to support model transition to opera-
 1373 tions. *Space Weather*147469–480. <http://doi.wiley.com/10.1002/2016SW001387>
 1374 10.1002/2016SW001387
- 1375 Glocer2009pwomGlocer, A., Tóth, G., Gombosi, T. Welling, D. 2009may. Mod-
 1376 eling ionospheric outflows and their impact on the magnetosphere, initial re-
 1377 sults Modeling ionospheric outflows and their impact on the magnetosphere, ini-
 1378 tial results. *Journal of Geophysical Research: Space Physics*114A5A05216.
 1379 <http://doi.wiley.com/10.1029/2009JA014053> 10.1029/2009JA014053
- 1380 Glocer2009multifluidGlocer, A., Tóth, G., Ma, Y., Gombosi, T., Zhang, JC. Kistler, LM.
 1381 2009dec. Multifluid Block-Adaptive-Tree Solar wind Roe-type Upwind Scheme: Mag-
 1382 netospheric composition and dynamics during geomagnetic storms-Initial results Multi-
 1383 fluid Block-Adaptive-Tree Solar wind Roe-type Upwind Scheme: Magnetospheric com-
 1384 position and dynamics during geomagnetic storms-Initial results. *Journal of Geophysical*
 1385 *Research: Space Physics*114A12A12203. <http://doi.wiley.com/10.1029/2009JA014418>
 1386 10.1029/2009JA014418
- 1387 Haiducek2017Haiducek, JD., Welling, DT., Ganushkina, NY., Morley, SK. Ozturk,
 1388 DS. 2017dec. SWMF Global Magnetosphere Simulations of January 2005: Ge-
 1389 omagnetic Indices and Cross-Polar Cap Potential SWMF Global Magnetosphere
 1390 Simulations of January 2005: Geomagnetic Indices and Cross-Polar Cap Poten-
 1391 tial. *Space Weather*15121567–1587. <http://doi.wiley.com/10.1002/2017SW001695>
 1392 10.1002/2017SW001695
- 1393 Hajra2016SupersubstormsHajra, R., Tsurutani, BT., Echer, E., Gonzalez, WD. Gjerloev,
 1394 JW. 201608. Supersubstorms (SML < -2500 nT): Magnetic Storm and Solar Cy-
 1395 cle Dependences Supersubstorms (SML < -2500 nT): Magnetic storm and solar cy-
 1396 cle dependences. *Journal of Geophysical Research: Space Physics*12187805-7816.
 1397 10.1002/2015JA021835
- 1398 Henderson2009Henderson, MG. 2009. Observational evidence for an inside-out sub-
 1399 storm onset scenario Observational evidence for an inside-out substorm onset scenario.
 1400 *Annales Geophysicae*2752129–2140. [http://www.ann-geophys.net/27/2129/2009/angeo-](http://www.ann-geophys.net/27/2129/2009/angeo-27-2129-2009.pdf)
 1401 [27-2129-2009.pdf](http://www.ann-geophys.net/27/2129/2009/angeo-27-2129-2009.pdf) 10.5194/angeo-27-2129-2009
- 1402 Hendry2013RapidRadiationBeltHendry, AT., Rodger, CJ., Clilverd, MA., Thomson, NR.,
 1403 Morley, SK. Raita, T. 201303. Rapid Radiation Belt Losses Occurring During
 1404 High-Speed Solar Wind Stream–Driven Storms: Importance of Energetic Electron

- 1405 Precipitation Rapid Radiation Belt Losses Occurring During High-Speed Solar Wind
 1406 Stream–Driven Storms: Importance of Energetic Electron Precipitation. *Dynamics of*
 1407 *the Earth’s Radiation Belts and Inner Magnetosphere Dynamics of the Earth’s Radiation*
 1408 *Belts and Inner Magnetosphere* (199, 213-224). Washington, DC American Geophysical
 1409 *Union (AGU). 10.1029/2012GM001299*
- 1410 Heppner1955Heppner, JP. 1955mar. Note on the occurrence of world-wide S.S.C.’s dur-
 1411 ing the onset of negative bays at College, Alaska Note on the occurrence of world-
 1412 wide S.S.C.’s during the onset of negative bays at College, Alaska. *Journal of*
 1413 *Geophysical Research*60129–32. <http://doi.wiley.com/10.1029/JZ060i001p00029>
 1414 [10.1029/JZ060i001p00029](http://doi.wiley.com/10.1029/JZ060i001p00029)
- 1415 Hones1984PlasmaSheetBehaviorHones, EW. 1984. Plasma Sheet Behavior dur-
 1416 ing Substorms Plasma sheet behavior during substorms. *Magnetic Reconnection*
 1417 *in Space and Laboratory Plasmas Magnetic Reconnection in Space and Laboratory*
 1418 *Plasmas* (30, 178-184). Washington, DC American Geophysical Union (AGU).
 1419 [10.1029/GM030p0178](http://doi.wiley.com/10.1029/GM030p0178)
- 1420 Hones1984Hones, EW., Birn, J., Baker, DN., Bame, SJ., Feldman, WC., Mc-
 1421 Comas, DJ. Tsurutani, BT. 1984oct. Detailed examination of a plas-
 1422 moid in the distant magnetotail with ISEE 3 Detailed examination of a plas-
 1423 moid in the distant magnetotail with ISEE 3. *Geophysical Research*
 1424 *Letters*11101046–1049. <http://dx.doi.org/10.1029/GL011i010p01046>
 1425 <http://doi.wiley.com/10.1029/GL011i010p01046> [10.1029/GL011i010p01046](http://doi.wiley.com/10.1029/GL011i010p01046)
- 1426 Honkonen2011aHonkonen, I., Palmroth, M., Pulkkinen, TI., Janhunen, P. Aikio, A.
 1427 2011jan. On large plasmoid formation in a global magnetohydrodynamic simulation
 1428 On large plasmoid formation in a global magnetohydrodynamic simulation. *Annales*
 1429 *Geophysicae*291167–179. <http://www.ann-geophys.net/29/167/2011/> [10.5194/angeo-](http://doi.wiley.com/10.5194/angeo-29-167-2011)
 1430 [29-167-2011](http://doi.wiley.com/10.5194/angeo-29-167-2011)
- 1431 Hsu2003Hsu, TS. McPherron, RL. 2003jul. Occurrence frequencies of IMF
 1432 triggered and nontriggered substorms Occurrence frequencies of IMF triggered
 1433 and nontriggered substorms. *Journal of Geophysical Research*108A71307.
 1434 <http://doi.wiley.com/10.1029/2002JA009442> [10.1029/2002JA009442](http://doi.wiley.com/10.1029/2002JA009442)
- 1435 Hsu2004Hsu, TS. McPherron, RL. 2004jul. Average characteristics of trig-
 1436 gered and nontriggered substorms Average characteristics of triggered and
 1437 nontriggered substorms. *Journal of Geophysical Research*109A7A07208.

- 1438 <http://doi.wiley.com/10.1029/2003JA009933> 10.1029/2003JA009933
- 1439 Hsu2012Hsu, TS. McPherron, RL. 2012nov. A statistical analysis
1440 of substorm associated tail activity A statistical analysis of substorm as-
1441 sociated tail activity. *Advances in Space Research*50101317–1343.
1442 <https://www.sciencedirect.com/science/article/pii/S0273117712004371>
1443 10.1016/J.ASR.2012.06.034
- 1444 Ieda2001Ieda, A., Fairfield, DH., Mukai, T., Saito, Y., Kokubun, S., Liou, K.Brittacher,
1445 MJ. 2001mar. Plasmoid ejection and auroral brightenings Plasmoid ejection and au-
1446 roral brightenings. *Journal of Geophysical Research: Space Physics*106A33845–3857.
1447 <http://doi.wiley.com/10.1029/1999JA000451> <http://dx.doi.org/10.1029/1999JA000451>
1448 10.1029/1999JA000451
- 1449 Iyemori1996Iyemori, T. Rao, DRK. 1996. Decay of the Dst field of geomagnetic dis-
1450 turbance after substorm onset and its implication to storm-substorm relation Decay
1451 of the Dst field of geomagnetic disturbance after substorm onset and its implication
1452 to storm-substorm relation. *Annales Geophysicae*146608–618. [http://www.ann-
1453 geophys.net/14/608/1996/](http://www.ann-geophys.net/14/608/1996/) 10.1007/s00585-996-0608-3
- 1454 Johnson2014triggeringJohnson, JR. Wing, S. 2014. External versus Internal Trig-
1455 gering of Substorms: An Information-Theoretical Approach External versus internal
1456 triggering of substorms: An information-theoretical approach. *Geophysical Research
1457 Letters*41165748-5754. 10.1002/2014GL060928
- 1458 Jordanova2017Jordanova, V., Delzanno, G., Henderson, M., Godinez, H., Jeffery,
1459 C., Lawrence, E.Horne, R. 2017nov. Specification of the near-Earth space
1460 environment with SHIELDS Specification of the near-Earth space environment
1461 with SHIELDS. *Journal of Atmospheric and Solar-Terrestrial Physics*177148-
1462 159. <https://www.sciencedirect.com/science/article/pii/S1364682617302729>
1463 10.1016/j.jastp.2017.11.006
- 1464 Juusola2011Juusola, L., Østgaard, N., Tanskanen, E., Partamies, N. Snekvik, K.
1465 2011oct. Earthward plasma sheet flows during substorm phases Earthward
1466 plasma sheet flows during substorm phases. *Journal of Geophysical Research:
1467 Space Physics*116A10A10228. <http://doi.wiley.com/10.1029/2011JA016852>
1468 10.1029/2011JA016852
- 1469 Kamide1974bKamide, Y. McIlwain, CE. 1974nov. The onset time of magne-
1470 topheric substorms determined from ground and synchronous satellite records

- 1471 The onset time of magnetospheric substorms determined from ground and syn-
 1472 chronous satellite records. *Journal of Geophysical Research*79314787–4790.
 1473 <http://doi.wiley.com/10.1029/JA079i031p04787> 10.1029/JA079i031p04787
- 1474 Kamide1974Kamide, Y., Yasuhara, F. Akasofu, SI. 1974aug. On the cause of
 1475 northward magnetic field along the negative X axis during magnetospheric sub-
 1476 storms On the cause of northward magnetic field along the negative X axis dur-
 1477 ing magnetospheric substorms. *Planetary and Space Science*2281219–1229.
 1478 <https://www.sciencedirect.com/science/article/pii/0032063374900063> 10.1016/0032-
 1479 0633(74)90006-3
- 1480 Katus2013GeomagneticIndicesKatus, RM. Liemohn, MW. 201308. Similarities and Dif-
 1481 ferences in Low- to Middle-Latitude Geomagnetic Indices Similarities and differences in
 1482 low- to middle-latitude geomagnetic indices. *Journal of Geophysical Research: Space*
 1483 *Physics*11885149-5156. 10.1002/jgra.50501
- 1484 Kaufmann1987Kaufmann, RL. 1987. Substorm currents: Growth phase and onset Sub-
 1485 storm currents: Growth phase and onset. *Journal of Geophysical Research*92A77471.
 1486 <http://doi.wiley.com/10.1029/JA092iA07p07471> 10.1029/JA092iA07p07471
- 1487 Kauristie2017Kauristie, K., Morschhauser, A., Olsen, N., Finlay, CC., McPherron, RL.,
 1488 Gjerloev, JW. Opgenoorth, HJ. 2017mar. On the Usage of Geomagnetic Indices
 1489 for Data Selection in Internal Field Modelling On the Usage of Geomagnetic Indices
 1490 for Data Selection in Internal Field Modelling. *Space Science Reviews*2061-461–90.
 1491 <http://link.springer.com/10.1007/s11214-016-0301-0> 10.1007/s11214-016-0301-0
- 1492 Kepko2004RelativeTimingSubstormKepko, L. 2004. Relative Timing of Substorm On-
 1493 set Phenomena Relative timing of substorm onset phenomena. *Journal of Geophysical*
 1494 *Research*109A4. 10.1029/2003JA010285
- 1495 Kepko2001CommentLowLatitudePi2Kepko, L. McPherron, RL. 2001. Comment on
 1496 “Evaluation of Low-Latitude Pi2 Pulsations as Indicators of Substorm Onset Using Po-
 1497 lar Ultraviolet Imagery” by K. Liou, et Al. Comment on “Evaluation of low-latitude
 1498 Pi2 pulsations as indicators of substorm onset using Polar ultraviolet imagery” by K.
 1499 Liou, et al. *Journal of Geophysical Research: Space Physics*106A918919-18922.
 1500 10.1029/2000JA000189
- 1501 Kepko2015Kepko, L., McPherron, RL., Amm, O., Apatenkov, S., Baumjohann, W., Birn,
 1502 J.Sergeev, V. 2015jul. Substorm Current Wedge Revisited Substorm Current Wedge
 1503 Revisited. *Space Science Reviews*1901-41–46. <http://link.springer.com/10.1007/s11214->

1504 014-0124-9 10.1007/s11214-014-0124-9

1505 Kim2005Kim, KH., Takahashi, K., Lee, D., Sutcliffe, PR. Yumoto, K. 2005. Pi2

1506 pulsations associated with poleward boundary intensifications during the absence of

1507 substorms Pi2 pulsations associated with poleward boundary intensifications dur-

1508 ing the absence of substorms. *Journal of Geophysical Research*110A1A01217.

1509 <http://doi.wiley.com/10.1029/2004JA010780> 10.1029/2004JA010780

1510 Korth1991Korth, A., Pu, ZY., Kremser, G. Roux, A. 1991mar. A Statistical Study of

1511 Substorm Onset Conditions at Geostationary Orbit A Statistical Study of Substorm On-

1512 set Conditions at Geostationary Orbit. *JR. Kan, TA. Potemra, S. Kokubun T. Iijima*

1513 (*), Magnetospheric Substorms Magnetospheric substorms (64, 343–351). Washington,*

1514 *D. C.American Geophysical Union (AGU). <http://doi.wiley.com/10.1029/GM064p0343>*

1515 10.1029/GM064p0343

1516 Koskinen1993Koskinen, HEJ., Lopez, RE., Pellinen, RJ., Pulkkinen, TI., Baker, DN.

1517 Bössinger, T. 1993apr. Pseudobreakup and substorm growth phase in the ionosphere

1518 and magnetosphere Pseudobreakup and substorm growth phase in the ionosphere and

1519 magnetosphere. *Journal of Geophysical Research: Space Physics*98A45801–5813.

1520 <http://doi.wiley.com/10.1029/92JA02482> 10.1029/92JA02482

1521 Kullen2009SubstormsPseudobreakupsKullen, A., Ohtani, S. Karlsson, T. 200904. Geo-

1522 magnetic Signatures of Auroral Substorms Preceded by Pseudobreakups Geomagnetic

1523 signatures of auroral substorms preceded by pseudobreakups. *Journal of Geophysical*

1524 *Research: Space Physics*114A4A04201. 10.1029/2008JA013712

1525 Lee2004Lee, DY. Lyons, LR. 2004apr. Geosynchronous magnetic field response to

1526 solar wind dynamic pressure pulse Geosynchronous magnetic field response to so-

1527 lar wind dynamic pressure pulse. *Journal of Geophysical Research*109A4A04201.

1528 <http://doi.wiley.com/10.1029/2003JA010076> 10.1029/2003JA010076

1529 Lezniak1968Lezniak, TW., Arnoldy, RL., Parks, GK. Winckler, JR. 1968jul. Measure-

1530 ment and Intensity of Energetic Electrons at the Equator at 6.6 Re Measurement and

1531 Intensity of Energetic Electrons at the Equator at 6.6 Re. *Radio Science*37710–714.

1532 <http://doi.wiley.com/10.1002/rds196837710> 10.1002/rds196837710

1533 Liemohn2018ModelEvaluationGuidelinesLiemohn, MW., McCollough, JP., Jordanova,

1534 VK., Ngwira, CM., Morley, SK., Cid, C.Vasile, R. 201811. Model Evaluation Guide-

1535 lines for Geomagnetic Index Predictions Model evaluation guidelines for geomagnetic

1536 index predictions. *Space Weather*16122079-2102. 10.1029/2018SW002067

- 1537 Liou2010Liou, K. 2010dec. Polar Ultraviolet Imager observation of auroral breakup
 1538 Polar Ultraviolet Imager observation of auroral breakup. *Journal of Geophysical Re-*
 1539 *search: Space Physics*115A12A12219. <http://doi.wiley.com/10.1029/2010JA015578>
 1540 10.1029/2010JA015578
- 1541 Liou2002Liou, K., Meng, CI., Lui, ATY., Newell, PT. Wing, S. 2002. Magnetic
 1542 dipolarization with substorm expansion onset Magnetic dipolarization with substorm
 1543 expansion onset. *Magnetospheric Physics: Magnetosphere—inner*107A121131.
 1544 <https://agupubs.onlinelibrary.wiley.com/doi/pdf/10.1029/2001JA000179>
 1545 10.1029/2001JA000179
- 1546 Liou1999RelativeTimingSubstormLiou, K., Meng, CI., Lui, TY., Newell, PT., Brittnacher,
 1547 M., Parks, G.Yumoto, K. 1999. On Relative Timing in Substorm Onset Signatures On
 1548 relative timing in substorm onset signatures. *Journal of Geophysical Research: Space*
 1549 *Physics*104A1022807-22817. 10.1029/1999JA900206
- 1550 Liou2000LowLatitudePi2Liou, K., Meng, CI., Newell, PT., Takahashi, K., Ohtani, SI., Lui,
 1551 ATY.Parks, G. 2000. Evaluation of Low-Latitude Pi2 Pulsations as Indicators of Sub-
 1552 storm Onset Using Polar Ultraviolet Imagery Evaluation of low-latitude Pi2 pulsations
 1553 as indicators of substorm onset using Polar ultraviolet imagery. *Journal of Geophysical*
 1554 *Research: Space Physics*105A22495-2505. 10.1029/1999JA900416
- 1555 Liu2013Liu, J., Angelopoulos, V., Runov, A. Zhou, XZ. 2013may. On the current
 1556 sheets surrounding dipolarizing flux bundles in the magnetotail: The case for wedgelets
 1557 On the current sheets surrounding dipolarizing flux bundles in the magnetotail: The
 1558 case for wedgelets. *Journal of Geophysical Research: Space Physics*11852000–2020.
 1559 <http://doi.wiley.com/10.1002/jgra.50092> 10.1002/jgra.50092
- 1560 Lopez2007Lopez, RE., Hernandez, S., Wiltberger, M., Huang, CL., Kepko, EL.,
 1561 Spence, H.Lyon, JG. 2007jan. Predicting magnetopause crossings at geosyn-
 1562 chronous orbit during the Halloween storms Predicting magnetopause crossings
 1563 at geosynchronous orbit during the Halloween storms. *Space Weather*51S01005.
 1564 <http://doi.wiley.com/10.1029/2006SW000222> 10.1029/2006SW000222
- 1565 Lui1978Lui, ATY. 1978oct. Estimates of current changes in the geomagneto-
 1566 tail associated with a substorm Estimates of current changes in the geomagne-
 1567 totail associated with a substorm. *Geophysical Research Letters*510853–856.
 1568 <http://doi.wiley.com/10.1029/GL005i010p00853> 10.1029/GL005i010p00853
- 1569 Lui1991SubstormSynthesisLui, ATY. 1991. Extended Consideration of a Synthesis Model

- 1570 for Magnetospheric Substorms Extended Consideration of a Synthesis Model for Mag-
 1571 netospheric Substorms. *Magnetospheric Substorms Magnetospheric Substorms* (64,
 1572 43-60). Washington, DC American Geophysical Union (AGU). 10.1029/GM064p0043
- 1573 Lyon1981Lyon, JG., Brecht, SH., Huba, JD., Fedder, JA. Palmadesso, PJ.
 1574 1981apr. Computer Simulation of a Geomagnetic Substorm Computer Simu-
 1575 lation of a Geomagnetic Substorm. *Physical Review Letters*46151038–1041.
 1576 <https://link.aps.org/doi/10.1103/PhysRevLett.46.1038> 10.1103/PhysRevLett.46.1038
- 1577 Lyons1997Lyons, LR., Blanchard, GT., Samson, JC., Lepping, RP., Yamamoto, T.
 1578 Moretto, T. 1997dec. Coordinated observations demonstrating external sub-
 1579 storm triggering Coordinated observations demonstrating external substorm trig-
 1580 gering. *Journal of Geophysical Research: Space Physics*102A1227039–27051.
 1581 <http://doi.wiley.com/10.1029/97JA02639> 10.1029/97JA02639
- 1582 McPherron1972McPherron, R. 1972sep. Substorm related changes in the
 1583 geomagnetic tail: the growth phase Substorm related changes in the geomag-
 1584 netic tail: the growth phase. *Planetary and Space Science*2091521–1539.
 1585 <https://www.sciencedirect.com/science/article/pii/0032063372900542> 10.1016/0032-
 1586 0633(72)90054-2
- 1587 McPherron1970McPherron, RL. 1970oct. Growth phase of magnetospheric
 1588 substorms Growth phase of magnetospheric substorms. *Journal of Geophys-
 1589 ical Research*75285592–5599. <http://doi.wiley.com/10.1029/JA075i028p05592>
 1590 10.1029/JA075i028p05592
- 1591 McPherron2015McPherron, RL. 2015jan. Earth's Magnetotail Earth's Magnetotail.
 1592 A. Keiling, CM. Jackman PA. Delamere (), *Magnetotails in the Solar System Magne-
 1593 totails in the solar system* (61–84). Hoboken, NJ American Geophysical Union (AGU).
 1594 <http://doi.wiley.com/10.1002/9781118842324.ch4> 10.1002/9781118842324.ch4
- 1595 McPherron2017McPherron, RL. Chu, X. 2017mar. The Mid-Latitude Positive
 1596 Bay and the MPB Index of Substorm Activity The Mid-Latitude Positive Bay and
 1597 the MPB Index of Substorm Activity. *Space Science Reviews*2061-491–122.
 1598 <http://link.springer.com/10.1007/s11214-016-0316-6> 10.1007/s11214-016-0316-6
- 1599 McPherron2018McPherron, RL. Chu, X. 2018apr. The Midlatitude Positive Bay
 1600 Index and the Statistics of Substorm Occurrence The Midlatitude Positive Bay
 1601 Index and the Statistics of Substorm Occurrence. *Journal of Geophysical Re-
 1602 search: Space Physics*12342831-2850. <http://doi.wiley.com/10.1002/2017JA024766>

- 1603 10.1002/2017JA024766
- 1604 McPherron1973McPherron, RL., Russell, CT. Aubry, MP. 1973jun. Satellite studies
1605 of magnetospheric substorms on August 15, 1968: 9. Phenomenological model for
1606 substorms Satellite studies of magnetospheric substorms on August 15, 1968: 9. Phe-
1607 nomenological model for substorms. *Journal of Geophysical Research*78163131–3149.
1608 <http://doi.wiley.com/10.1029/JA078i016p03131> 10.1029/JA078i016p03131
- 1609 Meng2013Meng, X., Tóth, G., Glocer, A., Fok, MC. Gombosi, TI. 2013sep. Pres-
1610 sure anisotropy in global magnetospheric simulations: Coupling with ring current
1611 models Pressure anisotropy in global magnetospheric simulations: Coupling with ring
1612 current models. *Journal of Geophysical Research: Space Physics*11895639–5658.
1613 <http://doi.wiley.com/10.1002/jgra.50539> 10.1002/jgra.50539
- 1614 Meng2012bMeng, X., Tóth, G., Liemohn, MW., Gombosi, TI. Runov, A. 2012aug.
1615 Pressure anisotropy in global magnetospheric simulations: A magneto-hydrodynam-
1616 ics model Pressure anisotropy in global magnetospheric simulations: A magneto-
1617 hydrodynamics model. *Journal of Geophysical Research: Space Physics*117A8.
1618 <http://doi.wiley.com/10.1029/2012JA017791> 10.1029/2012JA017791
- 1619 Moldwin1993Moldwin, MB. Hughes, WJ. 1993jan. Geomagnetic substorm associa-
1620 tion of plasmoids Geomagnetic substorm association of plasmoids. *Journal of Geo-*
1621 *physical Research: Space Physics*98A181–88. <http://doi.wiley.com/10.1029/92JA02153>
1622 10.1029/92JA02153
- 1623 MorleySpacepy2014Morley, S., Koller, J., Welling, D., Larsen, B. Niehof, J. 201401.
1624 SpacePy: Python-Based Tools for the Space Science Community SpacePy: Python-
1625 Based Tools for the Space Science Community. *Astrophysics Source Code Li-*
1626 *brary*ascl:1401.002.
- 1627 Morley2009Morley, S., Rouillard, A. Freeman, M. 2009. Recurrent substorm activity dur-
1628 ing the passage of a corotating interaction region Recurrent substorm activity during the
1629 passage of a corotating interaction region. *Journal of Atmospheric and Solar-Terrestrial*
1630 *Physics*71101073–1081. 10.1016/j.jastp.2008.11.009
- 1631 Morley2007ObservationsMagnetosphericSubstormsMorley, SK. 2007. Observations of
1632 Magnetospheric Substorms during the Passage of a Corotating Interaction Region Ob-
1633 servations of magnetospheric substorms during the passage of a corotating interaction
1634 region. W. Short I. Cairns (), *Proceedings from 7th Australian Space Science Con-*
1635 *ference, 2007 Proceedings from 7th Australian Space Science Conference, 2007* (118-

- 1636 129). Sydney National Space Society of Australia Ltd.
- 1637 Morley2007AssociationNorthwardTurningsMorley, SK. Freeman, MP. 200704. On the
1638 Association between Northward Turnings of the Interplanetary Magnetic Field and
1639 Substorm Onsets On the association between northward turnings of the interplane-
1640 tary magnetic field and substorm onsets. *Geophysical Research Letters*348L08104.
1641 10.1029/2006GL028891
- 1642 Morley2010DropoutsOuterElectronMorley, SK., Friedel, RHW., Spanswick, EL., Reeves,
1643 G., Steinberg, JT., Koller, J.Noveroske, E. 201011. Dropouts of the Outer Electron
1644 Radiation Belt in Response to Solar Wind Stream Interfaces: Global Positioning Sys-
1645 tem Observations Dropouts of the outer electron radiation belt in response to solar
1646 wind stream interfaces: Global positioning system observations. *Proceedings of the*
1647 *Royal Society A: Mathematical, Physical and Engineering Sciences*46621233329-3350.
1648 10.1098/rspa.2010.0078
- 1649 Morley2011Morley, SK., Welling, DT., Koller, J., Larsen, BA., Henderson, MG. Niehof,
1650 J. 2011. SpacePy - A Python-Based Library of Tools for the Space Sciences SpacePy -
1651 A Python-based Library of Tools for the Space Sciences. *Proceedings of the 9th Python*
1652 *in Science Conference*39-45.
- 1653 Morley2018PerturbedInputEnsembleMorley, SK., Welling, DT. Woodroffe, JR. 201808.
1654 Perturbed Input Ensemble Modeling with the Space Weather Modeling Framework Per-
1655 turbed Input Ensemble Modeling with the Space Weather Modeling Framework. *Space*
1656 *Weather*1691330-1347. 10.1029/2018SW002000
- 1657 Mukhopadhyay2018AguConductanceMukhopadhyay, A., Welling, DT., Liemohn, MW.,
1658 Zou, S. Ridley, AJ. 201812. Challenges in Space Weather Prediction: Estimation of
1659 Auroral Conductance. *Challenges in Space Weather Prediction: Estimation of Auroral*
1660 *Conductance*. Washington, DC.
- 1661 Nagai1987Nagai, T. 1987mar. Field-aligned currents associated with substorms
1662 in the vicinity of synchronous orbit: 2. GOES 2 and GOES 3 observations Field-
1663 aligned currents associated with substorms in the vicinity of synchronous orbit: 2.
1664 GOES 2 and GOES 3 observations. *Journal of Geophysical Research*92A32432.
1665 <http://doi.wiley.com/10.1029/JA092iA03p02432> 10.1029/JA092iA03p02432
- 1666 Nagai1998Nagai, T., Fujimoto, M., Saito, Y., Machida, S., Terasawa, T., Nakamura,
1667 R.Kokubun, S. 1998mar. Structure and dynamics of magnetic reconnection for sub-
1668 storm onsets with Geotail observations Structure and dynamics of magnetic recon-

- 1669 nection for substorm onsets with Geotail observations. *Journal of Geophysical Re-*
 1670 search: *Space Physics*103A34419–4440. <http://doi.wiley.com/10.1029/97JA02190>
 1671 10.1029/97JA02190
- 1672 Newell2011aNewell, PT. Gjerloev, JW. 2011dec. Evaluation of SuperMAG
 1673 auroral electrojet indices as indicators of substorms and auroral power *Evalu-*
 1674 ation of SuperMAG auroral electrojet indices as indicators of substorms and au-
 1675 roral power. *Journal of Geophysical Research: Space Physics*116A12A12211.
 1676 <http://doi.wiley.com/10.1029/2011JA016779> 10.1029/2011JA016779
- 1677 Newell2011bNewell, PT. Gjerloev, JW. 2011dec. Substorm and magnetosphere
 1678 characteristic scales inferred from the SuperMAG auroral electrojet indices *Substorm*
 1679 and magnetosphere characteristic scales inferred from the SuperMAG auroral elec-
 1680 trojet indices. *Journal of Geophysical Research: Space Physics*116A12A12232.
 1681 <http://doi.wiley.com/10.1029/2011JA016936> 10.1029/2011JA016936
- 1682 Newell2011cNewell, PT. Liou, K. 2011mar. Solar wind driving and substorm trig-
 1683 gering *Solar wind driving and substorm triggering. Journal of Geophysical Re-*
 1684 search: *Space Physics*116A3A03229. <http://doi.wiley.com/10.1029/2010JA016139>
 1685 10.1029/2010JA016139
- 1686 Newell2001Newell, PT., Liou, K., Sotirelis, T. Meng, CI. 2001dec. Auroral precipi-
 1687 tation power during substorms: A Polar UV Imager-based superposed epoch analysis
 1688 Auroral precipitation power during substorms: A Polar UV Imager-based superposed
 1689 epoch analysis. *Journal of Geophysical Research: Space Physics*106A1228885–28896.
 1690 <http://doi.wiley.com/10.1029/2000JA000428> 10.1029/2000JA000428
- 1691 Nishida1986Nishida, A., Scholer, M., Terasawa, T., Bame, SJ., Gloeckler, G., Smith,
 1692 EJ. Zwickl, RD. 1986apr. Quasi-stagnant plasmoid in the middle tail: A new pre-
 1693 expansion phase phenomenon *Quasi-stagnant plasmoid in the middle tail: A new*
 1694 preexpansion phase phenomenon. *Journal of Geophysical Research*91A44245.
 1695 <http://doi.wiley.com/10.1029/JA091iA04p04245> 10.1029/JA091iA04p04245
- 1696 Noah2013Noah, MA. Burke, WJ. 2013aug. Sawtooth-substorm connections: A closer
 1697 look *Sawtooth-substorm connections: A closer look. Journal of Geophysical Re-*
 1698 search: *Space Physics*11885136–5148. <http://doi.wiley.com/10.1002/jgra.50440>
 1699 10.1002/jgra.50440
- 1700 Nose2009Nosé, M., Iyemori, T., Takeda, M., Toh, H., Ookawa, T., Cifuentes-Nava,
 1701 G.Curto, JJ. 2009. New substorm index derived from high-resolution ge-

- 1702 omagnetic field data at low latitude and its comparison with AE and ASY in-
 1703 dices New substorm index derived from high-resolution geomagnetic field data
 1704 at low latitude and its comparison with AE and ASY indices. J. Love (),
 1705 Proc. XIII IAGA Workshop Proc. xiii iaga workshop (202–207). Golden, CO.
 1706 [https://geomag.usgs.gov/downloads/publications/Proceedings202 – 207.pdf](https://geomag.usgs.gov/downloads/publications/Proceedings202-207.pdf)
- 1707 Ohtani1993Ohtani, S., Anderson, BJ., Sibeck, DG., Newell, PT., Zanetti, LJ., Potemra,
 1708 TA.Russell, CT. 1993nov. A multisatellite study of a pseudo-substorm onset in the
 1709 near-Earth magnetotail A multisatellite study of a pseudo-substorm onset in the near-
 1710 Earth magnetotail. *Journal of Geophysical Research: Space Physics*98A1119355–19367.
 1711 <http://doi.wiley.com/10.1029/93JA01421> 10.1029/93JA01421
- 1712 Ohtani2004Ohtani, Si. Raeder, J. 2004jan. Tail current surge: New insights
 1713 from a global MHD simulation and comparison with satellite observations Tail
 1714 current surge: New insights from a global MHD simulation and comparison
 1715 with satellite observations. *Journal of Geophysical Research*109A1A01207.
 1716 <http://doi.wiley.com/10.1029/2002JA009750> 10.1029/2002JA009750
- 1717 Øieroset2001Øieroset, M., Phan, TD., Fujimoto, M., Lin, RP. Lepping, RP. 2001. In situ
 1718 detection of reconnection in the Earth’s magnetotail In situ detection of reconnection in
 1719 the Earth’s magnetotail. *Letters to Nature*412July414–416. 10.1038/35086520
- 1720 Øieroset1999Øieroset, M., Yamauchi, M., Liszka, L., Christon, SP. Hultqvist, B. 1999apr.
 1721 A statistical study of ion beams and conics from the dayside ionosphere during dif-
 1722 ferent phases of a substorm A statistical study of ion beams and conics from the day-
 1723 side ionosphere during different phases of a substorm. *Journal of Geophysical Re-*
 1724 *search: Space Physics*104A46987–6998. <http://doi.wiley.com/10.1029/1998JA900177>
 1725 10.1029/1998JA900177
- 1726 Parzen1962Parzen, E. 1962sep. On Estimation of a Probability Density Function and
 1727 Mode On Estimation of a Probability Density Function and Mode. *The Annals of*
 1728 *Mathematical Statistics*3331065–1076. <http://projecteuclid.org/euclid.aoms/1177704472>
 1729 10.1214/aoms/1177704472
- 1730 Perreault1978Perreault, P. Akasofu, SI. 1978sep. A study of geomagnetic storms
 1731 A study of geomagnetic storms. *Geophysical Journal International*543547–573.
 1732 <https://academic.oup.com/gji/article-lookup/doi/10.1111/j.1365-246X.1978.tb05494.x>
 1733 10.1111/j.1365-246X.1978.tb05494.x
- 1734 Powell1999Powell, KG., Roe, PL., Linde, TJ., Gombosi, TI. De Zeeuw, DL. 1999sep.

- 1735 A Solution-Adaptive Upwind Scheme for Ideal Magnetohydrodynamics A Solution-
 1736 Adaptive Upwind Scheme for Ideal Magnetohydrodynamics. *Journal of Computational*
 1737 *Physics*1542284–309. <http://linkinghub.elsevier.com/retrieve/pii/S002199919996299X>
 1738 10.1006/jcph.1999.6299
- 1739 Pulkkinen2013Pulkkinen, A., Rastätter, L., Kuznetsova, M., Singer, H., Balch, C., Weimer,
 1740 D.Weigel, R. 2013jun. Community-wide validation of geospace model ground
 1741 magnetic field perturbation predictions to support model transition to operations
 1742 Community-wide validation of geospace model ground magnetic field perturbation
 1743 predictions to support model transition to operations. *Space Weather*116369–385.
 1744 <http://doi.wiley.com/10.1002/swe.20056> 10.1002/swe.20056
- 1745 Pytte1976GroundSignaturesPytte, T., Mcpherron, R. Kokubun, S. 197612. The Ground
 1746 Signatures of the Expansion Phase during Multiple Onset Substorms The ground sig-
 1747 natures of the expansion phase during multiple onset substorms. *Planetary and Space*
 1748 *Science*24121115-IN4. 10.1016/0032-0633(76)90149-5
- 1749 Pytte1978Pytte, T., McPherron, RL., Hones, EW. West, HI. 1978. Multiple-
 1750 satellite studies of magnetospheric substorms: Distinction between polar mag-
 1751 netic substorms and convection-driven negative bays Multiple-satellite studies of
 1752 magnetospheric substorms: Distinction between polar magnetic substorms and
 1753 convection-driven negative bays. *Journal of Geophysical Research*83A2663.
 1754 <http://doi.wiley.com/10.1029/JA083iA02p00663> 10.1029/JA083iA02p00663
- 1755 Pytte1976MultiplesatelliteStudiesPytte, T., McPherron, RL., Kivelson, MG., West, HI.
 1756 Hones, EW. 197612. Multiple-Satellite Studies of Magnetospheric Substorms: Radial
 1757 Dynamics of the Plasma Sheet Multiple-satellite studies of magnetospheric substorms:
 1758 Radial dynamics of the plasma sheet. *Journal of Geophysical Research*81345921-5933.
 1759 10.1029/JA081i034p05921
- 1760 Rae2009Rae, IJ., Mann, IR., Murphy, KR., Milling, DK., Parent, A., Angelopou-
 1761 los, V.Russell, CT. 2009jan. Timing and localization of ionospheric sig-
 1762 natures associated with substorm expansion phase onset Timing and local-
 1763 ization of ionospheric signatures associated with substorm expansion phase
 1764 onset. *Journal of Geophysical Research: Space Physics*114A1A00C09.
 1765 <https://agupubs.onlinelibrary.wiley.com/doi/full/10.1029/2008JA013559>
 1766 10.1029/2008JA013559
- 1767 Raeder2001bRaeder, J., McPherron, RL., Frank, LA., Kokubun, S., Lu, G., Mukai,

- 1768 T.Slavin, JA. 2001jan. Global simulation of the Geospace Environment Model-
1769 ing substorm challenge event Global simulation of the Geospace Environment Mod-
1770 eling substorm challenge event. *Journal of Geophysical Research*106A1381–395.
1771 <http://doi.wiley.com/10.1029/2000JA000605> 10.1029/2000JA000605
- 1772 Raeder2010aRaeder, J., Zhu, P., Ge, Y. Siscoe, G. 2010dec. Open Geospace General
1773 Circulation Model simulation of a substorm: Axial tail instability and ballooning mode
1774 preceding substorm onset Open Geospace General Circulation Model simulation of a
1775 substorm: Axial tail instability and ballooning mode preceding substorm onset. *Journal*
1776 *of Geophysical Research*115A5A00I16. <http://doi.wiley.com/10.1029/2010JA015876>
1777 10.1029/2010JA015876
- 1778 Ridley2004Ridley, A., Gombosi, T. Dezeew, D. 200402. Ionospheric control of the
1779 magnetosphere: conductance Ionospheric control of the magnetosphere: conductance.
1780 *Annales Geophysicae*22567-584. 10.5194/angeo-22-567-2004
- 1781 Ridley2003Ridley, AJ., Gombosi, TI., De~Zeeuw, DL., Clauer, CR. Richmond, AD.
1782 2003. Ionospheric control of the magnetosphere: Thermospheric neutral winds Iono-
1783 spheric control of the magnetosphere: Thermospheric neutral winds. *J. Geophys.*
1784 *Res.*108A81328. 10.1029/2002JA009464
- 1785 Rostoker2002Rostoker, G. 2002jul. Identification of substorm expansive phase
1786 onsets Identification of substorm expansive phase onsets. *Journal of Geo-*
1787 *physical Research*107A71137. <http://doi.wiley.com/10.1029/2001JA003504>
1788 10.1029/2001JA003504
- 1789 Rostoker1980Rostoker, G., Akasofu, SI., Foster, J., Greenwald, R., Kamide, Y.,
1790 Kawasaki, K.Russell, C. 1980apr. Magnetospheric substorms—definition and
1791 signatures Magnetospheric substorms—definition and signatures. *Journal of Geo-*
1792 *physical Research*85A41663. <http://doi.wiley.com/10.1029/JA085iA04p01663>
1793 10.1029/JA085iA04p01663
- 1794 Runov2009Runov, A., Angelopoulos, V., Sitnov, MI., Sergeev, VA., Bonnell, J., McFadden,
1795 JP.Auster, U. 2009jul. THEMIS observations of an earthward-propagating dipolarization
1796 front THEMIS observations of an earthward-propagating dipolarization front. *Geo-*
1797 *physical Research Letters*3614L14106. <http://doi.wiley.com/10.1029/2009GL038980>
1798 10.1029/2009GL038980
- 1799 Runov2012Runov, A., Angelopoulos, V. Zhou, XZ. 2012may. Multipoint observations
1800 of dipolarization front formation by magnetotail reconnection Multipoint observations

- 1801 of dipolarization front formation by magnetotail reconnection. *Journal of Geophysical*
 1802 *Research: Space Physics*117A5A05230. <http://doi.wiley.com/10.1029/2011JA017361>
 1803 10.1029/2011JA017361
- 1804 Russell2000Russell, CT. 2000oct. How northward turnings of the IMF can
 1805 lead to substorm expansion onsets How northward turnings of the IMF can lead
 1806 to substorm expansion onsets. *Geophysical Research Letters*27203257–3259.
 1807 <http://doi.wiley.com/10.1029/2000GL011910> 10.1029/2000GL011910
- 1808 Samson1986Samson, J. Yeung, K. 1986nov. Some generalizations on the
 1809 method of superposed epoch analysis Some generalizations on the method of
 1810 superposed epoch analysis. *Planetary and Space Science*34111133–1142.
 1811 <http://linkinghub.elsevier.com/retrieve/pii/0032063386900255> 10.1016/0032-
 1812 0633(86)90025-5
- 1813 Sauvaud1980Sauvaud, JA. Winckler, J. 1980. Dynamics of plasma, energetic par-
 1814 ticles, and fields near synchronous orbit in the nighttime sector during magneto-
 1815 spheric substorms Dynamics of plasma, energetic particles, and fields near syn-
 1816 chronous orbit in the nighttime sector during magnetospheric substorms. *Journal of*
 1817 *Geophysical Research*85A52043. <http://doi.wiley.com/10.1029/JA085iA05p02043>
 1818 10.1029/JA085iA05p02043
- 1819 Sazykin2000Sazykin, SY. 2000. Theoretical Studies of Penetration of Magnetospheric
 1820 Electric Fields to the Ionosphere Theoretical Studies of Penetration of Magnetospheric
 1821 Electric Fields to the Ionosphere . Logan, UtahUtah State University.
- 1822 Schmid2011Schmid, D., Volwerk, M., Nakamura, R., Baumjohann, W. Heyn, M.
 1823 2011sep. A statistical and event study of magnetotail dipolarization fronts A statistical
 1824 and event study of magnetotail dipolarization fronts. *Annales Geophysicae*2991537–
 1825 1547. <http://www.ann-geophys.net/29/1537/2011/> 10.5194/angeo-29-1537-2011
- 1826 Sergeev2012Sergeev, VA., Angelopoulos, V. Nakamura, R. 2012mar. Re-
 1827 cent advances in understanding substorm dynamics Recent advances in un-
 1828 derstanding substorm dynamics. *Geophysical Research Letters*395L05101.
 1829 <http://doi.wiley.com/10.1029/2012GL050859> 10.1029/2012GL050859
- 1830 Sergeev1990Sergeev, VA., Tanskanen, P., Mursula, K., Korth, A. Elphic, RC.
 1831 1990apr. Current sheet thickness in the near-Earth plasma sheet during sub-
 1832 storm growth phase Current sheet thickness in the near-Earth plasma sheet dur-
 1833 ing substorm growth phase. *Journal of Geophysical Research*95A43819.

- 1834 <http://doi.wiley.com/10.1029/JA095iA04p03819> 10.1029/JA095iA04p03819
- 1835 Singer1996Singer, H., Matheson, L., Grubb, R., Newman, A. Bouwer, D. 1996oct.
- 1836 Monitoring space weather with the GOES magnetometers Monitoring space weather
- 1837 with the GOES magnetometers. ER. Washwell (), Proceedings of SPIE Pro-
- 1838 ceedings of spie (2812, 299–308). International Society for Optics and Photon-
- 1839 ics. <http://proceedings.spiedigitallibrary.org/proceeding.aspx?articleid=1021197>
- 1840 10.1117/12.254077
- 1841 Slavin1989Slavin, JA., Baker, DN., Craven, JD., Elphic, RC., Fairfield, DH., Frank,
- 1842 LA.Zwickl, RD. 1989nov. CDAW 8 observations of plasmoid signatures in the ge-
- 1843 omagnetic tail: An assessment CDAW 8 observations of plasmoid signatures in the
- 1844 geomagnetic tail: An assessment. Journal of Geophysical Research94A1115153.
- 1845 <http://doi.wiley.com/10.1029/JA094iA11p15153> 10.1029/JA094iA11p15153
- 1846 Slavin1992Slavin, JA., Smith, MF., Mazur, EL., Baker, DN., Iyemori, T., Singer, HJ.
- 1847 Greenstadt, EW. 1992apr. ISEE 3 plasmoid and TCR observations during an ex-
- 1848 tended interval of substorm activity ISEE 3 plasmoid and TCR observations during
- 1849 an extended interval of substorm activity. Geophysical Research Letters198825–828.
- 1850 <http://doi.wiley.com/10.1029/92GL00394> 10.1029/92GL00394
- 1851 Slinker1995Slinker, SP., Fedder, JA. Lyon, JG. 1995apr. Plasmoid formation and evo-
- 1852 lution in a numerical simulation of a substorm Plasmoid formation and evolution in
- 1853 a numerical simulation of a substorm. Geophysical Research Letters227859–862.
- 1854 <http://doi.wiley.com/10.1029/95GL00300> 10.1029/95GL00300
- 1855 Stephenson2000Stephenson, DB. 2000apr. Use of the “Odds Ratio” for Diagnos-
- 1856 ing Forecast Skill Use of the “Odds Ratio” for Diagnosing Forecast Skill. Weather
- 1857 and Forecasting152221–232. <http://journals.ametsoc.org/doi/abs/10.1175/1520-0434>
- 1858 10.1175/1520-0434(2000)015<0221:UOTORF>2.0.CO;2
- 1859 Sugiura1968Sugiura, M., Skillman, TL., Ledley, BG. Heppner, JP. 1968nov. Propa-
- 1860 gation of the sudden commencement of July 8, 1966, to the magnetotail Propagation
- 1861 of the sudden commencement of July 8, 1966, to the magnetotail. Journal of Geo-
- 1862 physical Research73216699–6709. <http://doi.wiley.com/10.1029/JA073i021p06699>
- 1863 10.1029/JA073i021p06699
- 1864 Toffoletto2003Toffoletto, F., Sazykin, S., Spiro, R. Wolf, R. 2003. Inner magne-
- 1865 tospheric modeling with the Rice Convection Model Inner magnetospheric mod-
- 1866 eling with the Rice Convection Model. Space Science Reviews1071-2175–196.

- 1867 <http://link.springer.com/10.1023/A:1025532008047> 10.1023/A:1025532008047
- 1868 Toth2016Tóth, G., Jia, X., Markidis, S., Peng, IB., Chen, Y., Daldorff, LKS.Dorelli, JC.
1869 2016feb. Extended magnetohydrodynamics with embedded particle-in-cell simula-
1870 tion of Ganymede's magnetosphere Extended magnetohydrodynamics with embedded
1871 particle-in-cell simulation of Ganymede's magnetosphere. *Journal of Geophysical Re-*
1872 *search: Space Physics*12121273–1293. <http://doi.wiley.com/10.1002/2015JA021997>
1873 10.1002/2015JA021997
- 1874 Toth2008Tóth, G., Ma, Y. Gombosi, TI. 2008jul. Hall magneto-
1875 hydrodynamics on block-adaptive grids Hall magnetohydrodynamics on
1876 block-adaptive grids. *Journal of Computational Physics*227146967–
1877 6984. <http://linkinghub.elsevier.com/retrieve/pii/S0021999108002076>
1878 10.1016/j.jcp.2008.04.010
- 1879 Toth2005Tóth, G., Sokolov, IV., Gombosi, TI., Chesney, DR., Clauer, CR., De Zeeuw,
1880 DL.Kóta, J. 2005. Space Weather Modeling Framework: A new tool for the space
1881 science community Space Weather Modeling Framework: A new tool for the space
1882 science community. *Journal of Geophysical Research: Space Physics*110A12A12226.
1883 <http://dx.doi.org/10.1029/2005JA011126> 10.1029/2005JA011126
- 1884 Toth2012Tóth, G., van der Holst, B., Sokolov, IV., Zeeuw, DLD., Gombosi, TI., Fang,
1885 F.Opher, M. 2012. Adaptive Numerical Algorithms in Space Weather Modeling Adap-
1886 tive Numerical Algorithms in Space Weather Modeling. *J. Comput. Phys.*2313870–903.
1887 10.1016/j.jcp.2011.02.006
- 1888 Walach2015Walach, MT. Milan, SE. 2015mar. Are steady magnetospheric convec-
1889 tion events prolonged substorms? Are steady magnetospheric convection events pro-
1890 longed substorms? *Journal of Geophysical Research: Space Physics*12031751–1758.
1891 <http://doi.wiley.com/10.1002/2014JA020631> 10.1002/2014JA020631
- 1892 Wang2010Wang, H., Ma, S. Ridley, AJ. 2010mar. Comparative study of a substorm event
1893 by satellite observation and model simulation Comparative study of a substorm event
1894 by satellite observation and model simulation. *Chinese Science Bulletin*559857–864.
1895 <http://link.springer.com/10.1007/s11434-009-0282-4> 10.1007/s11434-009-0282-4
- 1896 Welling2017ExploringPredictivePerformanceWelling, DT., Anderson, BJ., Crowley, G.,
1897 Pulkkinen, AA. Rastätter, L. 201701. Exploring Predictive Performance: A Reanal-
1898 ysis of the Geospace Model Transition Challenge Exploring predictive performance:
1899 A reanalysis of the geospace model transition challenge. *Space Weather*151192-203.

- 1900 10.1002/2016SW001505
- 1901 Welling2016gpwWelling, DT., Barakat, AR., Eccles, JV., Schunk, RW. Chappell, CR.
1902 2016. Coupling the Generalized Polar Wind Model to Global Magnetohydrodynamics:
1903 Initial Results Coupling the Generalized Polar Wind Model to Global Magneto-
1904 dynamics: Initial Results. *Magnetosphere-Ionosphere Coupling in the Solar System*
1905 *Magnetosphere-ionosphere coupling in the solar system* (222, 179–194). Washington,
1906 DC American Geophysical Union (AGU). 10.15142/T3C88J
- 1907 Welling2010aWelling, DT. Ridley, AJ. 2010mar. Validation of SWMF magnetic field
1908 and plasma Validation of SWMF magnetic field and plasma. *Space Weather*83S03002.
1909 <http://doi.wiley.com/10.1029/2009SW000494> 10.1029/2009SW000494
- 1910 Weygand2008Weygand, JM., McPherron, R., Kauristie, K., Frey, H. Hsu, TS. 2008dec.
1911 Relation of auroral substorm onset to local AL index and dispersionless particle in-
1912 jections Relation of auroral substorm onset to local AL index and dispersionless par-
1913 ticle injections. *Journal of Atmospheric and Solar-Terrestrial Physics*70182336–
1914 2345. <https://www.sciencedirect.com/science/article/pii/S1364682608002563>
1915 10.1016/J.JASTP.2008.09.030
- 1916 Wild2009aWild, JA., Woodfield, EE. Morley, SK. 2009sep. On the triggering of au-
1917 roral substorms by northward turnings of the interplanetary magnetic field On the
1918 triggering of auroral substorms by northward turnings of the interplanetary magnetic
1919 field. *Annales Geophysicae*2793559–3570. <http://www.ann-geophys.net/27/3559/2009/>
1920 10.5194/angeo-27-3559-2009
- 1921 Wilks2011Wilks, DS. 2011. Statistical methods in the atmospheric sciences Statistical
1922 methods in the atmospheric sciences. Cambridge, MA Elsevier/Academic Press.
- 1923 Wilson2004Wilson, GR., Ober, DM., Germany, GA. Lund, EJ. 2004feb. Night-
1924 side auroral zone and polar cap ion outflow as a function of substorm size and
1925 phase Nightside auroral zone and polar cap ion outflow as a function of substorm
1926 size and phase. *Journal of Geophysical Research: Space Physics*109A2A02206.
1927 <http://doi.wiley.com/10.1029/2003JA009835> 10.1029/2003JA009835
- 1928 Wiltberger2010Wiltberger, M., Lotko, W., Lyon, JG., Damiano, P. Merkin, V. 2010oct.
1929 Influence of cusp O+ outflow on magnetotail dynamics in a multifluid MHD model
1930 of the magnetosphere Influence of cusp O+ outflow on magnetotail dynamics in
1931 a multifluid MHD model of the magnetosphere. *Journal of Geophysical Re-*
1932 *search: Space Physics*115A10A00J05. <http://doi.wiley.com/10.1029/2010JA015579>

- 1933 10.1029/2010JA015579
- 1934 Winglee2002Winglee, RM., Chua, D., Brittnacher, M., Parks, GK. Lu, G. 2002sep.
1935 Global impact of ionospheric outflows on the dynamics of the magnetosphere and cross-
1936 polar cap potential Global impact of ionospheric outflows on the dynamics of the mag-
1937 netosphere and cross-polar cap potential. *Journal of Geophysical Research*107A91237.
1938 <http://doi.wiley.com/10.1029/2001JA000214> 10.1029/2001JA000214
- 1939 Wolf1982Wolf, RA., Harel, M., Spiro, RW., Voigt, GH., Reiff, PH. Chen, CKK. 1982.
1940 Computer simulation of inner magnetospheric dynamics for the magnetic storm of
1941 July 29, 1977 Computer simulation of inner magnetospheric dynamics for the mag-
1942 netic storm of July 29, 1977. *Journal of Geophysical Research*87A85949–5962.
1943 <http://doi.wiley.com/10.1029/JA087iA08p05949> 10.1029/JA087iA08p05949
- 1944 Yu2008bYu, Y. Ridley, AJ. 2008may. Validation of the space weather mod-
1945 eling framework using ground-based magnetometers Validation of the space
1946 weather modeling framework using ground-based magnetometers. *Space*
1947 *Weather*65S05002. <http://www.agu.org/pubs/crossref/2008/2007SW000345.shtml>
1948 <http://doi.wiley.com/10.1029/2007SW000345> 10.1029/2007SW000345
- 1949 Yu2010cYu, Y., Ridley, AJ., Welling, DT. Tóth, G. 201008. Including Gap Region Field-
1950 Aligned Currents and Magnetospheric Currents in the MHD Calculation of Ground-
1951 Based Magnetic Field Perturbations Including gap region field-aligned currents and
1952 magnetospheric currents in the MHD calculation of ground-based magnetic field per-
1953 turbations. *Journal of Geophysical Research*115A8A08207. 10.1029/2009JA014869
- 1954 Zhu2004Zhu, P., Bhattacharjee, A. Ma, ZW. 2004nov. Finite k y balloon-
1955 ing instability in the near-Earth magnetotail Finite k y ballooning instability in
1956 the near-Earth magnetotail. *Journal of Geophysical Research*109A11A11211.
1957 <http://doi.wiley.com/10.1029/2004JA010505> 10.1029/2004JA010505

1958 **References**

- 1959 Aikio1999Aikio, AT., Sergeev, VA., Shukhtina, MA., Vagina, LI., Angelopoulos, V.
1960 Reeves, GD. 1999jun. Characteristics of pseudobreakups and substorms observed in
1961 the ionosphere, at the geosynchronous orbit, and in the midtail Characteristics of pseu-
1962 dobreakups and substorms observed in the ionosphere, at the geosynchronous orbit, and
1963 in the midtail. *Journal of Geophysical Research: Space Physics*104A612263–12287.
1964 <http://doi.wiley.com/10.1029/1999JA900118> 10.1029/1999JA900118

- 1965 Akasofu1960Akasofu, SI. 1960sep. Large-scale auroral motions and polar magnetic distur-
 1966 bances—I A polar disturbance at about 1100 hours on 23 september 1957 Large-scale
 1967 auroral motions and polar magnetic disturbances—I A polar disturbance at about 1100
 1968 hours on 23 september 1957. *Journal of Atmospheric and Terrestrial Physics*19110–25.
 1969 <http://www.sciencedirect.com/science/article/pii/0021916960901033> 10.1016/0021-
 1970 9169(60)90103-3
- 1971 Akasofu1964Akasofu, SI. 1964apr. The development of the auroral substorm
 1972 The development of the auroral substorm. *Planetary and Space Science*1014273.
 1973 <https://www.sciencedirect.com/science/article/pii/0032063364901515> 10.1016/0032-
 1974 0633(64)90151-5
- 1975 Akasofu1968PolarMagnetosphericSubstormsAkasofu, SI. 1968. *Polar and Magnetospheric*
 1976 *Substorms Polar and Magnetospheric Substorms*. Dordrecht, The NetherlandsSpringer
 1977 Netherlands.
- 1978 Akasofu1969Akasofu, SI. Meng, CI. 1969jan. A study of polar magnetic substorms
 1979 A study of polar magnetic substorms. *Journal of Geophysical Research*741293–313.
 1980 <http://doi.wiley.com/10.1029/JA074i001p00293> 10.1029/JA074i001p00293
- 1981 Angelopoulos2008Angelopoulos, V., McFadden, JP., Larson, D., Carlson, CW., Mende,
 1982 SB., Frey, H.Kepko, L. 2008aug. Tail reconnection triggering substorm onset. Tail
 1983 reconnection triggering substorm onset. *Science (New York, N.Y.)*3215891931–5.
 1984 <http://www.ncbi.nlm.nih.gov/pubmed/18653845> 10.1126/science.1160495
- 1985 Baker1996NeutralLineModelBaker, DN., Pulkkinen, TI., Angelopoulos, V., Baumjohann,
 1986 W. McPherron, RL. 199606. Neutral Line Model of Substorms: Past Results and
 1987 Present View Neutral line model of substorms: Past results and present view. *Journal of*
 1988 *Geophysical Research: Space Physics*101A612975-13010. 10.1029/95JA03753
- 1989 Barnston1999Barnston, AG., Leetmaa, A., Kousky, VE., Livezey, RE., O’Lenic,
 1990 E., Van den Dool, H.Unger, DA. 1999sep. NCEP Forecasts of the El Niño
 1991 of 1997-98 and Its U.S. Impacts NCEP Forecasts of the El Niño of 1997-98 and
 1992 Its U.S. Impacts. *Bulletin of the American Meteorological Society*8091829–
 1993 1852. <http://journals.ametsoc.org/doi/abs/10.1175/1520-0477> 10.1175/1520-
 1994 0477(1999)080<1829:NFOTEN>2.0.CO;2
- 1995 Birn2013Birn, J. Hesse, M. 2013jun. The substorm current wedge in MHD simu-
 1996 lations The substorm current wedge in MHD simulations. *Journal of Geophysical*
 1997 *Research: Space Physics*11863364–3376. <http://doi.wiley.com/10.1002/jgra.50187>

- 1998 10.1002/jgra.50187
- 1999 Birn1981Birn, J. Hones Jr., EW. 1981. Three-Dimensional Computer Modeling of Dy-
2000 namic Reconnection in the Geomagnetic Tail Three-Dimensional Computer Modeling
2001 of Dynamic Reconnection in the Geomagnetic Tail. *J. Geophys. Res.*86A86802–6808.
2002 <http://dx.doi.org/10.1029/JA086iA08p06802> 10.1029/JA086iA08p06802
- 2003 Birn2011Birn, J., Nakamura, R., Panov, EV. Hesse, M. 2011jan. Bursty bulk flows and
2004 dipolarization in MHD simulations of magnetotail reconnection Bursty bulk flows and
2005 dipolarization in MHD simulations of magnetotail reconnection. *Journal of Geophysical*
2006 *Research: Space Physics*116A1A01210. <http://doi.wiley.com/10.1029/2010JA016083>
2007 10.1029/2010JA016083
- 2008 Birn1998Birn, J., Thomsen, MF., Borovsky, JE., Reeves, GD., McComas, DJ., Belian, RD.
2009 Hesse, M. 1998may. Substorm electron injections: Geosynchronous observations and
2010 test particle simulations Substorm electron injections: Geosynchronous observations and
2011 test particle simulations. *Journal of Geophysical Research: Space Physics*103A59235–
2012 9248. <http://doi.wiley.com/10.1029/97JA02635> 10.1029/97JA02635
- 2013 Boakes2009Boakes, PD., Milan, SE., Abel, GA., Freeman, MP., Chisham, G. Hubert, B.
2014 2009. A statistical study of the open magnetic flux content of the magnetosphere at
2015 the time of substorm onset A statistical study of the open magnetic flux content of the
2016 magnetosphere at the time of substorm onset. *Geophysical Research Letters*364L04105.
2017 <http://dx.doi.org/10.1029/2008GL037059> L04105 10.1029/2008GL037059
- 2018 Bonnevier1970Bonnevier, B., Boström, R. Rostoker, G. 1970jan. A three-dimensional
2019 model current system for polar magnetic substorms A three-dimensional model current
2020 system for polar magnetic substorms. *Journal of Geophysical Research*751107–122.
2021 <http://doi.wiley.com/10.1029/JA075i001p00107> 10.1029/JA075i001p00107
- 2022 Borovsky1993Borovsky, JE., Nemzek, RJ. Belian, RD. 1993mar. The occur-
2023 rence rate of magnetospheric-substorm onsets: Random and periodic substorms
2024 The occurrence rate of magnetospheric-substorm onsets: Random and periodic
2025 substorms. *Journal of Geophysical Research: Space Physics*98A33807–3813.
2026 <http://doi.wiley.com/10.1029/92JA02556> 10.1029/92JA02556
- 2027 Borovsky2017Borovsky, JE. Yakymenko, K. 2017mar. Substorm occurrence rates,
2028 substorm recurrence times, and solar wind structure Substorm occurrence rates,
2029 substorm recurrence times, and solar wind structure. *Journal of Geophysical Re-*
2030 *search: Space Physics*12232973–2998. <http://doi.wiley.com/10.1002/2016JA023625>

- 2031 10.1002/2016JA023625
- 2032 Burrell2018SnakesOnASpaceshipBurrell, AG., Halford, AJ., Klenzing, J., Stoneback, RA.,
2033 Morley, SK., Annex, AM.Ma, J. 201811. Snakes on a Spaceship - An Overview
2034 of Python in Heliophysics Snakes on a Spaceship - An Overview of Python in He-
2035 liophysics. *Journal of Geophysical Research: Space Physics*1231210384-10402.
2036 10.1029/2018JA025877
- 2037 Caan1975Caan, MN., McPherron, RL. Russell, CT. 1975jan. Substorm and in-
2038 terplanetary magnetic field effects on the geomagnetic tail lobes Substorm and in-
2039 terplanetary magnetic field effects on the geomagnetic tail lobes. *Journal of Geo-*
2040 *physical Research*801191–194. <http://doi.wiley.com/10.1029/JA080i001p00191>
2041 10.1029/JA080i001p00191
- 2042 Caan1977Caan, MN., McPherron, RL. Russell, CT. 1977oct. Characteristics of the as-
2043 sociation between the interplanetary magnetic field and substorms Characteristics of
2044 the association between the interplanetary magnetic field and substorms. *Journal of*
2045 *Geophysical Research*82294837–4842. <http://doi.wiley.com/10.1029/JA082i029p04837>
2046 10.1029/JA082i029p04837
- 2047 Caan1978Caan, MN., McPherron, RL. Russell, CT. 1978mar. The statistical
2048 magnetic signature of magnetospheric substorms The statistical magnetic signa-
2049 ture of magnetospheric substorms. *Planetary and Space Science*263269–279.
2050 <https://www.sciencedirect.com/science/article/pii/0032063378900922> 10.1016/0032-
2051 0633(78)90092-2
- 2052 Carter2016ROCingCarter, JV., Pan, J., Rai, SN. Galandiuk, S. 201606. ROC-Ing
2053 along: Evaluation and Interpretation of Receiver Operating Characteristic Curves ROC-
2054 ing along: Evaluation and interpretation of receiver operating characteristic curves.
2055 *Surgery*15961638-1645. 10.1016/j.surg.2015.12.029
- 2056 Cayton2007Cayton, T. Belian, RD. 2007. Numerical modeling of the Syn-
2057 chronous Orbit Particle Analyzer (SOPA, Version 2) that flew on S/C 1990-095 Nu-
2058 merical modeling of the Synchronous Orbit Particle Analyzer (SOPA, Version 2)
2059 that flew on S/C 1990-095 . Los Alamos, NMLos Alamos National Laboratory.
2060 <http://permalink.lanl.gov/object/tr?what=info:lanl-repo/lareport/LA-14335>
- 2061 Chen2017Chen, Y., Tóth, G., Cassak, P., Jia, X., Gombosi, TI., Slavin, JA.Henderson,
2062 MG. 2017oct. Global Three-Dimensional Simulation of Earth's Dayside Recon-
2063 nection Using a Two-Way Coupled Magnetohydrodynamics With Embedded Particle-

- 2064 in-Cell Model: Initial Results Global Three-Dimensional Simulation of Earth's Day-
 2065 side Reconnection Using a Two-Way Coupled Magnetohydrodynamics With Em-
 2066 bedded Particle-in-Cell Model: Initial Results. *Journal of Geophysical Research:*
 2067 *Space Physics*1221010,318–10,335. <http://doi.wiley.com/10.1002/2017JA024186>
 2068 10.1002/2017JA024186
- 2069 Chu2015Chu, X., McPherron, R.L., Hsu, T.S. Angelopoulos, V. 2015apr. So-
 2070 lar cycle dependence of substorm occurrence and duration: Implications for on-
 2071 set Solar cycle dependence of substorm occurrence and duration: Implications
 2072 for onset. *Journal of Geophysical Research A: Space Physics*12042808–2818.
 2073 <http://doi.wiley.com/10.1002/2015JA021104> 10.1002/2015JA021104
- 2074 Clauer1985Clauer, C.R. Kamide, Y. 1985. DP 1 and DP 2 current sys-
 2075 tems for the March 22, 1979 substorms DP 1 and DP 2 current systems for
 2076 the March 22, 1979 substorms. *Journal of Geophysical Research*90A21343.
 2077 <http://doi.wiley.com/10.1029/JA090iA02p01343> 10.1029/JA090iA02p01343
- 2078 Conover1999Conover, W.J. 1999. Practical nonparametric statistics Practical nonparametric
 2079 statistics (3rd). Hoboken, NJWiley.
- 2080 Coroniti1972Coroniti, F.V. Kennel, C.F. 1972jul. Changes in magnetospheric config-
 2081 uration during the substorm growth phase Changes in magnetospheric configuration
 2082 during the substorm growth phase. *Journal of Geophysical Research*77193361–3370.
 2083 <http://doi.wiley.com/10.1029/JA077i019p03361> 10.1029/JA077i019p03361
- 2084 Cummings1968Cummings, W.D. Coleman, P.J. 1968jul. Simultaneous Magnetic Field
 2085 Variations at the Earth's Surface and at Synchronous, Equatorial Distance. Part I. Bay-
 2086 Associated Events Simultaneous Magnetic Field Variations at the Earth's Surface and at
 2087 Synchronous, Equatorial Distance. Part I. Bay-Associated Events. *Radio Science*37758–
 2088 761. <http://doi.wiley.com/10.1002/rds196837758> 10.1002/rds196837758
- 2089 Davis1966Davis, T.N. Sugiura, M. 1966feb. Auroral electrojet ac-
 2090 tivity index AE and its universal time variations Auroral electrojet activ-
 2091 ity index AE and its universal time variations. *Journal of Geophysi-*
 2092 *cal Research*713785–801. <http://dx.doi.org/10.1029/JZ071i003p00785>
 2093 <http://doi.wiley.com/10.1029/JZ071i003p00785> 10.1029/JZ071i003p00785
- 2094 DeZeeuw2000De Zeeuw, D., Gombosi, T., Groth, C., Powell, K. Stout, Q. 2000. An
 2095 adaptive MHD method for global space weather simulations An adaptive MHD method
 2096 for global space weather simulations. *IEEE Transactions on Plasma Science*2861956–

- 2097 1965. <http://ieeexplore.ieee.org/document/902224/> 10.1109/27.902224
- 2098 DeForest1971DeForest, SE. McIlwain, CE. 1971jun. Plasma clouds in the magnetosphere
2099 Plasma clouds in the magnetosphere. *Journal of Geophysical Research*76163587–3611.
2100 <http://doi.wiley.com/10.1029/JA076i016p03587> 10.1029/JA076i016p03587
- 2101 Eastwood2005Eastwood, JP., Sibeck, DG., Slavin, JA., Goldstein, ML., Lavraud, B., Sit-
2102 nov, M.Dandouras, I. 2005jun. Observations of multiple X-line structure in the
2103 Earth's magnetotail current sheet: A Cluster case study Observations of multiple X-
2104 line structure in the Earth's magnetotail current sheet: A Cluster case study. *Geo-
2105 physical Research Letters*3211L11105. <http://doi.wiley.com/10.1029/2005GL022509>
2106 10.1029/2005GL022509
- 2107 Ekelund2012ROCCurvesEkelund, S. 201203. ROC Curves—What Are They and How
2108 Are They Used? ROC Curves—What are They and How are They Used? *Point of
2109 Care*11116-21. 10.1097/POC.0b013e318246a642
- 2110 El-Alaoui2009El-Alaoui, M., Ashour-Abdalla, M., Walker, RJ., Perroomian, V., Richard,
2111 RL., Angelopoulos, V. Runov, A. 2009aug. Substorm evolution as revealed
2112 by THEMIS satellites and a global MHD simulation Substorm evolution as re-
2113 vealed by THEMIS satellites and a global MHD simulation. *Journal of Geo-
2114 physical Research*114A8A08221. <http://doi.wiley.com/10.1029/2009JA014133>
2115 10.1029/2009JA014133
- 2116 Forsyth2014Forsyth, C., Fazakerley, AN., Rae, IJ., J. Watt, CE., Murphy, K., Wild,
2117 JA.Zhang, Y. 2014feb. In situ spatiotemporal measurements of the detailed azimuthal
2118 substructure of the substorm current wedge In situ spatiotemporal measurements of the
2119 detailed azimuthal substructure of the substorm current wedge. *Journal of Geophysical
2120 Research: Space Physics*1192927–946. <http://doi.wiley.com/10.1002/2013JA019302>
2121 10.1002/2013JA019302
- 2122 Forsyth2015Forsyth, C., Rae, IJ., Coxon, JC., Freeman, MP., Jackman, CM., Gjer-
2123 loev, J. Fazakerley, AN. 2015dec. A new technique for determining Sub-
2124 storm Onsets and Phases from Indices of the Electrojet (SOPHIE) A new tech-
2125 nique for determining Substorm Onsets and Phases from Indices of the Electrojet
2126 (SOPHIE). *Journal of Geophysical Research: Space Physics*1201210,592–10,606.
2127 <http://doi.wiley.com/10.1002/2015JA021343> 10.1002/2015JA021343
- 2128 Freeman2004Freeman, MP. Morley, SK. 2004jun. A minimal substorm
2129 model that explains the observed statistical distribution of times between sub-

- 2130 storms A minimal substorm model that explains the observed statistical distribu-
 2131 tion of times between substorms. *Geophysical Research Letters*3112L12807.
 2132 <http://doi.wiley.com/10.1029/2004GL019989> <http://dx.doi.org/10.1029/2004GL019989>
 2133 10.1029/2004GL019989
- 2134 Freeman2009Freeman, MP. Morley, SK. 2009nov. No evidence for externally trig-
 2135 gered substorms based on superposed epoch analysis of IMF B z No evidence for ex-
 2136 ternally triggered substorms based on superposed epoch analysis of IMF B z. *Geo-*
 2137 *physical Research Letters*3621L21101. <http://doi.wiley.com/10.1029/2009GL040621>
 2138 10.1029/2009GL040621
- 2139 Frey2010CommentSubstormTriggeringFrey, HU. 2010. Comment on “Substorm Triggering
 2140 by New Plasma Intrusion: THEMIS All-Sky Imager Observations” by Y. Nishimura
 2141 et Al. Comment on “Substorm triggering by new plasma intrusion: THEMIS all-sky
 2142 imager observations” by Y. Nishimura et al. *Journal of Geophysical Research: Space*
 2143 *Physics*115A12A12232. 10.1029/2010JA016113
- 2144 Frey2004Frey, HU., Mende, SB., Angelopoulos, V. Donovan, EF. 2004oct.
 2145 Substorm onset observations by IMAGE-FUV Substorm onset observa-
 2146 tions by IMAGE-FUV. *Journal of Geophysical Research*109A10A10304.
 2147 <http://doi.wiley.com/10.1029/2004JA010607> 10.1029/2004JA010607
- 2148 Fruhauff2017Frühauff, D. Glassmeier, KH. 2017nov. The Plasma Sheet as Natu-
 2149 ral Symmetry Plane for Dipolarization Fronts in the Earth’s Magnetotail The Plasma
 2150 Sheet as Natural Symmetry Plane for Dipolarization Fronts in the Earth’s Mag-
 2151 netotail. *Journal of Geophysical Research: Space Physics*1221111,373–11,388.
 2152 <http://doi.wiley.com/10.1002/2017JA024682> 10.1002/2017JA024682
- 2153 Fu2012Fu, HS., Khotyaintsev, YV., Vaivads, A., André, M. Huang, SY. 2012may.
 2154 Occurrence rate of earthward-propagating dipolarization fronts Occurrence rate of
 2155 earthward-propagating dipolarization fronts. *Geophysical Research Letters*3910L10101.
 2156 <http://doi.wiley.com/10.1029/2012GL051784> 10.1029/2012GL051784
- 2157 Ganushkina2015Ganushkina, NY., Amariutei, OA., Welling, D. Heynderickx, D. 2015jan.
 2158 Nowcast model for low-energy electrons in the inner magnetosphere Nowcast model
 2159 for low-energy electrons in the inner magnetosphere. *Space Weather*13116–34.
 2160 <http://doi.wiley.com/10.1002/2014SW001098> 10.1002/2014SW001098
- 2161 Gjerloev2012SuperMAGDataProcessingGjerloev, JW. 201209. The SuperMAG Data Pro-
 2162 cessing Technique The SuperMAG data processing technique. *Journal of Geophysical*

- 2163 Research: Space Physics117A9. 10.1029/2012JA017683
- 2164 Glocer2016Glocer, A., Rastätter, L., Kuznetsova, M., Pulkkinen, A., Singer, HJ., Balch,
2165 C.Wing, S. 2016jul. Community-wide validation of geospace model local K-index
2166 predictions to support model transition to operations Community-wide validation
2167 of geospace model local K-index predictions to support model transition to opera-
2168 tions. *Space Weather*147469–480. <http://doi.wiley.com/10.1002/2016SW001387>
2169 10.1002/2016SW001387
- 2170 Glocer2009pwomGlocer, A., Tóth, G., Gombosi, T. Welling, D. 2009may. Mod-
2171 eling ionospheric outflows and their impact on the magnetosphere, initial re-
2172 sults Modeling ionospheric outflows and their impact on the magnetosphere, ini-
2173 tial results. *Journal of Geophysical Research: Space Physics*114A5A05216.
2174 <http://doi.wiley.com/10.1029/2009JA014053> 10.1029/2009JA014053
- 2175 Glocer2009multifluidGlocer, A., Tóth, G., Ma, Y., Gombosi, T., Zhang, JC. Kistler, LM.
2176 2009dec. Multifluid Block-Adaptive-Tree Solar wind Roe-type Upwind Scheme: Mag-
2177 netospheric composition and dynamics during geomagnetic storms-Initial results Multi-
2178 fluid Block-Adaptive-Tree Solar wind Roe-type Upwind Scheme: Magnetospheric com-
2179 position and dynamics during geomagnetic storms-Initial results. *Journal of Geophysical*
2180 *Research: Space Physics*114A12A12203. <http://doi.wiley.com/10.1029/2009JA014418>
2181 10.1029/2009JA014418
- 2182 Haiducek2017Haiducek, JD., Welling, DT., Ganushkina, NY., Morley, SK. Ozturk,
2183 DS. 2017dec. SWMF Global Magnetosphere Simulations of January 2005: Ge-
2184 omagnetic Indices and Cross-Polar Cap Potential SWMF Global Magnetosphere
2185 Simulations of January 2005: Geomagnetic Indices and Cross-Polar Cap Poten-
2186 tial. *Space Weather*15121567–1587. <http://doi.wiley.com/10.1002/2017SW001695>
2187 10.1002/2017SW001695
- 2188 Hajra2016SupersubstormsHajra, R., Tsurutani, BT., Echer, E., Gonzalez, WD. Gjerloev,
2189 JW. 201608. Supersubstorms (SML < -2500 nT): Magnetic Storm and Solar Cy-
2190 cle Dependences Supersubstorms (SML < -2500 nT): Magnetic storm and solar cy-
2191 cle dependences. *Journal of Geophysical Research: Space Physics*12187805-7816.
2192 10.1002/2015JA021835
- 2193 Henderson2009Henderson, MG. 2009. Observational evidence for an inside-out sub-
2194 storm onset scenario Observational evidence for an inside-out substorm onset scenario.
2195 *Annales Geophysicae*2752129–2140. <http://www.ann-geophys.net/27/2129/2009/angeo->

- 2196 27-2129-2009.pdf 10.5194/angeo-27-2129-2009
- 2197 Hendry2013RapidRadiationBeltHendry, AT., Rodger, CJ., Clilverd, MA., Thomson, NR.,
 2198 Morley, SK. Raita, T. 201303. Rapid Radiation Belt Losses Occurring During
 2199 High-Speed Solar Wind Stream–Driven Storms: Importance of Energetic Electron
 2200 Precipitation Rapid Radiation Belt Losses Occurring During High-Speed Solar Wind
 2201 Stream–Driven Storms: Importance of Energetic Electron Precipitation. Dynamics of
 2202 the Earth’s Radiation Belts and Inner Magnetosphere Dynamics of the Earth’s Radiation
 2203 Belts and Inner Magnetosphere (199, 213-224). Washington, DC American Geophysical
 2204 cal Union (AGU). 10.1029/2012GM001299
- 2205 Heppner1955Heppner, JP. 1955mar. Note on the occurrence of world-wide S.S.C.’s dur-
 2206 ing the onset of negative bays at College, Alaska Note on the occurrence of world-
 2207 wide S.S.C.’s during the onset of negative bays at College, Alaska. Journal of
 2208 Geophysical Research60129–32. <http://doi.wiley.com/10.1029/JZ060i001p00029>
 2209 10.1029/JZ060i001p00029
- 2210 Hones1984PlasmaSheetBehaviorHones, EW. 1984. Plasma Sheet Behavior dur-
 2211 ing Substorms Plasma sheet behavior during substorms. Magnetic Reconnection
 2212 in Space and Laboratory Plasmas Magnetic Reconnection in Space and Laboratory
 2213 Plasmas (30, 178-184). Washington, DC American Geophysical Union (AGU).
 2214 10.1029/GM030p0178
- 2215 Hones1984Hones, EW., Birn, J., Baker, DN., Bame, SJ., Feldman, WC., Mc-
 2216 Comas, DJ.Tsurutani, BT. 1984oct. Detailed examination of a plas-
 2217 moid in the distant magnetotail with ISEE 3 Detailed examination of a plas-
 2218 moid in the distant magnetotail with ISEE 3. Geophysical Research
 2219 Letters11101046–1049. <http://dx.doi.org/10.1029/GL011i010p01046>
 2220 <http://doi.wiley.com/10.1029/GL011i010p01046> 10.1029/GL011i010p01046
- 2221 Honkonen2011aHonkonen, I., Palmroth, M., Pulkkinen, TI., Janhunen, P. Aikio, A.
 2222 2011jan. On large plasmoid formation in a global magnetohydrodynamic simulation
 2223 On large plasmoid formation in a global magnetohydrodynamic simulation. Annales
 2224 Geophysicae291167–179. <http://www.ann-geophys.net/29/167/2011/> 10.5194/angeo-
 2225 29-167-2011
- 2226 Hsu2003Hsu, TS. McPherron, RL. 2003jul. Occurrence frequencies of IMF
 2227 triggered and nontriggered substorms Occurrence frequencies of IMF triggered
 2228 and nontriggered substorms. Journal of Geophysical Research108A71307.

- 2229 <http://doi.wiley.com/10.1029/2002JA009442> 10.1029/2002JA009442
- 2230 Hsu2004Hsu, TS. McPherron, RL. 2004jul. Average characteristics of trig-
2231 gered and nontriggered substorms Average characteristics of triggered and
2232 nontriggered substorms. *Journal of Geophysical Research*109A7A07208.
2233 <http://doi.wiley.com/10.1029/2003JA009933> 10.1029/2003JA009933
- 2234 Hsu2012Hsu, TS. McPherron, RL. 2012nov. A statistical analysis
2235 of substorm associated tail activity A statistical analysis of substorm as-
2236 sociated tail activity. *Advances in Space Research*50101317–1343.
2237 <https://www.sciencedirect.com/science/article/pii/S0273117712004371>
2238 10.1016/J.ASR.2012.06.034
- 2239 Ieda2001Ieda, A., Fairfield, DH., Mukai, T., Saito, Y., Kokubun, S., Liou, K.Brittacher,
2240 MJ. 2001mar. Plasmoid ejection and auroral brightenings Plasmoid ejection and au-
2241 roral brightenings. *Journal of Geophysical Research: Space Physics*106A33845–3857.
2242 <http://doi.wiley.com/10.1029/1999JA000451> <http://dx.doi.org/10.1029/1999JA000451>
2243 10.1029/1999JA000451
- 2244 Iyemori1996Iyemori, T. Rao, DRK. 1996. Decay of the Dst field of geomagnetic dis-
2245 turbance after substorm onset and its implication to storm-substorm relation Decay
2246 of the Dst field of geomagnetic disturbance after substorm onset and its implication
2247 to storm-substorm relation. *Annales Geophysicae*146608–618. [http://www.ann-
2248 geophys.net/14/608/1996/](http://www.ann-geophys.net/14/608/1996/) 10.1007/s00585-996-0608-3
- 2249 Johnson2014triggeringJohnson, JR. Wing, S. 2014. External versus Internal Trig-
2250 gering of Substorms: An Information-Theoretical Approach External versus internal
2251 triggering of substorms: An information-theoretical approach. *Geophysical Research*
2252 *Letters*41165748-5754. 10.1002/2014GL060928
- 2253 Jordanova2017Jordanova, V., Delzanno, G., Henderson, M., Godinez, H., Jeffery,
2254 C., Lawrence, E.Horne, R. 2017nov. Specification of the near-Earth space
2255 environment with SHIELDS Specification of the near-Earth space environment
2256 with SHIELDS. *Journal of Atmospheric and Solar-Terrestrial Physics*177148-
2257 159. <https://www.sciencedirect.com/science/article/pii/S1364682617302729>
2258 10.1016/j.jastp.2017.11.006
- 2259 Juusola2011Juusola, L., Østgaard, N., Tanskanen, E., Partamies, N. Snekvik, K.
2260 2011oct. Earthward plasma sheet flows during substorm phases Earthward
2261 plasma sheet flows during substorm phases. *Journal of Geophysical Research:*

- 2262 Space Physics116A10A10228. <http://doi.wiley.com/10.1029/2011JA016852>
2263 10.1029/2011JA016852
- 2264 Kamide1974bKamide, Y. McIlwain, CE. 1974nov. The onset time of magne-
2265 topheric substorms determined from ground and synchronous satellite records
2266 The onset time of magnetospheric substorms determined from ground and syn-
2267 chronous satellite records. *Journal of Geophysical Research*79314787–4790.
2268 <http://doi.wiley.com/10.1029/JA079i031p04787> 10.1029/JA079i031p04787
- 2269 Kamide1974Kamide, Y., Yasuhara, F. Akasofu, SI. 1974aug. On the cause of
2270 northward magnetic field along the negative X axis during magnetospheric sub-
2271 storms On the cause of northward magnetic field along the negative X axis dur-
2272 ing magnetospheric substorms. *Planetary and Space Science*2281219–1229.
2273 <https://www.sciencedirect.com/science/article/pii/0032063374900063> 10.1016/0032-
2274 0633(74)90006-3
- 2275 Katus2013GeomagneticIndicesKatus, RM. Liemohn, MW. 201308. Similarities and Dif-
2276 ferences in Low- to Middle-Latitude Geomagnetic Indices Similarities and differences in
2277 low- to middle-latitude geomagnetic indices. *Journal of Geophysical Research: Space*
2278 *Physics*11885149-5156. 10.1002/jgra.50501
- 2279 Kaufmann1987Kaufmann, RL. 1987. Substorm currents: Growth phase and onset Sub-
2280 storm currents: Growth phase and onset. *Journal of Geophysical Research*92A77471.
2281 <http://doi.wiley.com/10.1029/JA092iA07p07471> 10.1029/JA092iA07p07471
- 2282 Kauristie2017Kauristie, K., Morschhauser, A., Olsen, N., Finlay, CC., McPherron, RL.,
2283 Gjerloev, JW. Opgenoorth, HJ. 2017mar. On the Usage of Geomagnetic Indices
2284 for Data Selection in Internal Field Modelling On the Usage of Geomagnetic Indices
2285 for Data Selection in Internal Field Modelling. *Space Science Reviews*2061-461–90.
2286 <http://link.springer.com/10.1007/s11214-016-0301-0> 10.1007/s11214-016-0301-0
- 2287 Kepko2004RelativeTimingSubstormKepko, L. 2004. Relative Timing of Substorm On-
2288 set Phenomena Relative timing of substorm onset phenomena. *Journal of Geophysical*
2289 *Research*109A4. 10.1029/2003JA010285
- 2290 Kepko2001CommentLowLatitudePi2Kepko, L. McPherron, RL. 2001. Comment on
2291 “Evaluation of Low-Latitude Pi2 Pulsations as Indicators of Substorm Onset Using Po-
2292 lar Ultraviolet Imagery” by K. Liou, et Al. Comment on “Evaluation of low-latitude
2293 Pi2 pulsations as indicators of substorm onset using Polar ultraviolet imagery” by K.
2294 Liou, et al. *Journal of Geophysical Research: Space Physics*106A918919-18922.

- 2295 10.1029/2000JA000189
- 2296 Kepko2015Kepko, L., McPherron, RL., Amm, O., Apatenkov, S., Baumjohann, W., Birn,
2297 J.Sergeev, V. 2015jul. Substorm Current Wedge Revisited Substorm Current Wedge
2298 Revisited. *Space Science Reviews*1901-41–46. [http://link.springer.com/10.1007/s11214-](http://link.springer.com/10.1007/s11214-014-0124-9)
2299 [014-0124-9](http://link.springer.com/10.1007/s11214-014-0124-9) 10.1007/s11214-014-0124-9
- 2300 Kim2005Kim, KH., Takahashi, K., Lee, D., Sutcliffe, PR. Yumoto, K. 2005. Pi2
2301 pulsations associated with poleward boundary intensifications during the absence of
2302 substorms Pi2 pulsations associated with poleward boundary intensifications dur-
2303 ing the absence of substorms. *Journal of Geophysical Research*110A1A01217.
2304 <http://doi.wiley.com/10.1029/2004JA010780> 10.1029/2004JA010780
- 2305 Korth1991Korth, A., Pu, ZY., Kremser, G. Roux, A. 1991mar. A Statistical Study of
2306 Substorm Onset Conditions at Geostationary Orbit A Statistical Study of Substorm On-
2307 set Conditions at Geostationary Orbit. *JR. Kan, TA. Potemra, S. Kokubun T. Iijima*
2308 *(), Magnetospheric Substorms Magnetospheric substorms (64, 343–351). Washington,*
2309 *D. C.American Geophysical Union (AGU).* <http://doi.wiley.com/10.1029/GM064p0343>
2310 [10.1029/GM064p0343](http://doi.wiley.com/10.1029/GM064p0343)
- 2311 Koskinen1993Koskinen, HEJ., Lopez, RE., Pellinen, RJ., Pulkkinen, TI., Baker, DN.
2312 Bösinger, T. 1993apr. Pseudobreakup and substorm growth phase in the ionosphere
2313 and magnetosphere Pseudobreakup and substorm growth phase in the ionosphere and
2314 magnetosphere. *Journal of Geophysical Research: Space Physics*98A45801–5813.
2315 <http://doi.wiley.com/10.1029/92JA02482> 10.1029/92JA02482
- 2316 Kullen2009SubstormsPseudobreakupsKullen, A., Ohtani, S. Karlsson, T. 200904. Geo-
2317 magnetic Signatures of Auroral Substorms Preceded by Pseudobreakups Geomagnetic
2318 signatures of auroral substorms preceded by pseudobreakups. *Journal of Geophysical*
2319 *Research: Space Physics*114A4A04201. 10.1029/2008JA013712
- 2320 Lee2004Lee, DY. Lyons, LR. 2004apr. Geosynchronous magnetic field response to
2321 solar wind dynamic pressure pulse Geosynchronous magnetic field response to so-
2322 lar wind dynamic pressure pulse. *Journal of Geophysical Research*109A4A04201.
2323 <http://doi.wiley.com/10.1029/2003JA010076> 10.1029/2003JA010076
- 2324 Lezniak1968Lezniak, TW., Arnoldy, RL., Parks, GK. Winckler, JR. 1968jul. Measure-
2325 ment and Intensity of Energetic Electrons at the Equator at 6.6 Re Measurement and
2326 Intensity of Energetic Electrons at the Equator at 6.6 Re. *Radio Science*37710–714.
2327 <http://doi.wiley.com/10.1002/rds196837710> 10.1002/rds196837710

- 2328 Liemohn2018ModelEvaluationGuidelinesLiemohn, MW., McCollough, JP., Jordanova,
2329 VK., Ngwira, CM., Morley, SK., Cid, C.Vasile, R. 201811. Model Evaluation Guide-
2330 lines for Geomagnetic Index Predictions Model evaluation guidelines for geomagnetic
2331 index predictions. *Space Weather*16122079-2102. 10.1029/2018SW002067
- 2332 Liou2010Liou, K. 2010dec. Polar Ultraviolet Imager observation of auroral breakup
2333 Polar Ultraviolet Imager observation of auroral breakup. *Journal of Geophysical Re-*
2334 *search: Space Physics*115A12A12219. <http://doi.wiley.com/10.1029/2010JA015578>
2335 10.1029/2010JA015578
- 2336 Liou2002Liou, K., Meng, CI., Lui, ATY., Newell, PT. Wing, S. 2002. Magnetic
2337 dipolarization with substorm expansion onset Magnetic dipolarization with substorm
2338 expansion onset. *Magnetospheric Physics: Magnetosphere—inner*107A121131.
2339 <https://agupubs.onlinelibrary.wiley.com/doi/pdf/10.1029/2001JA000179>
2340 10.1029/2001JA000179
- 2341 Liou1999RelativeTimingSubstormLiou, K., Meng, CI., Lui, TY., Newell, PT., Brittnacher,
2342 M., Parks, G.Yumoto, K. 1999. On Relative Timing in Substorm Onset Signatures On
2343 relative timing in substorm onset signatures. *Journal of Geophysical Research: Space*
2344 *Physics*104A1022807-22817. 10.1029/1999JA900206
- 2345 Liou2000LowLatitudePi2Liou, K., Meng, CI., Newell, PT., Takahashi, K., Ohtani, SI., Lui,
2346 ATY.Parks, G. 2000. Evaluation of Low-Latitude Pi2 Pulsations as Indicators of Sub-
2347 storm Onset Using Polar Ultraviolet Imagery Evaluation of low-latitude Pi2 pulsations
2348 as indicators of substorm onset using Polar ultraviolet imagery. *Journal of Geophysical*
2349 *Research: Space Physics*105A22495-2505. 10.1029/1999JA900416
- 2350 Liu2013Liu, J., Angelopoulos, V., Runov, A. Zhou, XZ. 2013may. On the current
2351 sheets surrounding dipolarizing flux bundles in the magnetotail: The case for wedgelets
2352 On the current sheets surrounding dipolarizing flux bundles in the magnetotail: The
2353 case for wedgelets. *Journal of Geophysical Research: Space Physics*11852000–2020.
2354 <http://doi.wiley.com/10.1002/jgra.50092> 10.1002/jgra.50092
- 2355 Lopez2007Lopez, RE., Hernandez, S., Wiltberger, M., Huang, CL., Kepko, EL.,
2356 Spence, H.Lyon, JG. 2007jan. Predicting magnetopause crossings at geosyn-
2357 chronous orbit during the Halloween storms Predicting magnetopause crossings
2358 at geosynchronous orbit during the Halloween storms. *Space Weather*51S01005.
2359 <http://doi.wiley.com/10.1029/2006SW000222> 10.1029/2006SW000222
- 2360 Lui1978Lui, ATY. 1978oct. Estimates of current changes in the geomagneto-

- 2361 tail associated with a substorm Estimates of current changes in the geomagne-
 2362 totail associated with a substorm. *Geophysical Research Letters*510853–856.
 2363 <http://doi.wiley.com/10.1029/GL005i010p00853> 10.1029/GL005i010p00853
- 2364 Lui1991SubstormSynthesisLui, ATY. 1991. Extended Consideration of a Synthesis Model
 2365 for Magnetospheric Substorms Extended Consideration of a Synthesis Model for Mag-
 2366 netospheric Substorms. *Magnetospheric Substorms Magnetospheric Substorms* (64,
 2367 43-60). Washington, DC American Geophysical Union (AGU). 10.1029/GM064p0043
- 2368 Lyon1981Lyon, JG., Brecht, SH., Huba, JD., Fedder, JA. Palmadesso, PJ.
 2369 1981apr. Computer Simulation of a Geomagnetic Substorm Computer Simu-
 2370 lation of a Geomagnetic Substorm. *Physical Review Letters*46151038–1041.
 2371 <https://link.aps.org/doi/10.1103/PhysRevLett.46.1038> 10.1103/PhysRevLett.46.1038
- 2372 Lyons1997Lyons, LR., Blanchard, GT., Samson, JC., Lepping, RP., Yamamoto, T.
 2373 Moretto, T. 1997dec. Coordinated observations demonstrating external sub-
 2374 storm triggering Coordinated observations demonstrating external substorm trig-
 2375 gering. *Journal of Geophysical Research: Space Physics*102A1227039–27051.
 2376 <http://doi.wiley.com/10.1029/97JA02639> 10.1029/97JA02639
- 2377 McPherron1972McPherron, R. 1972sep. Substorm related changes in the
 2378 geomagnetic tail: the growth phase Substorm related changes in the geomag-
 2379 netic tail: the growth phase. *Planetary and Space Science*2091521–1539.
 2380 <https://www.sciencedirect.com/science/article/pii/0032063372900542> 10.1016/0032-
 2381 0633(72)90054-2
- 2382 McPherron1970McPherron, RL. 1970oct. Growth phase of magnetospheric
 2383 substorms Growth phase of magnetospheric substorms. *Journal of Geophysi-
 2384 cal Research*75285592–5599. <http://doi.wiley.com/10.1029/JA075i028p05592>
 2385 10.1029/JA075i028p05592
- 2386 McPherron2015McPherron, RL. 2015jan. Earth's Magnetotail Earth's Magnetotail.
 2387 A. Keiling, CM. Jackman PA. Delamere (), Magnetotails in the Solar System Magne-
 2388 totails in the solar system (61–84). Hoboken, NJ American Geophysical Union (AGU).
 2389 <http://doi.wiley.com/10.1002/9781118842324.ch4> 10.1002/9781118842324.ch4
- 2390 McPherron2017McPherron, RL. Chu, X. 2017mar. The Mid-Latitude Positive
 2391 Bay and the MPB Index of Substorm Activity The Mid-Latitude Positive Bay and
 2392 the MPB Index of Substorm Activity. *Space Science Reviews*2061-491–122.
 2393 <http://link.springer.com/10.1007/s11214-016-0316-6> 10.1007/s11214-016-0316-6

- 2394 McPherron2018McPherron, RL. Chu, X. 2018apr. The Midlatitude Positive Bay
 2395 Index and the Statistics of Substorm Occurrence The Midlatitude Positive Bay
 2396 Index and the Statistics of Substorm Occurrence. *Journal of Geophysical Re-*
 2397 *search: Space Physics*12342831-2850. <http://doi.wiley.com/10.1002/2017JA024766>
 2398 10.1002/2017JA024766
- 2399 McPherron1973McPherron, RL., Russell, CT. Aubry, MP. 1973jun. Satellite studies
 2400 of magnetospheric substorms on August 15, 1968: 9. Phenomenological model for
 2401 substorms Satellite studies of magnetospheric substorms on August 15, 1968: 9. Phe-
 2402 nomenological model for substorms. *Journal of Geophysical Research*78163131–3149.
 2403 <http://doi.wiley.com/10.1029/JA078i016p03131> 10.1029/JA078i016p03131
- 2404 Meng2013Meng, X., Tóth, G., Glocer, A., Fok, MC. Gombosi, TI. 2013sep. Pres-
 2405 sure anisotropy in global magnetospheric simulations: Coupling with ring current
 2406 models Pressure anisotropy in global magnetospheric simulations: Coupling with ring
 2407 current models. *Journal of Geophysical Research: Space Physics*11895639–5658.
 2408 <http://doi.wiley.com/10.1002/jgra.50539> 10.1002/jgra.50539
- 2409 Meng2012bMeng, X., Tóth, G., Liemohn, MW., Gombosi, TI. Runov, A. 2012aug.
 2410 Pressure anisotropy in global magnetospheric simulations: A magnetohydrodynam-
 2411 ics model Pressure anisotropy in global magnetospheric simulations: A magneto-
 2412 hydrodynamics model. *Journal of Geophysical Research: Space Physics*117A8.
 2413 <http://doi.wiley.com/10.1029/2012JA017791> 10.1029/2012JA017791
- 2414 Moldwin1993Moldwin, MB. Hughes, WJ. 1993jan. Geomagnetic substorm associa-
 2415 tion of plasmoids Geomagnetic substorm association of plasmoids. *Journal of Geo-*
 2416 *physical Research: Space Physics*98A181–88. <http://doi.wiley.com/10.1029/92JA02153>
 2417 10.1029/92JA02153
- 2418 MorleySpacepy2014Morley, S., Koller, J., Welling, D., Larsen, B. Niehof, J. 201401.
 2419 SpacePy: Python-Based Tools for the Space Science Community SpacePy: Python-
 2420 Based Tools for the Space Science Community. *Astrophysics Source Code Li-*
 2421 *brary*ascl:1401.002.
- 2422 Morley2009Morley, S., Rouillard, A. Freeman, M. 2009. Recurrent substorm activity dur-
 2423 ing the passage of a corotating interaction region Recurrent substorm activity during the
 2424 passage of a corotating interaction region. *Journal of Atmospheric and Solar-Terrestrial*
 2425 *Physics*71101073–1081. 10.1016/j.jastp.2008.11.009
- 2426 Morley2007ObservationsMagnetosphericSubstormsMorley, SK. 2007. Observations of

- 2427 Magnetospheric Substorms during the Passage of a Corotating Interaction Region Ob-
 2428 servations of magnetospheric substorms during the passage of a corotating interaction
 2429 region. W. Short I. Cairns (), Proceedings from 7th Australian Space Science Con-
 2430 ference, 2007 Proceedings from 7th Australian Space Science Conference, 2007 (118-
 2431 129). SydneyNational Space Society of Australia Ltd.
- 2432 Morley2007AssociationNorthwardTurningsMorley, SK. Freeman, MP. 200704. On the
 2433 Association between Northward Turnings of the Interplanetary Magnetic Field and
 2434 Substorm Onsets On the association between northward turnings of the interplane-
 2435 tary magnetic field and substorm onsets. *Geophysical Research Letters*348L08104.
 2436 10.1029/2006GL028891
- 2437 Morley2010DropoutsOuterElectronMorley, SK., Friedel, RHW., Spanswick, EL., Reeves,
 2438 G., Steinberg, JT., Koller, J.Noveroske, E. 201011. Dropouts of the Outer Electron
 2439 Radiation Belt in Response to Solar Wind Stream Interfaces: Global Positioning Sys-
 2440 tem Observations Dropouts of the outer electron radiation belt in response to solar
 2441 wind stream interfaces: Global positioning system observations. *Proceedings of the*
 2442 *Royal Society A: Mathematical, Physical and Engineering Sciences*46621233329-3350.
 2443 10.1098/rspa.2010.0078
- 2444 Morley2011Morley, SK., Welling, DT., Koller, J., Larsen, BA., Henderson, MG. Niehof,
 2445 J. 2011. SpacePy - A Python-Based Library of Tools for the Space Sciences SpacePy -
 2446 A Python-based Library of Tools for the Space Sciences. *Proceedings of the 9th Python*
 2447 *in Science Conference*39-45.
- 2448 Morley2018PerturbedInputEnsembleMorley, SK., Welling, DT. Woodroffe, JR. 201808.
 2449 Perturbed Input Ensemble Modeling with the Space Weather Modeling Framework Per-
 2450 turbed Input Ensemble Modeling with the Space Weather Modeling Framework. *Space*
 2451 *Weather*1691330-1347. 10.1029/2018SW002000
- 2452 Mukhopadhyay2018AguConductanceMukhopadhyay, A., Welling, DT., Liemohn, MW.,
 2453 Zou, S. Ridley, AJ. 201812. Challenges in Space Weather Prediction: Estimation of
 2454 Auroral Conductance. *Challenges in Space Weather Prediction: Estimation of Auroral*
 2455 *Conductance*. Washington, DC.
- 2456 Nagai1987Nagai, T. 1987mar. Field-aligned currents associated with substorms
 2457 in the vicinity of synchronous orbit: 2. GOES 2 and GOES 3 observations Field-
 2458 aligned currents associated with substorms in the vicinity of synchronous orbit: 2.
 2459 GOES 2 and GOES 3 observations. *Journal of Geophysical Research*92A32432.

- 2460 <http://doi.wiley.com/10.1029/JA092iA03p02432> 10.1029/JA092iA03p02432
- 2461 Nagai1998Nagai, T., Fujimoto, M., Saito, Y., Machida, S., Terasawa, T., Nakamura,
2462 R.Kokubun, S. 1998mar. Structure and dynamics of magnetic reconnection for sub-
2463 storm onsets with Geotail observations Structure and dynamics of magnetic recon-
2464 nection for substorm onsets with Geotail observations. *Journal of Geophysical Re-*
2465 *search: Space Physics*103A34419–4440. <http://doi.wiley.com/10.1029/97JA02190>
2466 10.1029/97JA02190
- 2467 Newell2011aNewell, PT. Gjerloev, JW. 2011dec. Evaluation of SuperMAG
2468 auroral electrojet indices as indicators of substorms and auroral power Evalua-
2469 tion of SuperMAG auroral electrojet indices as indicators of substorms and au-
2470 roral power. *Journal of Geophysical Research: Space Physics*116A12A12211.
2471 <http://doi.wiley.com/10.1029/2011JA016779> 10.1029/2011JA016779
- 2472 Newell2011bNewell, PT. Gjerloev, JW. 2011dec. Substorm and magnetosphere
2473 characteristic scales inferred from the SuperMAG auroral electrojet indices Substorm
2474 and magnetosphere characteristic scales inferred from the SuperMAG auroral elec-
2475 trojet indices. *Journal of Geophysical Research: Space Physics*116A12A12232.
2476 <http://doi.wiley.com/10.1029/2011JA016936> 10.1029/2011JA016936
- 2477 Newell2011cNewell, PT. Liou, K. 2011mar. Solar wind driving and substorm trig-
2478 gering Solar wind driving and substorm triggering. *Journal of Geophysical Re-*
2479 *search: Space Physics*116A3A03229. <http://doi.wiley.com/10.1029/2010JA016139>
2480 10.1029/2010JA016139
- 2481 Newell2001Newell, PT., Liou, K., Sotirelis, T. Meng, CI. 2001dec. Auroral precipi-
2482 tation power during substorms: A Polar UV Imager-based superposed epoch analysis
2483 Auroral precipitation power during substorms: A Polar UV Imager-based superposed
2484 epoch analysis. *Journal of Geophysical Research: Space Physics*106A1228885–28896.
2485 <http://doi.wiley.com/10.1029/2000JA000428> 10.1029/2000JA000428
- 2486 Nishida1986Nishida, A., Scholer, M., Terasawa, T., Bame, SJ., Gloeckler, G., Smith,
2487 EJ. Zwickl, RD. 1986apr. Quasi-stagnant plasmoid in the middle tail: A new pre-
2488 expansion phase phenomenon Quasi-stagnant plasmoid in the middle tail: A new
2489 preexpansion phase phenomenon. *Journal of Geophysical Research*91A44245.
2490 <http://doi.wiley.com/10.1029/JA091iA04p04245> 10.1029/JA091iA04p04245
- 2491 Noah2013Noah, MA. Burke, WJ. 2013aug. Sawtooth-substorm connections: A closer
2492 look Sawtooth-substorm connections: A closer look. *Journal of Geophysical Re-*

- 2493 search: Space Physics11885136–5148. <http://doi.wiley.com/10.1002/jgra.50440>
 2494 10.1002/jgra.50440
- 2495 Nose2009Nosé, M., Iyemori, T., Takeda, M., Toh, H., Ookawa, T., Cifuentes-Nava,
 2496 G.Curto, JJ. 2009. New substorm index derived from high-resolution ge-
 2497 omagnetic field data at low latitude and its comparison with AE and ASY in-
 2498 dices New substorm index derived from high-resolution geomagnetic field data
 2499 at low latitude and its comparison with AE and ASY indices. J. Love (),
 2500 Proc. XIII IAGA Workshop Proc. xiii iaga workshop (202–207). Golden, CO.
 2501 <https://geomag.usgs.gov/downloads/publications/Proceedings202-207.pdf>
- 2502 Ohtani1993Ohtani, S., Anderson, BJ., Sibeck, DG., Newell, PT., Zanetti, LJ., Potemra,
 2503 TA.Russell, CT. 1993nov. A multisatellite study of a pseudo-substorm onset in the
 2504 near-Earth magnetotail A multisatellite study of a pseudo-substorm onset in the near-
 2505 Earth magnetotail. Journal of Geophysical Research: Space Physics98A1119355–19367.
 2506 <http://doi.wiley.com/10.1029/93JA01421> 10.1029/93JA01421
- 2507 Ohtani2004Ohtani, Si. Raeder, J. 2004jan. Tail current surge: New insights
 2508 from a global MHD simulation and comparison with satellite observations Tail
 2509 current surge: New insights from a global MHD simulation and comparison
 2510 with satellite observations. Journal of Geophysical Research109A1A01207.
 2511 <http://doi.wiley.com/10.1029/2002JA009750> 10.1029/2002JA009750
- 2512 Oieroset2001Øieroset, M., Phan, TD., Fujimoto, M., Lin, RP. Lepping, RP. 2001. In situ
 2513 detection of reconnection in the Earth’s magnetotail In situ detection of reconnection in
 2514 the Earth’s magnetotail. Letters to Nature412July414–416. 10.1038/35086520
- 2515 Oieroset1999Øieroset, M., Yamauchi, M., Liszka, L., Christon, SP. Hultqvist, B. 1999apr.
 2516 A statistical study of ion beams and conics from the dayside ionosphere during dif-
 2517 ferent phases of a substorm A statistical study of ion beams and conics from the day-
 2518 side ionosphere during different phases of a substorm. Journal of Geophysical Re-
 2519 search: Space Physics104A46987–6998. <http://doi.wiley.com/10.1029/1998JA900177>
 2520 10.1029/1998JA900177
- 2521 Parzen1962Parzen, E. 1962sep. On Estimation of a Probability Density Function and
 2522 Mode On Estimation of a Probability Density Function and Mode. The Annals of
 2523 Mathematical Statistics3331065–1076. <http://projecteuclid.org/euclid.aoms/1177704472>
 2524 10.1214/aoms/1177704472
- 2525 Perreault1978Perreault, P. Akasofu, SI. 1978sep. A study of geomagnetic storms

- 2526 A study of geomagnetic storms. *Geophysical Journal International* 54:3547–573.
 2527 <https://academic.oup.com/gji/article-lookup/doi/10.1111/j.1365-246X.1978.tb05494.x>
 2528 10.1111/j.1365-246X.1978.tb05494.x
- 2529 Powell 1999 Powell, KG., Roe, PL., Linde, TJ., Gombosi, TI. De Zeeuw, DL. 1999sep.
 2530 A Solution-Adaptive Upwind Scheme for Ideal Magnetohydrodynamics A Solution-
 2531 Adaptive Upwind Scheme for Ideal Magnetohydrodynamics. *Journal of Computational*
 2532 *Physics* 154:2284–309. <http://linkinghub.elsevier.com/retrieve/pii/S002199919996299X>
 2533 10.1006/jcph.1999.6299
- 2534 Pulkkinen 2013 Pulkkinen, A., Rastätter, L., Kuznetsova, M., Singer, H., Balch, C., Weimer,
 2535 D. Weigel, R. 2013jun. Community-wide validation of geospace model ground
 2536 magnetic field perturbation predictions to support model transition to operations
 2537 Community-wide validation of geospace model ground magnetic field perturbation
 2538 predictions to support model transition to operations. *Space Weather* 11:6369–385.
 2539 <http://doi.wiley.com/10.1002/swe.20056> 10.1002/swe.20056
- 2540 Pytte 1976 Ground Signatures Pytte, T., McPherron, R. Kokubun, S. 197612. The Ground
 2541 Signatures of the Expansion Phase during Multiple Onset Substorms The ground sig-
 2542 natures of the expansion phase during multiple onset substorms. *Planetary and Space*
 2543 *Science* 24:121115-IN4. 10.1016/0032-0633(76)90149-5
- 2544 Pytte 1978 Pytte, T., McPherron, RL., Hones, EW. West, HI. 1978. Multiple-
 2545 satellite studies of magnetospheric substorms: Distinction between polar mag-
 2546 netic substorms and convection-driven negative bays Multiple-satellite studies of
 2547 magnetospheric substorms: Distinction between polar magnetic substorms and
 2548 convection-driven negative bays. *Journal of Geophysical Research* 83A:2663.
 2549 <http://doi.wiley.com/10.1029/JA083iA02p00663> 10.1029/JA083iA02p00663
- 2550 Pytte 1976 Multiple Satellite Studies Pytte, T., McPherron, RL., Kivelson, MG., West, HI.
 2551 Hones, EW. 197612. Multiple-Satellite Studies of Magnetospheric Substorms: Radial
 2552 Dynamics of the Plasma Sheet Multiple-satellite studies of magnetospheric substorms:
 2553 Radial dynamics of the plasma sheet. *Journal of Geophysical Research* 81:345921-5933.
 2554 10.1029/JA081i034p05921
- 2555 Rae 2009 Rae, JJ., Mann, IR., Murphy, KR., Milling, DK., Parent, A., Angelopoulos,
 2556 V. Russell, CT. 2009jan. Timing and localization of ionospheric sig-
 2557 natures associated with substorm expansion phase onset Timing and local-
 2558 ization of ionospheric signatures associated with substorm expansion phase

- 2559 onset. *Journal of Geophysical Research: Space Physics*114A1A00C09.
 2560 <https://agupubs.onlinelibrary.wiley.com/doi/full/10.1029/2008JA013559>
 2561 10.1029/2008JA013559
- 2562 Raeder2001bRaeder, J., McPherron, RL., Frank, LA., Kokubun, S., Lu, G., Mukai,
 2563 T.Slavin, JA. 2001jan. Global simulation of the Geospace Environment Model-
 2564 ing substorm challenge event Global simulation of the Geospace Environment Mod-
 2565 eling substorm challenge event. *Journal of Geophysical Research*106A1381–395.
 2566 <http://doi.wiley.com/10.1029/2000JA000605> 10.1029/2000JA000605
- 2567 Raeder2010aRaeder, J., Zhu, P., Ge, Y. Siscoe, G. 2010dec. Open Geospace General
 2568 Circulation Model simulation of a substorm: Axial tail instability and ballooning mode
 2569 preceding substorm onset Open Geospace General Circulation Model simulation of a
 2570 substorm: Axial tail instability and ballooning mode preceding substorm onset. *Journal*
 2571 *of Geophysical Research*115A5A00I16. <http://doi.wiley.com/10.1029/2010JA015876>
 2572 10.1029/2010JA015876
- 2573 Ridley2004Ridley, A., Gombosi, T. Dezeew, D. 200402. Ionospheric control of the
 2574 magnetosphere: conductance Ionospheric control of the magnetosphere: conductance.
 2575 *Annales Geophysicae*22567-584. 10.5194/angeo-22-567-2004
- 2576 Ridley2003Ridley, AJ., Gombosi, TI., De~Zeeuw, DL., Clauer, CR. Richmond, AD.
 2577 2003. Ionospheric control of the magnetosphere: Thermospheric neutral winds Iono-
 2578 spheric control of the magnetosphere: Thermospheric neutral winds. *J. Geophys.*
 2579 *Res.*108A81328. 10.1029/2002JA009464
- 2580 Rostoker2002Rostoker, G. 2002jul. Identification of substorm expansive phase
 2581 onsets Identification of substorm expansive phase onsets. *Journal of Geo-*
 2582 *physical Research*107A71137. <http://doi.wiley.com/10.1029/2001JA003504>
 2583 10.1029/2001JA003504
- 2584 Rostoker1980Rostoker, G., Akasofu, SI., Foster, J., Greenwald, R., Kamide, Y.,
 2585 Kawasaki, K.Russell, C. 1980apr. Magnetospheric substorms—definition and
 2586 signatures Magnetospheric substorms—definition and signatures. *Journal of Geo-*
 2587 *physical Research*85A41663. <http://doi.wiley.com/10.1029/JA085iA04p01663>
 2588 10.1029/JA085iA04p01663
- 2589 Runov2009Runov, A., Angelopoulos, V., Sitnov, MI., Sergeev, VA., Bonnell, J., McFadden,
 2590 JP.Auster, U. 2009jul. THEMIS observations of an earthward-propagating dipolarization
 2591 front THEMIS observations of an earthward-propagating dipolarization front. *Geo-*

- 2592 physical Research Letters3614L14106. <http://doi.wiley.com/10.1029/2009GL038980>
 2593 10.1029/2009GL038980
- 2594 Runov2012Runov, A., Angelopoulos, V. Zhou, XZ. 2012may. Multipoint observations
 2595 of dipolarization front formation by magnetotail reconnection Multipoint observations
 2596 of dipolarization front formation by magnetotail reconnection. *Journal of Geophysical*
 2597 *Research: Space Physics*117A5A05230. <http://doi.wiley.com/10.1029/2011JA017361>
 2598 10.1029/2011JA017361
- 2599 Russell2000Russell, CT. 2000oct. How northward turnings of the IMF can
 2600 lead to substorm expansion onsets How northward turnings of the IMF can lead
 2601 to substorm expansion onsets. *Geophysical Research Letters*27203257–3259.
 2602 <http://doi.wiley.com/10.1029/2000GL011910> 10.1029/2000GL011910
- 2603 Samson1986Samson, J. Yeung, K. 1986nov. Some generalizations on the
 2604 method of superposed epoch analysis Some generalizations on the method of
 2605 superposed epoch analysis. *Planetary and Space Science*34111133–1142.
 2606 <http://linkinghub.elsevier.com/retrieve/pii/0032063386900255> 10.1016/0032-
 2607 0633(86)90025-5
- 2608 Sauvaud1980Sauvaud, JA. Winckler, J. 1980. Dynamics of plasma, energetic par-
 2609 ticles, and fields near synchronous orbit in the nighttime sector during magneto-
 2610 spheric substorms Dynamics of plasma, energetic particles, and fields near syn-
 2611 chronous orbit in the nighttime sector during magnetospheric substorms. *Journal of*
 2612 *Geophysical Research*85A52043. <http://doi.wiley.com/10.1029/JA085iA05p02043>
 2613 10.1029/JA085iA05p02043
- 2614 Sazykin2000Sazykin, SY. 2000. Theoretical Studies of Penetration of Magnetospheric
 2615 Electric Fields to the Ionosphere Theoretical Studies of Penetration of Magnetospheric
 2616 Electric Fields to the Ionosphere . Logan, UtahUtah State University.
- 2617 Schmid2011Schmid, D., Volwerk, M., Nakamura, R., Baumjohann, W. Heyn, M.
 2618 2011sep. A statistical and event study of magnetotail dipolarization fronts A statistical
 2619 and event study of magnetotail dipolarization fronts. *Annales Geophysicae*2991537–
 2620 1547. <http://www.ann-geophys.net/29/1537/2011/> 10.5194/angeo-29-1537-2011
- 2621 Sergeev2012Sergeev, VA., Angelopoulos, V. Nakamura, R. 2012mar. Re-
 2622 cent advances in understanding substorm dynamics Recent advances in un-
 2623 derstanding substorm dynamics. *Geophysical Research Letters*395L05101.
 2624 <http://doi.wiley.com/10.1029/2012GL050859> 10.1029/2012GL050859

- 2625 Sergeev1990Sergeev, VA., Tanskanen, P., Mursula, K., Korth, A. Elphic, RC.
 2626 1990apr. Current sheet thickness in the near-Earth plasma sheet during sub-
 2627 storm growth phase Current sheet thickness in the near-Earth plasma sheet dur-
 2628 ing substorm growth phase. *Journal of Geophysical Research*95A43819.
 2629 <http://doi.wiley.com/10.1029/JA095iA04p03819> 10.1029/JA095iA04p03819
- 2630 Singer1996Singer, H., Matheson, L., Grubb, R., Newman, A. Bouwer, D. 1996oct.
 2631 Monitoring space weather with the GOES magnetometers Monitoring space weather
 2632 with the GOES magnetometers. ER. Washwell (), *Proceedings of SPIE Pro-*
 2633 *ceedings of spie* (2812, 299–308). International Society for Optics and Photon-
 2634 ics. <http://proceedings.spiedigitallibrary.org/proceeding.aspx?articleid=1021197>
 2635 10.1117/12.254077
- 2636 Slavin1989Slavin, JA., Baker, DN., Craven, JD., Elphic, RC., Fairfield, DH., Frank,
 2637 LA.Zwickl, RD. 1989nov. CDAW 8 observations of plasmoid signatures in the ge-
 2638 omagnetic tail: An assessment CDAW 8 observations of plasmoid signatures in the
 2639 geomagnetic tail: An assessment. *Journal of Geophysical Research*94A1115153.
 2640 <http://doi.wiley.com/10.1029/JA094iA11p15153> 10.1029/JA094iA11p15153
- 2641 Slavin1992Slavin, JA., Smith, MF., Mazur, EL., Baker, DN., Iyemori, T., Singer, HJ.
 2642 Greenstadt, EW. 1992apr. ISEE 3 plasmoid and TCR observations during an ex-
 2643 tended interval of substorm activity ISEE 3 plasmoid and TCR observations during
 2644 an extended interval of substorm activity. *Geophysical Research Letters*198825–828.
 2645 <http://doi.wiley.com/10.1029/92GL00394> 10.1029/92GL00394
- 2646 Slinker1995Slinker, SP., Fedder, JA. Lyon, JG. 1995apr. Plasmoid formation and evo-
 2647 lution in a numerical simulation of a substorm Plasmoid formation and evolution in
 2648 a numerical simulation of a substorm. *Geophysical Research Letters*227859–862.
 2649 <http://doi.wiley.com/10.1029/95GL00300> 10.1029/95GL00300
- 2650 Stephenson2000Stephenson, DB. 2000apr. Use of the “Odds Ratio” for Diagnos-
 2651 ing Forecast Skill Use of the “Odds Ratio” for Diagnosing Forecast Skill. *Weather*
 2652 *and Forecasting*152221–232. <http://journals.ametsoc.org/doi/abs/10.1175/1520-0434>
 2653 10.1175/1520-0434(2000)015<0221:UOTORF>2.0.CO;2
- 2654 Sugiura1968Sugiura, M., Skillman, TL., Ledley, BG. Heppner, JP. 1968nov. Propa-
 2655 gation of the sudden commencement of July 8, 1966, to the magnetotail Propagation
 2656 of the sudden commencement of July 8, 1966, to the magnetotail. *Journal of Geo-*
 2657 *physical Research*73216699–6709. <http://doi.wiley.com/10.1029/JA073i021p06699>

- 2658 10.1029/JA073i021p06699
- 2659 Toffoletto2003Toffoletto, F., Sazykin, S., Spiro, R. Wolf, R. 2003. Inner magne-
 2660 tospheric modeling with the Rice Convection Model Inner magnetospheric mod-
 2661 eling with the Rice Convection Model. *Space Science Reviews*1071-2175–196.
 2662 <http://link.springer.com/10.1023/A:1025532008047> 10.1023/A:1025532008047
- 2663 Toth2016Tóth, G., Jia, X., Markidis, S., Peng, IB., Chen, Y., Daldorff, LKS.Dorelli, JC.
 2664 2016feb. Extended magnetohydrodynamics with embedded particle-in-cell simula-
 2665 tion of Ganymede’s magnetosphere Extended magnetohydrodynamics with embedded
 2666 particle-in-cell simulation of Ganymede’s magnetosphere. *Journal of Geophysical Re-*
 2667 *search: Space Physics*12121273–1293. <http://doi.wiley.com/10.1002/2015JA021997>
 2668 10.1002/2015JA021997
- 2669 Toth2008Tóth, G., Ma, Y. Gombosi, TI. 2008jul. Hall magneto-
 2670 hydrodynamics on block-adaptive grids Hall magnetohydrodynamics on
 2671 block-adaptive grids. *Journal of Computational Physics*227146967–
 2672 6984. <http://linkinghub.elsevier.com/retrieve/pii/S0021999108002076>
 2673 10.1016/j.jcp.2008.04.010
- 2674 Toth2005Tóth, G., Sokolov, IV., Gombosi, TI., Chesney, DR., Clauer, CR., De Zeeuw,
 2675 DL.Kóta, J. 2005. Space Weather Modeling Framework: A new tool for the space
 2676 science community Space Weather Modeling Framework: A new tool for the space
 2677 science community. *Journal of Geophysical Research: Space Physics*110A12A12226.
 2678 <http://dx.doi.org/10.1029/2005JA011126> 10.1029/2005JA011126
- 2679 Toth2012Tóth, G., van der Holst, B., Sokolov, IV., Zeeuw, DLD., Gombosi, TI., Fang,
 2680 F.Opher, M. 2012. Adaptive Numerical Algorithms in Space Weather Modeling Adap-
 2681 tive Numerical Algorithms in Space Weather Modeling. *J. Comput. Phys.*2313870–903.
 2682 10.1016/j.jcp.2011.02.006
- 2683 Walach2015Walach, MT. Milan, SE. 2015mar. Are steady magnetospheric convec-
 2684 tion events prolonged substorms? Are steady magnetospheric convection events pro-
 2685 longed substorms? *Journal of Geophysical Research: Space Physics*12031751–1758.
 2686 <http://doi.wiley.com/10.1002/2014JA020631> 10.1002/2014JA020631
- 2687 Wang2010Wang, H., Ma, S. Ridley, AJ. 2010mar. Comparative study of a substorm event
 2688 by satellite observation and model simulation Comparative study of a substorm event
 2689 by satellite observation and model simulation. *Chinese Science Bulletin*559857–864.
 2690 <http://link.springer.com/10.1007/s11434-009-0282-4> 10.1007/s11434-009-0282-4

- 2691 Welling2017ExploringPredictivePerformance Welling, DT., Anderson, BJ., Crowley, G.,
 2692 Pulkkinen, AA. Rastätter, L. 201701. Exploring Predictive Performance: A Reanal-
 2693 ysis of the Geospace Model Transition Challenge Exploring predictive performance:
 2694 A reanalysis of the geospace model transition challenge. *Space Weather*151192-203.
 2695 10.1002/2016SW001505
- 2696 Welling2016gpw Welling, DT., Barakat, AR., Eccles, JV., Schunk, RW. Chappell, CR.
 2697 2016. Coupling the Generalized Polar Wind Model to Global Magnetohydrodynamics:
 2698 Initial Results Coupling the Generalized Polar Wind Model to Global Magneto-hydro-
 2699 dynamics: Initial Results. *Magnetosphere-Ionosphere Coupling in the Solar System*
 2700 *Magnetosphere-ionosphere coupling in the solar system* (222, 179–194). Washington,
 2701 DC American Geophysical Union (AGU). 10.15142/T3C88J
- 2702 Welling2010a Welling, DT. Ridley, AJ. 2010mar. Validation of SWMF magnetic field
 2703 and plasma Validation of SWMF magnetic field and plasma. *Space Weather*83S03002.
 2704 <http://doi.wiley.com/10.1029/2009SW000494> 10.1029/2009SW000494
- 2705 Weygand2008 Weygand, JM., McPherron, R., Kauristie, K., Frey, H. Hsu, TS. 2008dec.
 2706 Relation of auroral substorm onset to local AL index and dispersionless particle in-
 2707 jections Relation of auroral substorm onset to local AL index and dispersionless par-
 2708 ticle injections. *Journal of Atmospheric and Solar-Terrestrial Physics*70182336–
 2709 2345. <https://www.sciencedirect.com/science/article/pii/S1364682608002563>
 2710 10.1016/J.JASTP.2008.09.030
- 2711 Wild2009a Wild, JA., Woodfield, EE. Morley, SK. 2009sep. On the triggering of au-
 2712 roral substorms by northward turnings of the interplanetary magnetic field On the
 2713 triggering of auroral substorms by northward turnings of the interplanetary magnetic
 2714 field. *Annales Geophysicae*2793559–3570. <http://www.ann-geophys.net/27/3559/2009/>
 2715 10.5194/angeo-27-3559-2009
- 2716 Wilks2011 Wilks, DS. 2011. Statistical methods in the atmospheric sciences Statistical
 2717 methods in the atmospheric sciences. Cambridge, MA Elsevier/Academic Press.
- 2718 Wilson2004 Wilson, GR., Ober, DM., Germany, GA. Lund, EJ. 2004feb. Night-
 2719 side auroral zone and polar cap ion outflow as a function of substorm size and
 2720 phase Nightside auroral zone and polar cap ion outflow as a function of substorm
 2721 size and phase. *Journal of Geophysical Research: Space Physics*109A2A02206.
 2722 <http://doi.wiley.com/10.1029/2003JA009835> 10.1029/2003JA009835
- 2723 Wiltberger2010 Wiltberger, M., Lotko, W., Lyon, JG., Damiano, P. Merkin, V. 2010oct.

- 2724 Influence of cusp O⁺ outflow on magnetotail dynamics in a multifluid MHD model
 2725 of the magnetosphere Influence of cusp O⁺ outflow on magnetotail dynamics in
 2726 a multifluid MHD model of the magnetosphere. *Journal of Geophysical Re-*
 2727 *search: Space Physics*115A10A00J05. <http://doi.wiley.com/10.1029/2010JA015579>
 2728 10.1029/2010JA015579
- 2729 Winglee2002Winglee, RM., Chua, D., Brittnacher, M., Parks, GK. Lu, G. 2002sep.
 2730 Global impact of ionospheric outflows on the dynamics of the magnetosphere and cross-
 2731 polar cap potential Global impact of ionospheric outflows on the dynamics of the mag-
 2732 netosphere and cross-polar cap potential. *Journal of Geophysical Research*107A91237.
 2733 <http://doi.wiley.com/10.1029/2001JA000214> 10.1029/2001JA000214
- 2734 Wolf1982Wolf, RA., Harel, M., Spiro, RW., Voigt, GH., Reiff, PH. Chen, CKK. 1982.
 2735 Computer simulation of inner magnetospheric dynamics for the magnetic storm of
 2736 July 29, 1977 Computer simulation of inner magnetospheric dynamics for the mag-
 2737 netic storm of July 29, 1977. *Journal of Geophysical Research*87A85949–5962.
 2738 <http://doi.wiley.com/10.1029/JA087iA08p05949> 10.1029/JA087iA08p05949
- 2739 Yu2008bYu, Y. Ridley, AJ. 2008may. Validation of the space weather mod-
 2740 eling framework using ground-based magnetometers Validation of the space
 2741 weather modeling framework using ground-based magnetometers. *Space*
 2742 *Weather*6S05002. <http://www.agu.org/pubs/crossref/2008/2007SW000345.shtml>
 2743 <http://doi.wiley.com/10.1029/2007SW000345> 10.1029/2007SW000345
- 2744 Yu2010cYu, Y., Ridley, AJ., Welling, DT. Tóth, G. 201008. Including Gap Region Field-
 2745 Aligned Currents and Magnetospheric Currents in the MHD Calculation of Ground-
 2746 Based Magnetic Field Perturbations Including gap region field-aligned currents and
 2747 magnetospheric currents in the MHD calculation of ground-based magnetic field per-
 2748 turbations. *Journal of Geophysical Research*115A8A08207. 10.1029/2009JA014869
- 2749 Zhu2004Zhu, P., Bhattacharjee, A. Ma, ZW. 2004nov. Finite k y balloon-
 2750 ing instability in the near-Earth magnetotail Finite k y ballooning instability in
 2751 the near-Earth magnetotail. *Journal of Geophysical Research*109A11A11211.
 2752 <http://doi.wiley.com/10.1029/2004JA010505> 10.1029/2004JA010505

Figure 1.

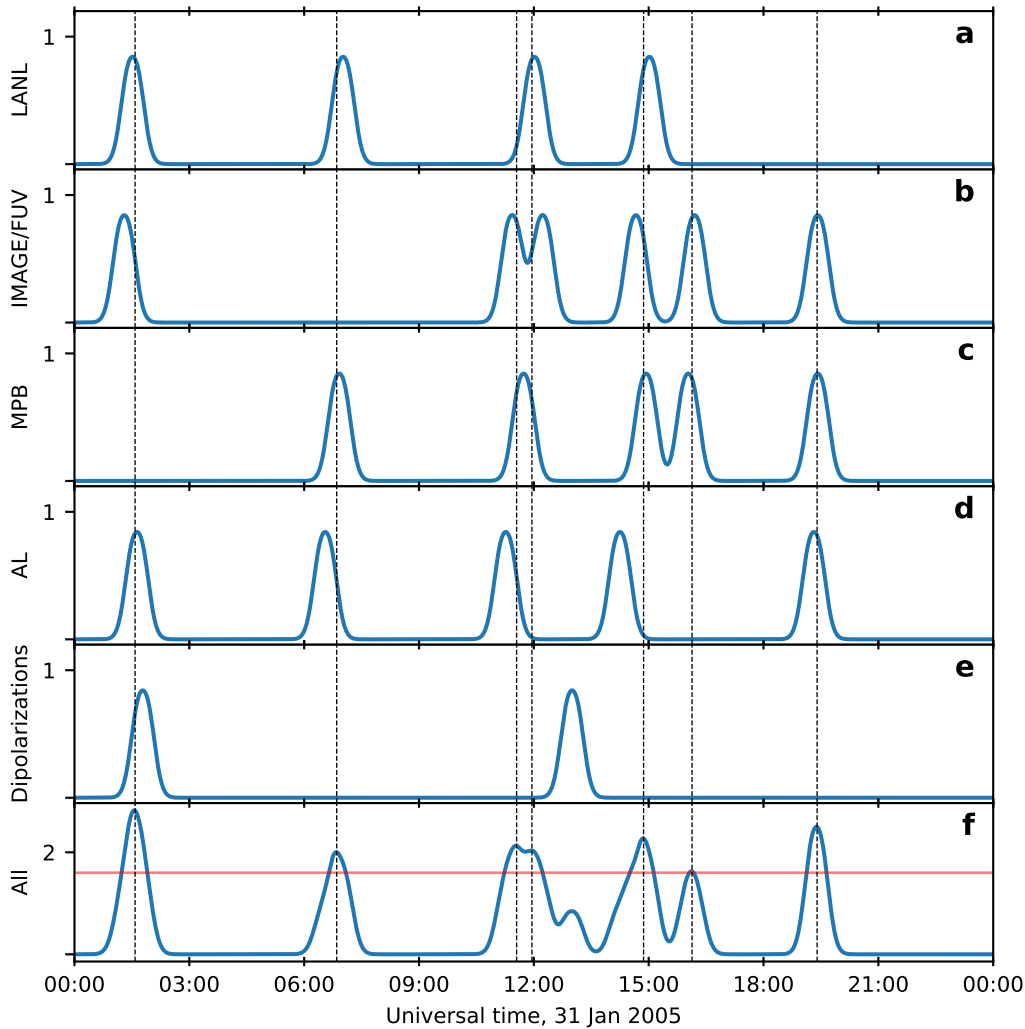


Figure 2.

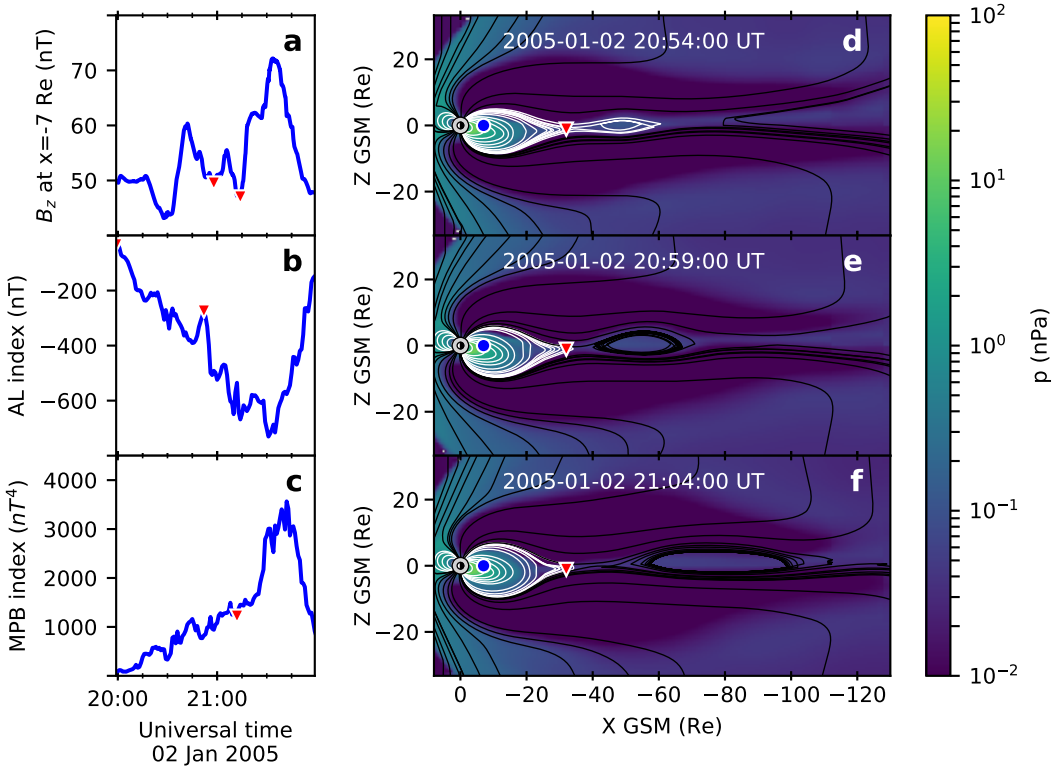


Figure 3.

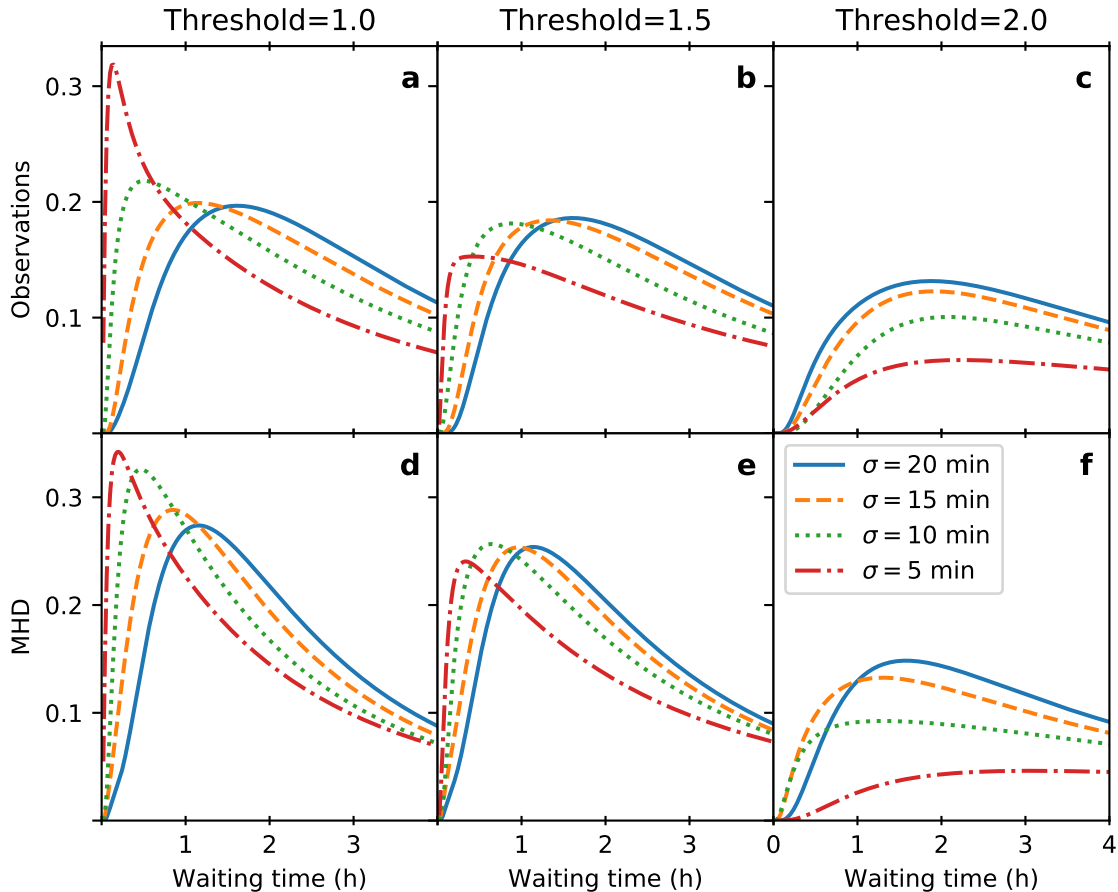


Figure 4.

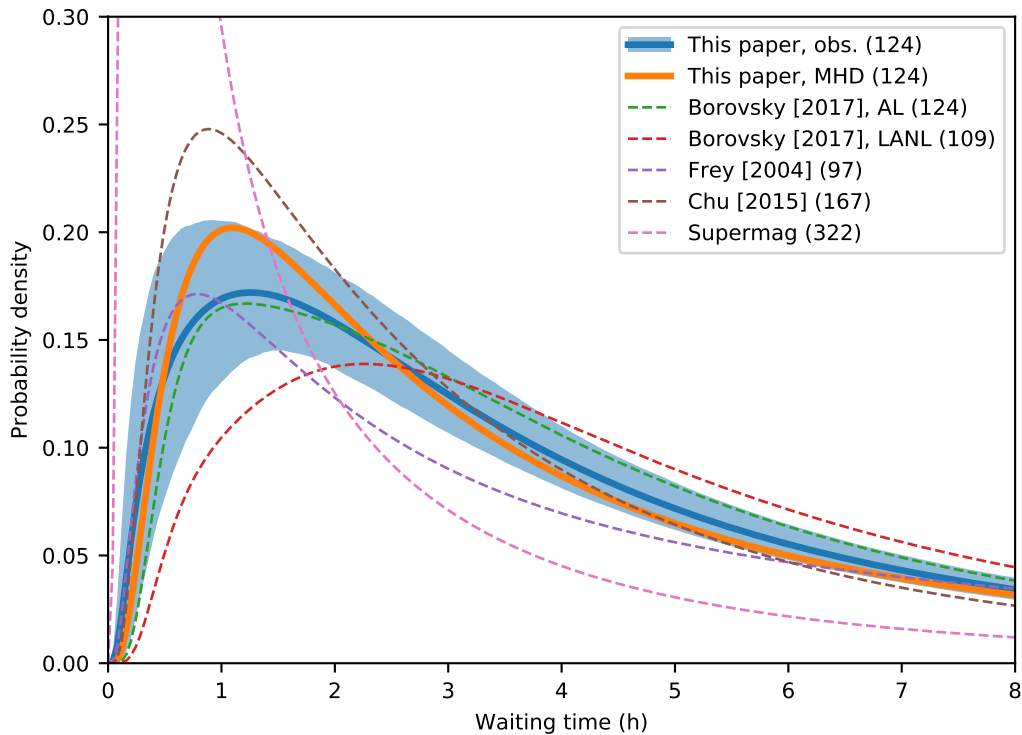


Figure 5.

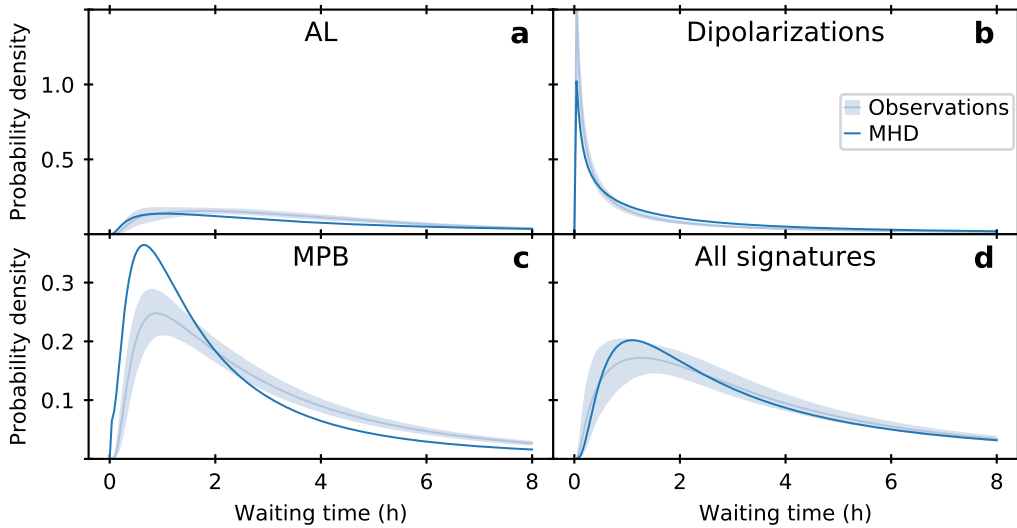


Figure 6.

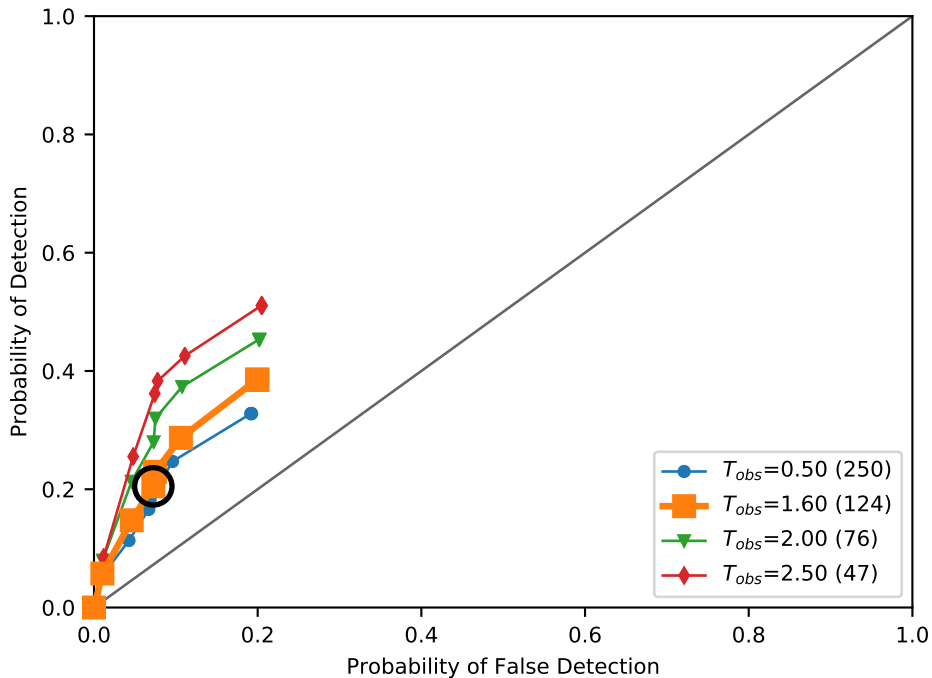


Figure 7.

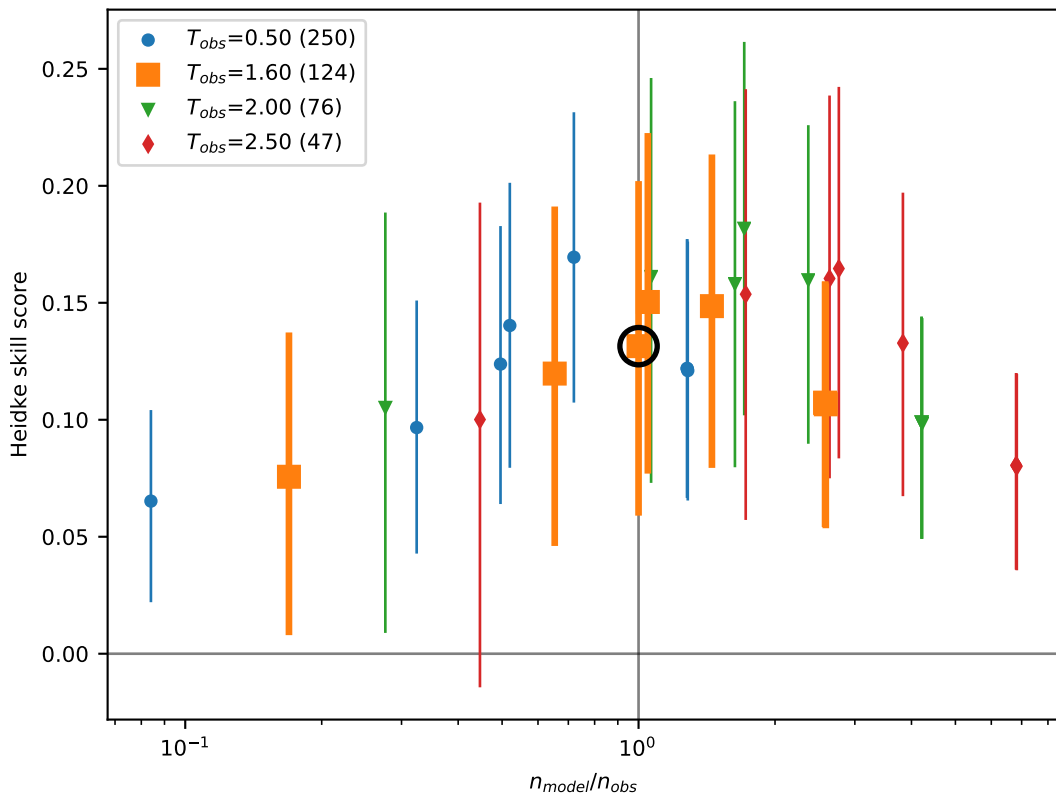


Figure 8.

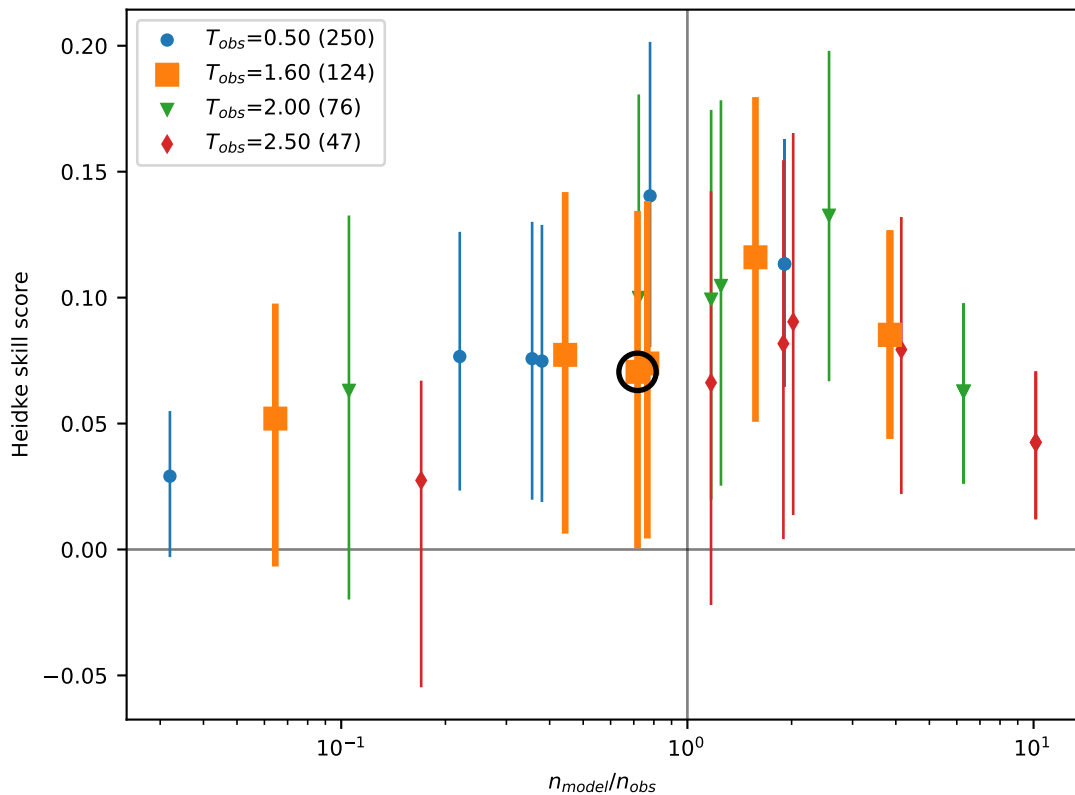


Figure 8.

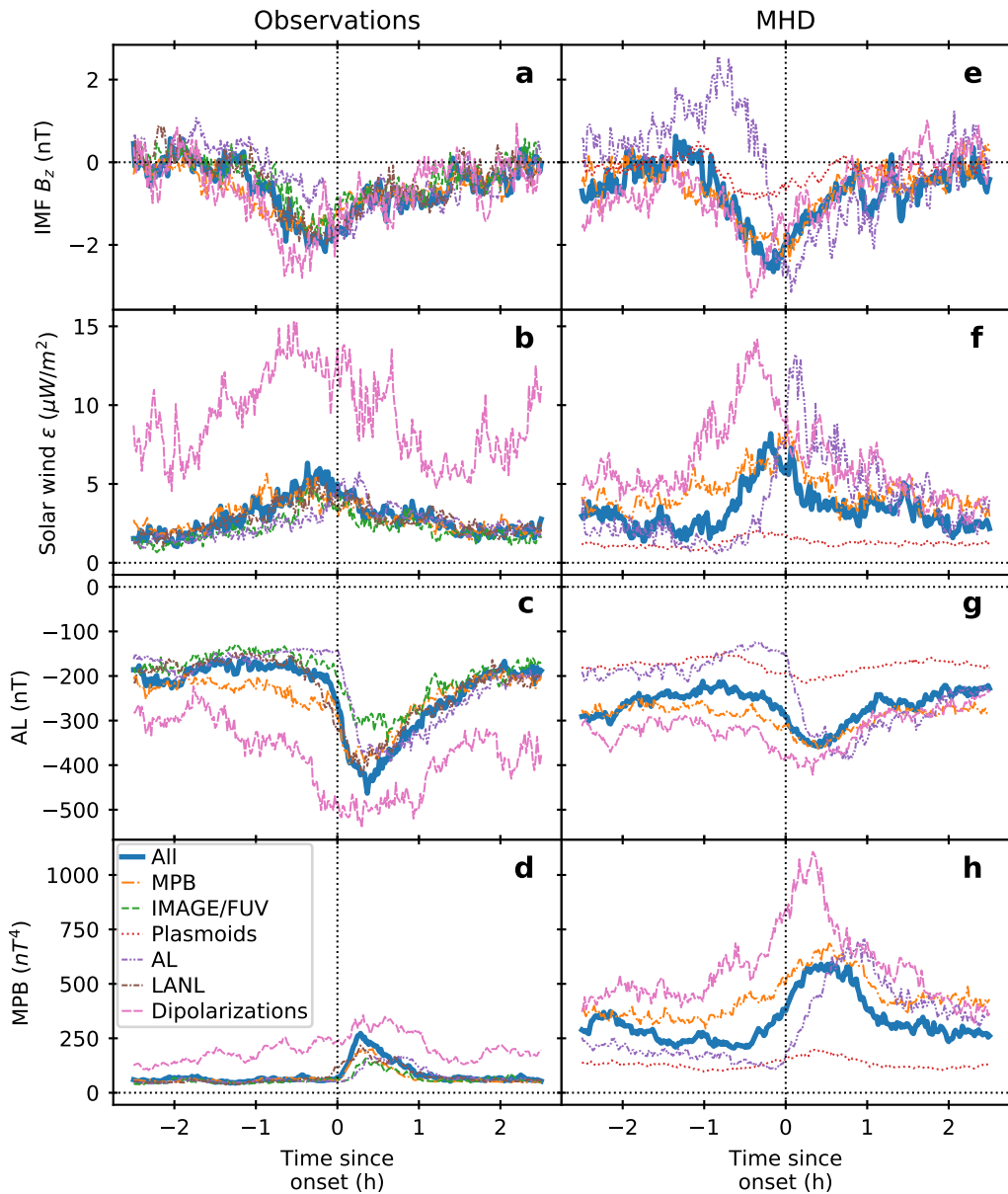


Figure 9.

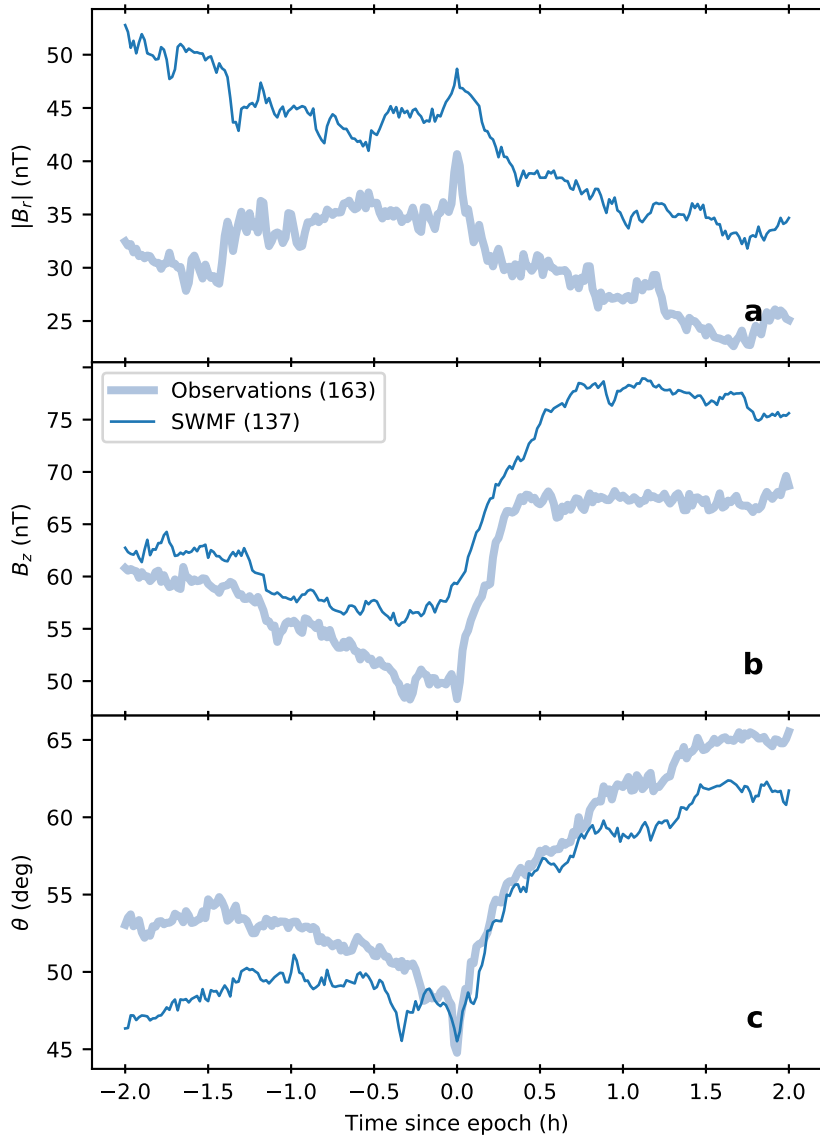


Figure 10.

